

1 **Supplementary Information**

2

3 **The AAA+ chaperone VCP disaggregates Tau fibrils and generates**
4 **aggregate seeds in a cellular system**

5 Itika Saha^{1,2}, Patricia Yuste-Checa^{1,2}, Miguel Da Silva Padilha^{3,4,7}, Qiang Guo^{5,#}, Roman
6 Körner¹, Hauke Holthausen¹, Victoria A. Trinkaus^{1,5,6}, Irina Dudanova^{3,4,7}, Rubén Fernández-
7 Busnadiego^{2,5,8,9}, Wolfgang Baumeister⁵, David W. Sanders^{10,‡}, Saurabh Gautam^{1,§}, Marc I.
8 Diamond¹⁰, F. Ulrich Hartl^{1,2,6,*} and Mark S. Hipp^{1,6,11,12*}

9 ¹Department of Cellular Biochemistry, Max Planck Institute of Biochemistry, Am Klopferspitz
10 18, 82152 Martinsried, Germany.

11 ²Aligning Science Across Parkinson's (ASAP) Collaborative Research Network, Chevy Chase,
12 MD, USA.

13 ³Molecular Neurodegeneration Group, Max Planck Institute for Biological Intelligence,
14 82152 Martinsried, Germany.

15 ⁴Department of Molecules – Signaling – Development, Max Planck Institute for Biological
16 Intelligence, Am Klopferspitz 18, 82152 Martinsried, Germany.

17 ⁵Department of Structural Molecular Biology, Max Planck Institute of Biochemistry, Am
18 Klopferspitz 18, 82152 Martinsried, Germany.

19 ⁶Munich Cluster for Systems Neurology (SyNergy), Munich, Germany.

20 ⁷Center for Anatomy, Faculty of Medicine and University Hospital Cologne, University of
21 Cologne, 50931 Cologne, Germany.

22 ⁸Institute of Neuropathology, University Medical Center Göttingen, 37099 Göttingen, Germany.

23 ⁹Cluster of Excellence “Multiscale Bioimaging: from Molecular Machines to Networks of
24 Excitable Cells” (MBExC), University of Göttingen, Germany.

25 ¹⁰Center for Alzheimer's and Neurodegenerative Diseases, Peter O'Donnell Jr. Brain Institute,
26 University of Texas Southwestern Medical Center, Dallas, 75390 Texas, USA.

27 ¹¹School of Medicine and Health Sciences, Carl von Ossietzky University Oldenburg,
28 Oldenburg, Germany.

29 ¹²Department of Biomedical Sciences of Cells and Systems, University Medical Center
30 Groningen, University of Groningen, Antonius Deusinglaan, 1, 9713 AV Groningen, The
31 Netherlands.

32

33 # Present address: State Key Laboratory of Protein and Plant Gene Research, School of Life
34 Sciences and Peking-Tsinghua Center for Life Sciences, Peking University, Beijing 100871,
35 China.

36 ‡ Present address: Department of Chemical and Biological Engineering, Princeton University,
37 Princeton, NJ 08544, USA

38 § Present address: Boehringer Ingelheim International GmbH, 55216 Ingelheim, Germany and
39 ViraTherapeutics GmbH, 6063 Rum, Austria.

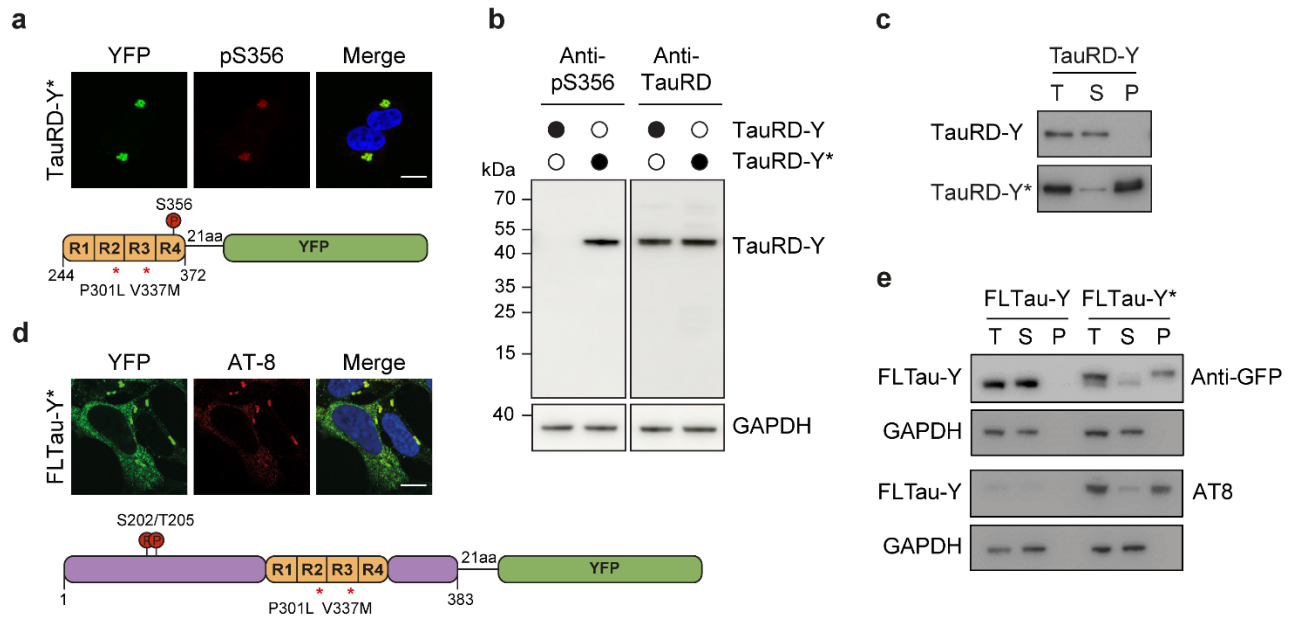
40

41 *Correspondence to uhartl@biochem.mpg.de and m.s.hipp@umcg.nl

42

43 Supplementary information includes 13 Supplementary Figures, Supplementary Table 1 and
44 uncropped scans of blots presented in supplementary figures.

45



46

47 **Supplementary Fig. 1: Tau aggregation in a constitutive expression model.**

48 **a** Immunofluorescence staining of TauRD-Y* cells with an antibody against Tau phosphorylation

49 at S356 (red) and YFP fluorescence of TauRD-Y (green). Scale bar, 10 μ m. **b** Analysis of Tau

50 S356 phosphorylation in lysates of TauRD-Y and TauRD-Y* cells by immunoblotting. Total

51 TauRD-Y was detected using antibody against TauRD. **c** Solubility of TauRD-Y in TauRD-Y and

52 TauRD-Y* cells at steady state, determined by fractionation of cell lysate by centrifugation,

53 followed by immunoblotting with anti-GFP antibody. T, total cell lysate, S, supernatant, P, pellet.

54 **d** Immunofluorescence staining of full-length Tau (FLTau-Y) in aggregate-containing FLTau-Y*

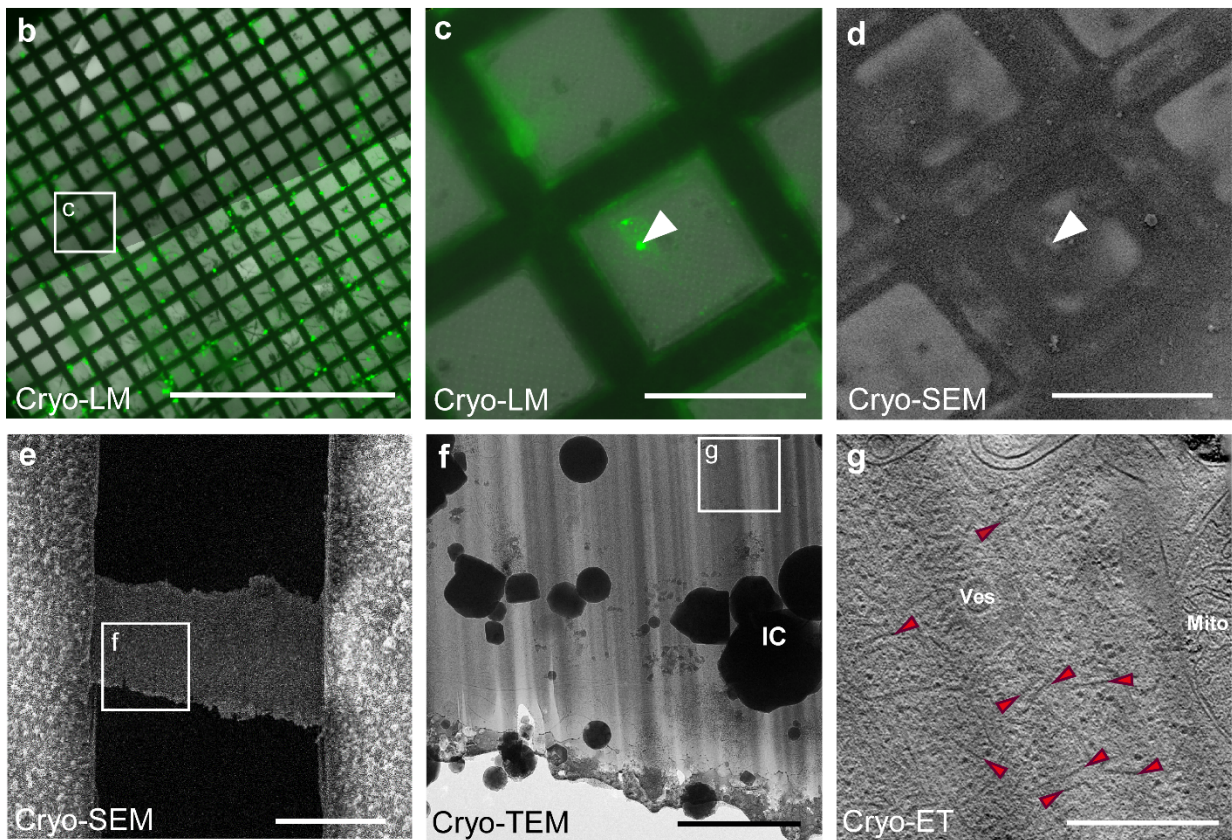
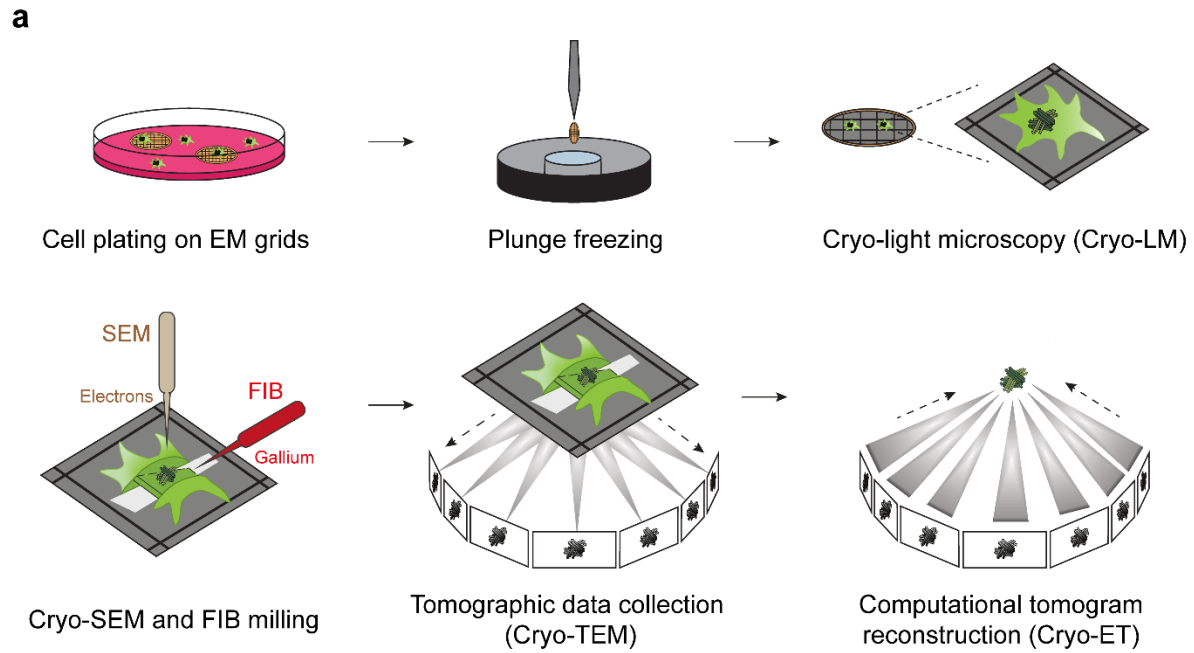
55 cells with AT-8 antibody specific for Tau phosphorylation at S202/T205 (red) and YFP

56 fluorescence of TauRD-Y (green). Scale bar, 10 μ m. **e** Solubility of phosphorylated FLTau-Y in

57 FLTau-Y and FLTau-Y* cells at steady state analyzed as in (c). Immunoblotting was with AT-8

58 antibody (bottom) and anti-GFP (top). GAPDH served as loading control.

59



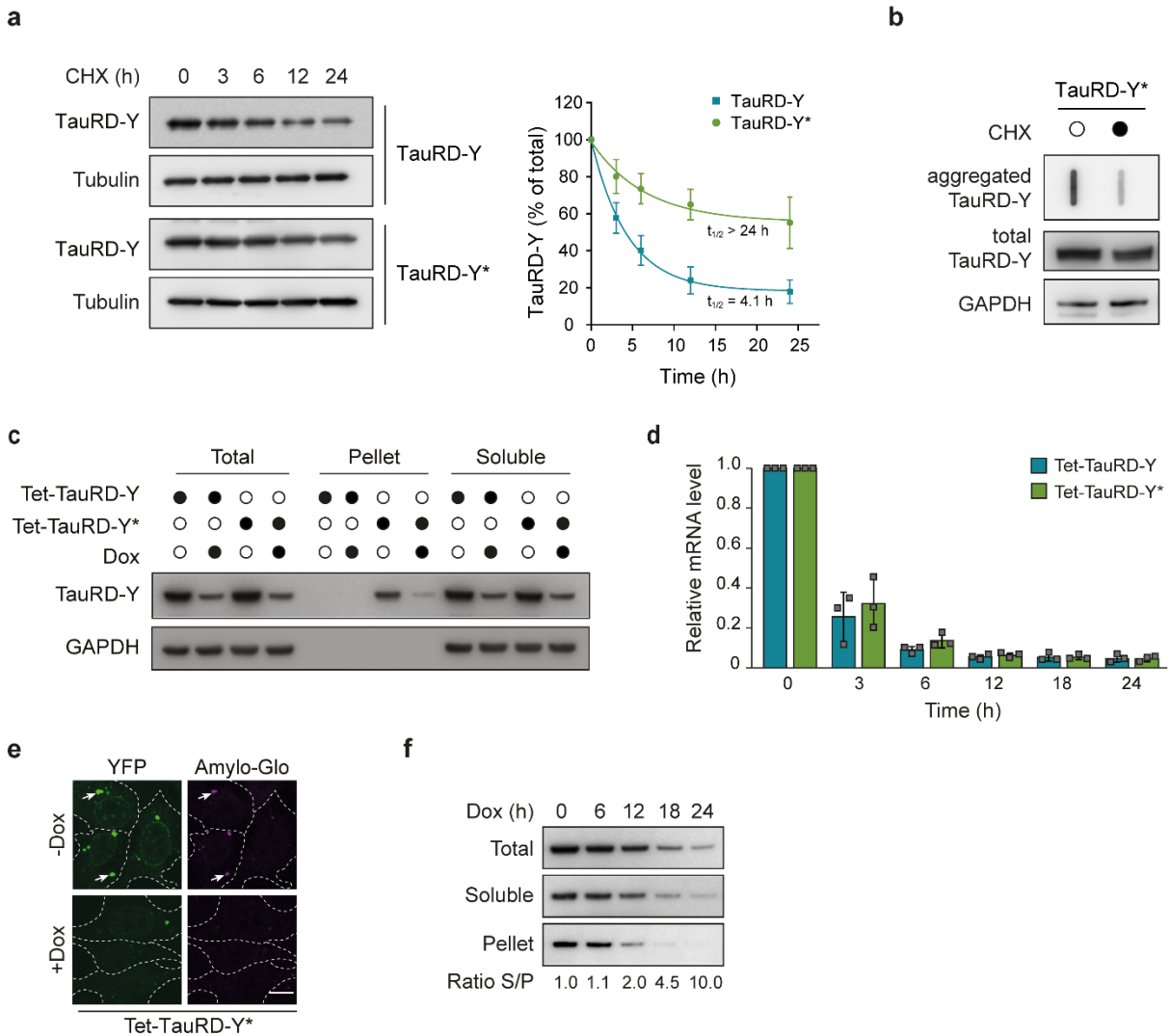
60

61 **Supplementary Fig. 2: Cryo-correlative-light-electron microscopy (cryo-CLEM) workflow.**

62 **a** Schematic representation of the cryo-CLEM workflow on cells containing TauRD-Y aggregates.

63 Cryo-LM (cryo-light microscopy), cryo-SEM (cryo-scanning electron microscopy), cryo-FIB

64 (focused ion beam), cryo-TEM (cryo-transmission electron microscopy), cryo-ET (cryo-electron
65 tomography). **b** Mouse primary neurons were cultured on EM grids for 10 days and transduced
66 with TauRD-Y followed by treatment with aggregate-containing cell lysates. 6 days after
67 transduction, grids were vitrified by plunge freezing. Thereafter, grids were imaged by cryo-light
68 microscopy (cryo-LM). An image of a grid with neurons containing aggregates is shown. Scale
69 bar, 1 mm. **c** Zoomed in cryo-LM image of the area marked in (b) by a white box. The arrowhead
70 indicates a neuronal TauRD-Y inclusion. Scale bar, 100 μm . **d** EM grids were transferred into the
71 cryo-FIB/SEM. Cryo-SEM image of the area shown in (c). The arrowhead indicates the same
72 location of the area shown in (c). Scale bar, 100 μm . **e** A \sim 200 nm thick lamella was generated at
73 that location by cryo-FIB milling. Scale bar, 10 μm . **f** Cryo-TEM overview of the lamella region
74 marked in (e). IC: Ice crystal. Scale bar, 2 μm . **g** 1.4 nm thick tomographic slice of a neuronal
75 TauRD-Y inclusion recorded in the area marked in (f). Red arrowheads indicate representative
76 TauRD-Y fibrils. Ves: Vesicle, Mito: Mitochondrion. Scale bar, 500 nm.



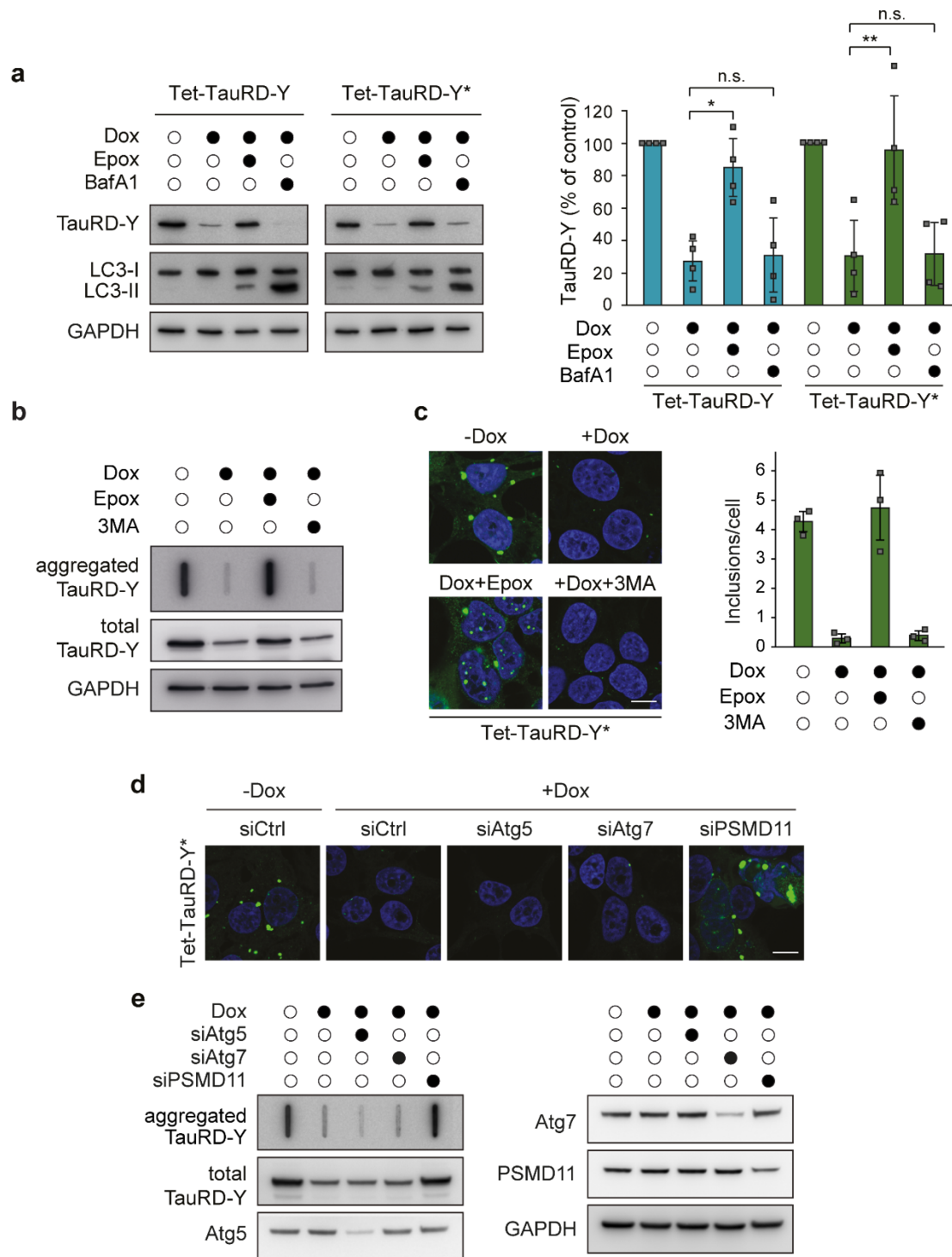
77

78 **Supplementary Fig. 3: TauRD-Y aggregation and clearance upon inhibition of expression in**
 79 **a constitutive and Tet-regulated TauRD-Y expression system.**

80 **a** Turnover of TauRD-Y in TauRD-Y and TauRD-Y* cells upon cycloheximide (CHX) shut-off
 81 (CHX; 50 μ g/mL). Left, anti-GFP immunoblots to determine TauRD-Y levels. Tubulin served as
 82 loading control. Right, exponential fits of CHX chase data and corresponding half-lives ($t_{1/2}$).
 83 Mean \pm s.d.; n=3. **b** Filter trap analysis of aggregated TauRD-Y upon CHX chase for 24 h.
 84 Aggregated and total TauRD-Y levels were determined by anti-GFP immunoblotting. GAPDH
 85 served as loading control. **c** Solubility of TauRD-Y in Tet-TauRD-Y and Tet-TauRD-Y* cells
 86 upon addition of 50 ng/mL doxycycline (Dox) for 24 h. Cell lysates were fractionated as in

87 Supplementary Fig. 1c. TauRD-Y was detected with anti-GFP antibody. GAPDH served as
88 loading control. **d** Quantitative PCR analysis of TauRD-Y mRNA in Tet-TauRD-Y and Tet-
89 TauRD-Y* cells treated with Dox for 0, 3, 6, 12, 18 and 24 h. mRNA levels were normalized to
90 the reference gene *RPS18*. Mean \pm s.d.; n=3. **e** Representative fluorescence images of Tet-TauRD-
91 Y* cells treated with Dox for 24 h showing staining of TauRD-Y inclusions (green) with Amylo-
92 Glo (magenta). White dashed lines indicate cell boundaries. Scale bar, 10 μ m. **f** Solubility of
93 TauRD-Y in Tet-TauRD-Y* cells upon addition of Dox for the indicated times. Normalized ratios
94 of TauRD-Y in soluble (S) and pellet (P) fractions are stated. Source data are provided as a Source
95 Data file.

96

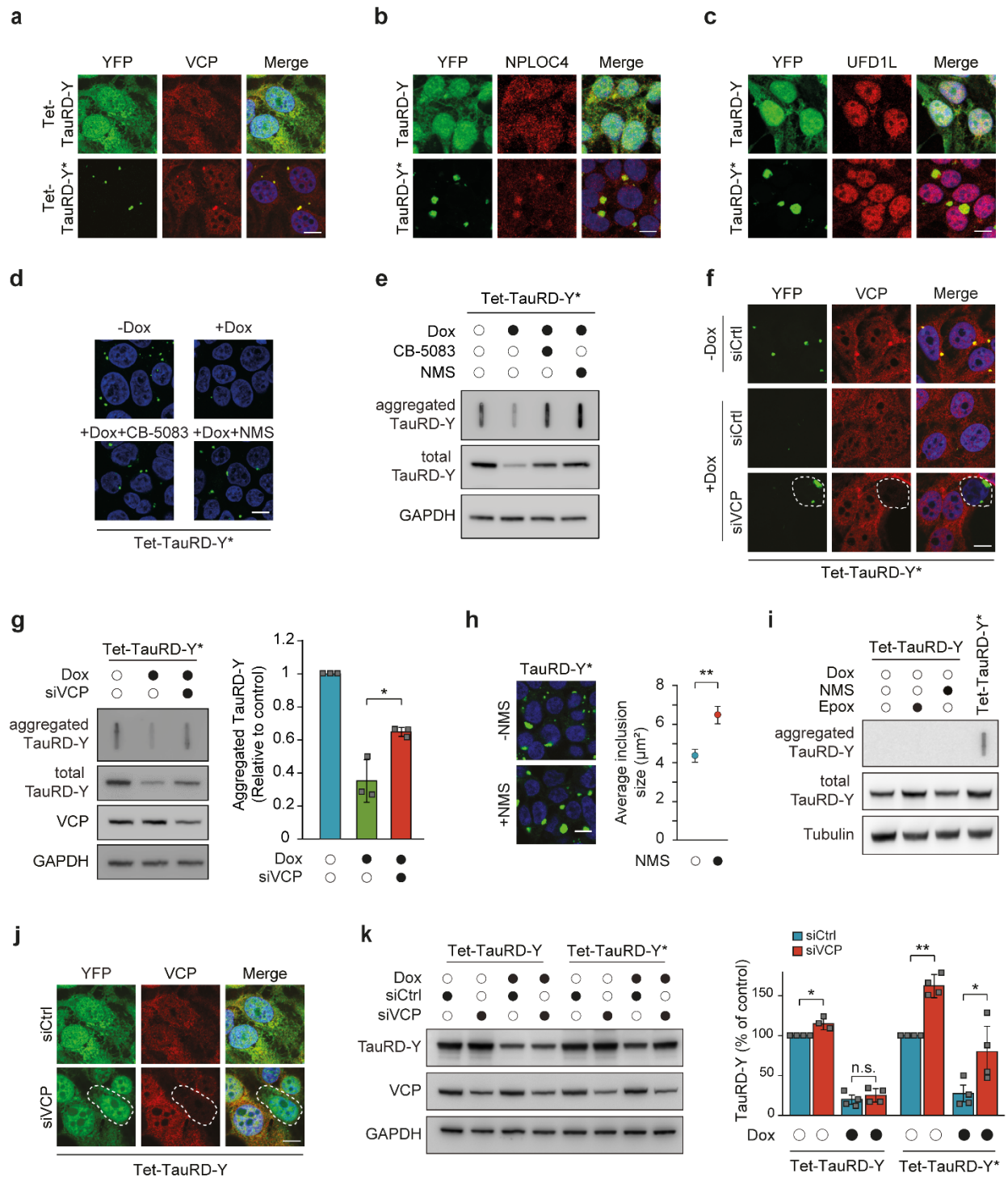


97

98 **Supplementary Fig. 4: Effect of UPS and autophagy inhibition on TauRD-Y levels and**
 99 **aggregate clearance.**

100 **a** Analysis of TauRD-Y levels in Tet-TauRD-Y and Tet-TauRD-Y* cells treated for 24 h with
 101 doxycycline (Dox; 50 ng/mL) alone or in combination with Epoxomicin (Epox; 50 nM) or

102 Bafilomycin A1 (BafA1; 50 nM). TauRD-Y and LC3 levels were determined by immunoblotting
103 against GFP and LC3B respectively. GAPDH served as loading control. Mean \pm s.d.; n=4. *p<0.05
104 (Tet-TauRD-Y: + Dox vs + Dox + Epox, p=0.0114), **p<0.01 (Tet-TauRD-Y*: + Dox vs + Dox
105 + Epox, p=0.0026); n.s. non-significant (Tet-TauRD-Y: + Dox vs + Dox + Epox, p= 0.6422; Tet-
106 TauRD-Y*: + Dox vs + Dox + Epox, p= 0.8799) from two-tailed Student's paired t-test. **b** Filter
107 trap analysis of Tet-TauRD-Y* cells treated for 24 h with Dox alone or in combination with
108 Epoxomicin (Epox; 50 nM) or 3-methyladenine (3MA; 5 mM). Aggregated and total TauRD-Y
109 was detected with anti-GFP antibody. **c** Left, representative images of Tet-TauRD-Y* cells treated
110 for 24 h with Dox alone or, in combination with Epoxomicin (Epox; 50 nM) or 3MA (5 mM).
111 Scale bar, 10 μ m. Right, quantification of TauRD-Y foci. 100-200 cells analyzed per experiment.
112 Mean \pm s.d.; n=3. **d** Representative images of Tet-TauRD-Y* cells transfected with non-targeted
113 (Ctrl) siRNA or siRNA against Atg5 (50 nM), Atg7 (50 nM) and PSMD11 (25 nM). 72 h after
114 transfection, doxycycline (Dox; 50 ng/mL) was added for another 24 h where indicated. Scale bar,
115 10 μ m. **e** Filter trap analysis of Tet-TauRD-Y* cells transfected with siRNAs and treated with Dox
116 as stated in (d). TauRD-Y was detected by immunoblotting with anti-GFP antibody. Source data
117 are provided as a Source Data file.



118

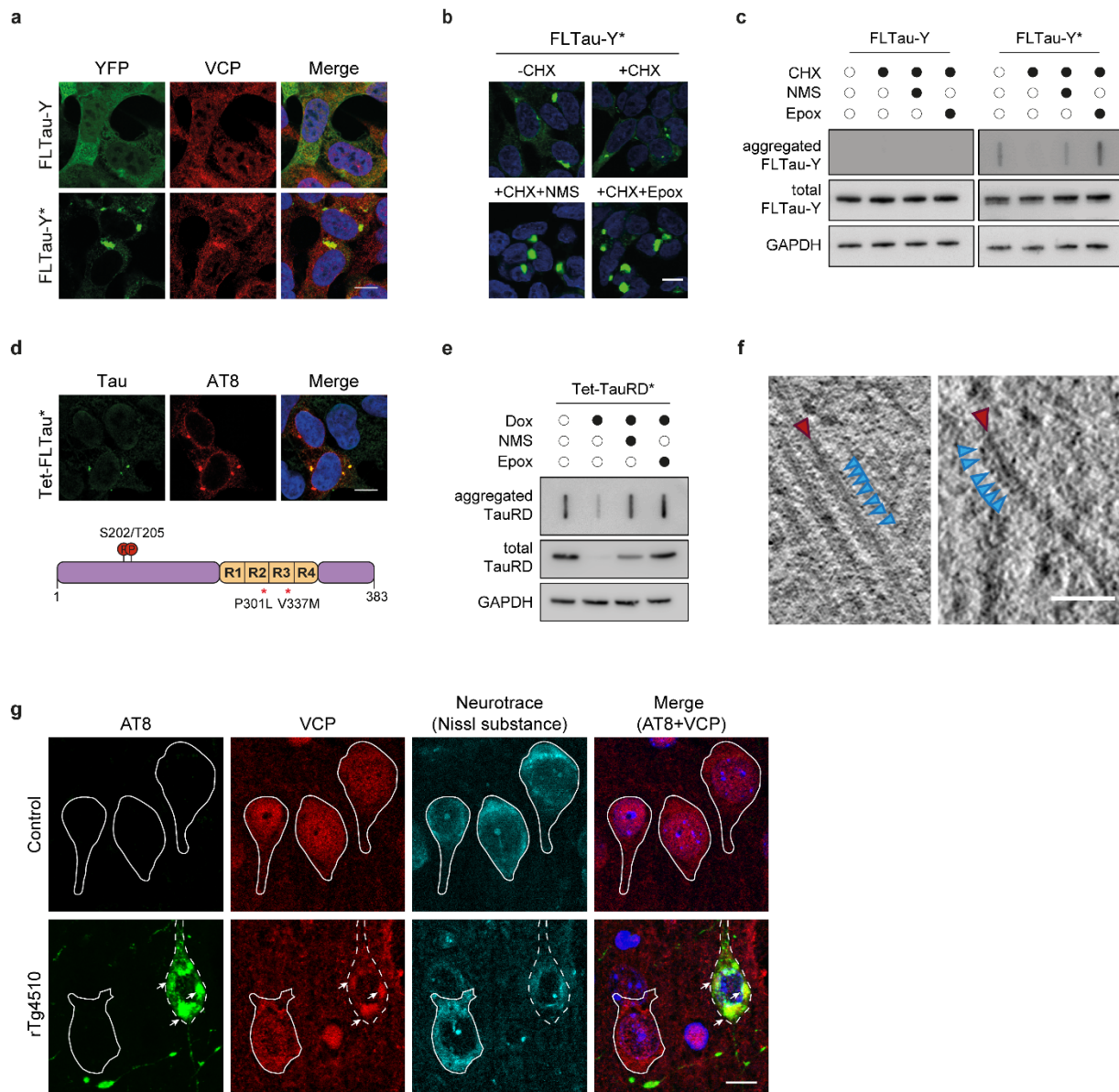
119 **Supplementary Fig. 5: Aggregation specific stabilization of Tau by VCP inactivation.**

120 **a** Immunofluorescence staining of VCP (red) and YFP fluorescence of TauRD-Y (green). **b** and **c**

121 Immunofluorescence staining of NPLOC4 (b) (red) and UFD1L (c) (red). Scale bars, 10 µm.

122 **d** Representative images of Tet-TauRD-Y* cells treated with doxycycline (Dox; 50 ng/mL) alone

123 or in combination with CB-5083 (1 μ M) or NMS-873 (NMS; 2.5 μ M). Scale bar, 10 μ m. **e** Filter
124 trap analysis of Tet-TauRD-Y* cells treated as in (d). **f** Immunofluorescence staining of VCP (red)
125 in Tet-TauRD-Y* cells treated with non-targeted (Ctrl) or VCP siRNA for 96 h. Doxycycline
126 (Dox; 50 ng/mL) was added for the last 24 h. Dashed lines indicate a cell with reduced VCP levels.
127 Scale bar, 10 μ m. **g** Left, filter trap analysis of aggregated TauRD-Y in Tet-TauRD-Y* lysates
128 treated as in (f). Right, quantification of aggregated TauRD-Y. Mean \pm s.d.; n=3. *p<0.05 (p=
129 0.0174) from two-tailed Student's paired t-test. **h** Representative images of TauRD-Y* cells
130 treated with NMS-873 (NMS; 5 μ M) and quantification of average inclusion size (μ m²). 200-400
131 cells analyzed per experiment. Mean \pm s.d.; n=5. **p<0.01 (p= 0.0022) from two-tailed Student's
132 paired t-test. **i** Filter trap analysis of Tet-TauRD-Y cells treated with Epoxomicin (Epox; 50 nM)
133 or NMS-873 (NMS; 2.5 μ M). Tet-TauRD-Y* lysate was used as control. **j** Immunofluorescence
134 staining of VCP (red) and YFP fluorescence of TauRD-Y (green) in Tet-TauRD-Y cells
135 transfected with non-targeted (Ctrl) or VCP siRNA. Dashed lines indicate a cell with reduced VCP
136 levels. Scale bar, 10 μ m. **k** Left, analysis of TauRD-Y level in Tet-TauRD-Y and Tet-TauRD-Y*
137 cells transfected for 96 h with non-targeted (Ctrl) or VCP siRNA. Doxycycline (Dox; 50 ng/mL)
138 was added for the last 24 h. TauRD-Y was detected with anti-TauRD antibody. Right,
139 quantification of TauRD-Y immunoblot. Mean \pm s.d.; n=4. *p<0.05 (Tet-TauRD-Y - Dox: siCtrl
140 vs siVCP, p= 0.0218; Tet-TauRD-Y* + Dox: siCtrl vs siVCP, p= 0.0156); **p<0.01 (Tet-TauRD-
141 Y* - Dox: siCtrl vs siVCP, p= 0.0023); n.s. non-significant (Tet-TauRD-Y + Dox: siCtrl vs siVCP,
142 p= 0.0539) from two-tailed paired Student's t-test. Source data are provided as a Source Data file.



143

144 **Supplementary Fig. 6: Role of VCP in full length Tau disaggregation.**

145 **a** Immunofluorescence staining of VCP (red) and YFP fluorescence of FLTau-Y (green) in FLTau-

146 Y and FLTau-Y* cells. Scale bar, 10 μ m. **b** Representative images of FLTau-Y* cells treated for

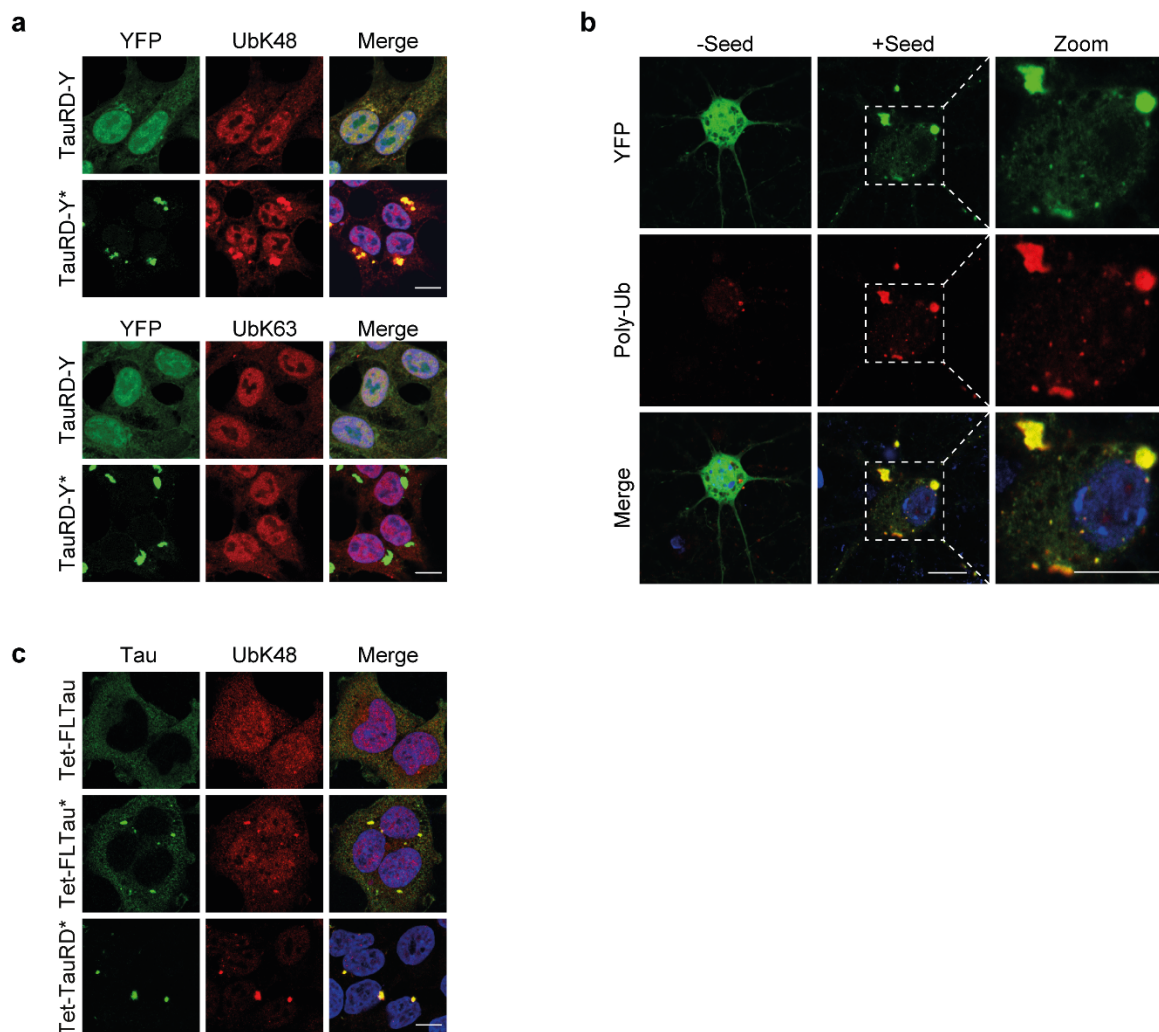
147 24 h with cycloheximide (CHX; 50 μ g/mL) alone or in combination with NMS-873 (NMS; 2.5

148 μ M) or Epoxomicin (Epox; 100 nM). Scale bar, 10 μ m. **c** Filter trap analysis of lysates from

149 FLTau-Y and FLTau-Y* cells treated for 24 h with Dox alone or in combination with NMS-873

150 (NMS; 2.5 μ M) or Epoxomicin (Epox; 50 nM). Aggregated and total FLTau-Y levels were

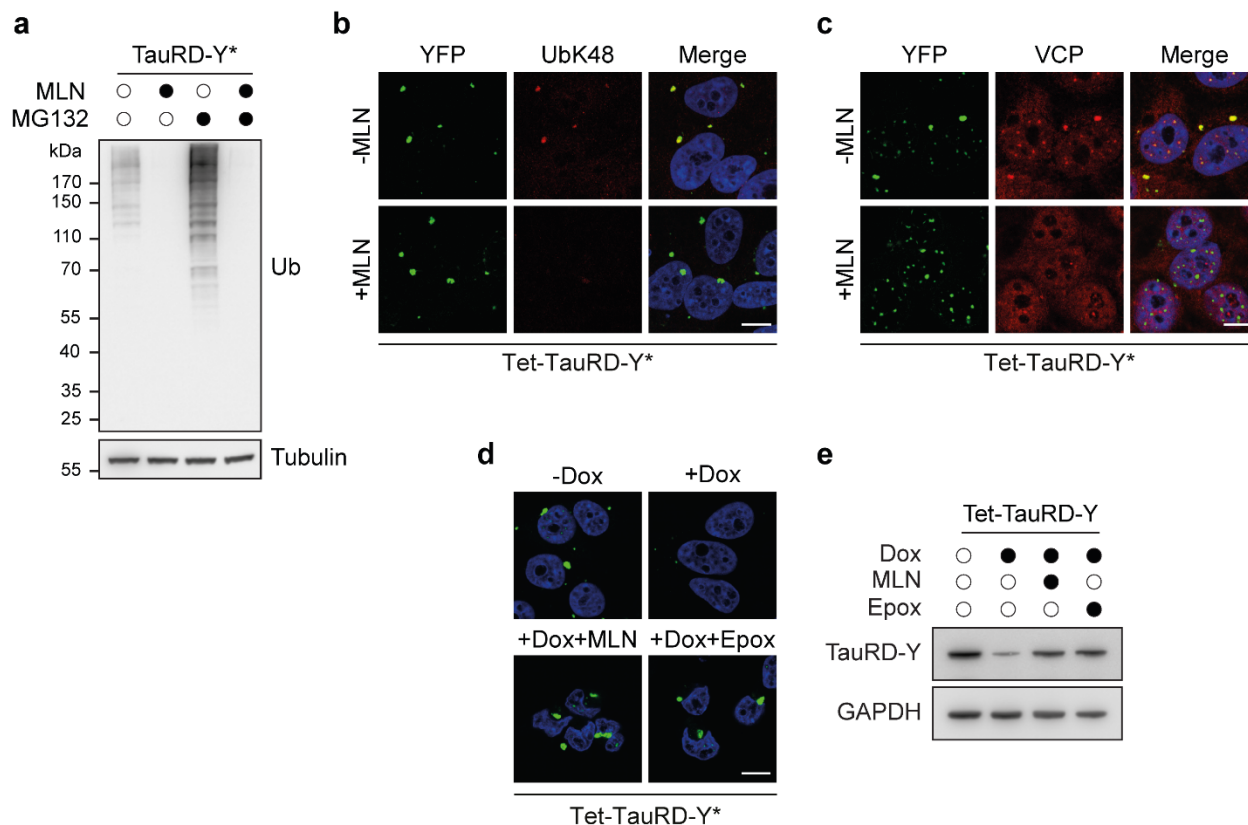
151 determined by immunoblotting against GFP. GAPDH served as loading control.
152 **d** Immunofluorescence staining of full-length Tau (FLTau) in aggregate-containing Tet-FLTau*
153 cells with Tau (green) and Tau S202/T205 phosphorylation specific AT-8 (red) antibody. Scale
154 bar, 10 μ m. **e** Filter trap analysis of lysates from Tet-TauRD* cells treated for 24 h with Dox alone
155 or in combination with NMS-873 (NMS; 2.5 μ M) or Epoxomicin (Epo; 50 nM). Aggregated and
156 total TauRD levels were determined by immunoblotting against myc and TauRD, respectively.
157 GAPDH served as loading control. **f** Examples of two TauRD-Y fibrils from a representative 1.4
158 nm thick tomographic slice of a TauRD inclusion from neurons. Red arrowheads indicate TauRD-
159 Y fibrils and blue arrowheads indicate globular densities along fibrils. Scale bar, 40 nm.
160 **g** Immunofluorescence staining of brain sections of 4-month-old control and Tau transgenic
161 rTg4510 mice with AT8 (green) and VCP (red) antibodies, Nissl substance (cyan) and DAPI (blue
162 in the merged image). The outline of a cell containing phosphorylated Tau (p-Tau) is marked by a
163 white dashed line. Cells not containing detectable p-Tau are marked by white continuous lines.
164 Arrows point to VCP colocalizing with Tau inclusions. Scale bar, 10 μ m.
165



166

167 **Supplementary Fig. 7: Ubiquitylation of TauRD-Y aggregates.**

168 **a** Immunofluorescence staining of (top) ubiquitin-K48 (UbK48) (red) and (bottom) ubiquitin K63
 169 (UbK63) (red) chains and YFP fluorescence of TauRD-Y (green) in TauRD-Y and TauRD-Y*
 170 cells. Scale bars, 10 μ m. **b** Immunofluorescence staining of ubiquitylated proteins (FK2 antibody)
 171 (red) in primary neurons expressing TauRD-Y (green) and treated with TauRD containing lysates
 172 (+Seed) where indicated. Scale bars, 20 μ m. **c** Immunofluorescence staining of ubiquitin-K48
 173 (UbK48) (red) chains and Tau (green) in Tet-FLTau, Tet-FLTau* and Tet-TauRD* cells. FLTau
 174 was detected using Tau-5 and TauRD using anti-myc antibody. Scale bar, 10 μ m.

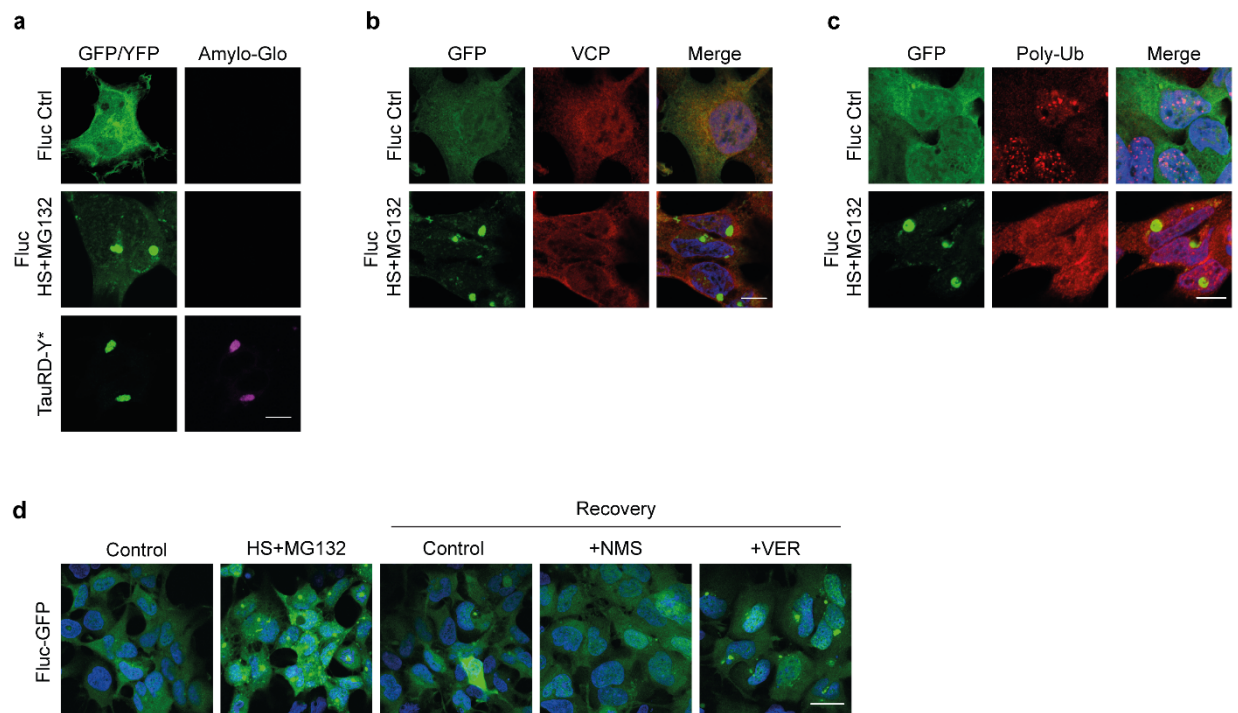


175

176 **Supplementary Fig. 8: Role of ubiquitylation in TauRD-Y disaggregation.**

177 **a** Analysis of ubiquitylated protein levels in lysates of TauRD-Y* cells treated with the ubiquitin
 178 activating enzyme E1 inhibitor MLN7243 (MLN; 0.5 μ M) alone or in combination with
 179 proteasome inhibitor MG132 (1 μ M) for 14 h. Ubiquitylated proteins were detected by
 180 immunoblotting against ubiquitin. Tubulin served as loading control. **b** Immunofluorescence
 181 staining of ubiquitin-K48 chains (UbK48) (red) and **c** VCP (red) in Tet-TauRD-Y* cells treated
 182 with MLN7243 (MLN; 0.5 μ M) for 12 h. Scale bars, 10 μ m. **d** Representative images of Tet-
 183 TauRD-Y* cells treated for 24 h with doxycycline (Dox; 50 ng/mL) alone or in combination with
 184 MLN7243 (MLN; 0.5 μ M) or Epoxomicin (Epox; 50 nM). Scale bar, 10 μ m. **e** Analysis of TauRD-
 185 Y levels in Tet-TauRD-Y cells treated for 24 h with Dox, MLN7243 and Epoxomicin as in (d).
 186 GAPDH served as loading control.

187

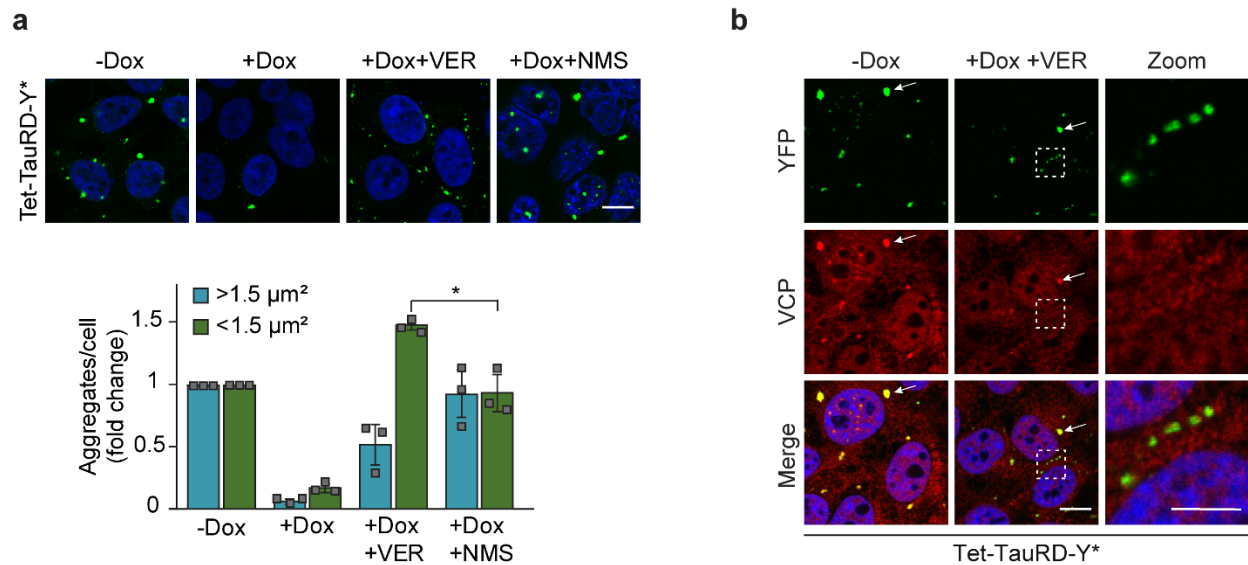


188

189 **Supplementary Fig. 9: Effect of VCP inhibition on firefly luciferase (Fluc) disaggregation.**

190 **a** Fluc-GFP expressing cells maintained at 37 °C (Fluc Ctrl) or heat-stressed at 43 °C in presence
 191 of 5 μM MG132 for 2 h (Fluc HS) were stained with the amyloid-specific dye Amylo-Glo
 192 (magenta). TauRD-Y* cells were used as control. Amylo-Glo fluorescence was imaged with
 193 similar exposure settings in all panels. Scale bar, 10 μm. **b** Immunofluorescence staining of VCP
 194 (red), and **c** ubiquitylated proteins (FK2 antibody) (red) in Fluc-GFP cells treated as in (a). Scale
 195 bars, 10 μm. **d** Effect of VCP and Hsp70 inhibition on Fluc-GFP disaggregation. Fluc-GFP
 196 aggregation was induced as in (a). Cells were then shifted to MG132 free media and allowed to
 197 recover at 37 °C for 8 h in presence of NMS-873 (NMS; 2.5 μM) and VER-155008 (VER; 10 μM)
 198 where indicated. Scale bar, 30 μm.

199



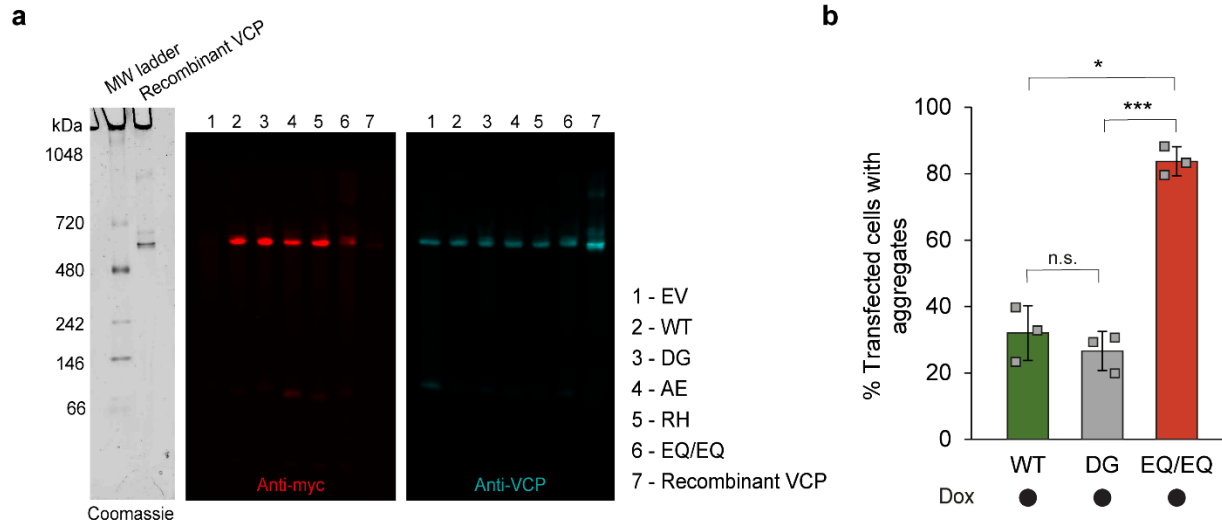
200

201 **Supplementary Fig. 10: Role of Hsp70 in TauRD-Y disaggregation.**

202 **a** Top, Representative images of Tet-TauRD-Y* cells treated for 24 h with doxycycline (Dox; 50
 203 ng/mL) alone or in combination with VER-155008 (VER; 10 μM) or NMS-873 (NMS; 2.5 μM).
 204 Bottom, quantification of large (>1.5 μm^2) and small (<1.5 μm^2) TauRD-Y foci. Mean \pm s.d.; n=3;
 205 ~100-200 cells were analyzed per experiment. *p<0.05 (p=0.0435) from two-tailed Student's
 206 paired t-test. Scale bar, 10 μm . **b** Immunofluorescence staining of VCP (red) and YFP fluorescence
 207 of TauRD-Y (green) in Tet-TauRD-Y* cells treated with a combination of doxycycline (Dox) and
 208 VER-155008 (VER) where indicated. White arrow points to large TauRD-Y inclusions co-
 209 localizing with VCP. Dashed lines enclose TauRD-Y foci that do not co-localize with VCP. Scale
 210 bar, 10 μm . Scale bar zoom, 5 μm . Source data are provided as a Source Data file.

211

212

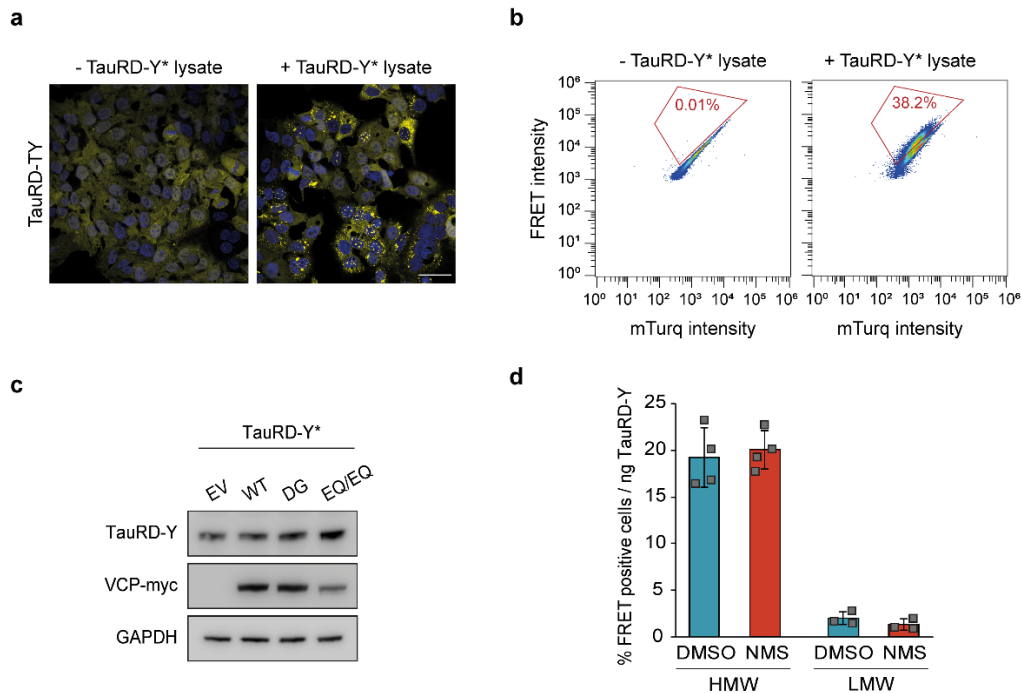


213
214
215

216 **Supplementary Fig. 11: Effect of VCP mutants on Tau disaggregation.**

217 **a** Native-PAGE analysis of recombinant VCP and lysates from Tet-TauRD-Y* cells transfected
218 with empty vector (EV) and myc-tagged wild type (WT), D395G (DG), A232E (AE), R155H (RH)
219 and E305Q/E578Q (EQ/EQ) VCP constructs. Immunoblot probed against myc (red) and VCP
220 (cyan) is shown. Non-tagged, recombinant VCP was analyzed as control. **b** Quantification of
221 aggregate foci in myc-positive Tet-TauRD-Y* cells transfected with myc-tagged WT, DG and
222 EQ/EQ VCP constructs for 24 h, and treated for another 24 h with doxycycline (Dox; 50 ng/mL).
223 Mean \pm s.d.; n=3; > 100 cells analyzed per experiment; *p<0.05 (WT vs EQ/EQ p=0.0192);
224 ***p<0.001 (DG vs EQ/EQ p=0.0008); n.s. non-significant (p=0.5646). Source data are provided
225 as a Source Data file.

226

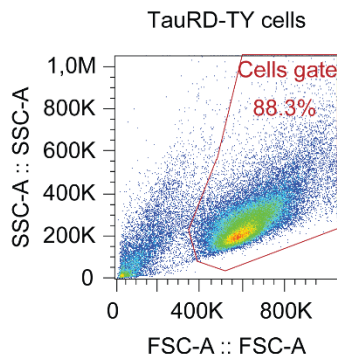


227

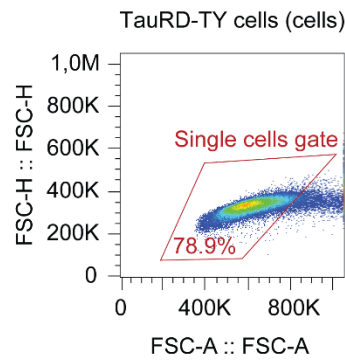
228 **Supplementary Fig. 12: Analysis of seeding-competent TauRD-Y.**

229 **a** Representative images of TauRD-TY FRET reporter cells treated with TauRD-Y* lysate where
 230 indicated showing TauRD-Y fluorescence in yellow. Scale bar, 40 μ m. **b** Representative
 231 pseudocolour dot plots for the analysis of FRET positive TauRD-TY cells by flow cytometry upon
 232 addition of TauRD-Y* lysate. FRET intensity is plotted against mTurquoise2 (mTurq) intensity
 233 and the % of FRET positive cells are indicated in red gates. **c** Analysis of TauRD-Y and VCP-myc
 234 levels in TauRD-Y* cells transfected for two days with empty vector (EV) and myc-tagged wild
 235 type (WT), D395G (DG) and E305Q/E578Q (EQ/EQ) VCP constructs. TauRD-Y and
 236 overexpressed VCP levels were determined by immunoblotting against GFP and myc,
 237 respectively. GAPDH served as loading control. **d** Comparison of seeding efficiencies of high
 238 molecular weight (HMW) and low molecular weight (LMW) species obtained by size exclusion
 239 chromatography of lysates from TauRD-Y* cells treated for 24 h with DMSO or NMS-873 (NMS;
 240 2 μ M). Mean \pm s.d.; HMW n=4, LMW n=3. Source data are provided as a Source Data file.

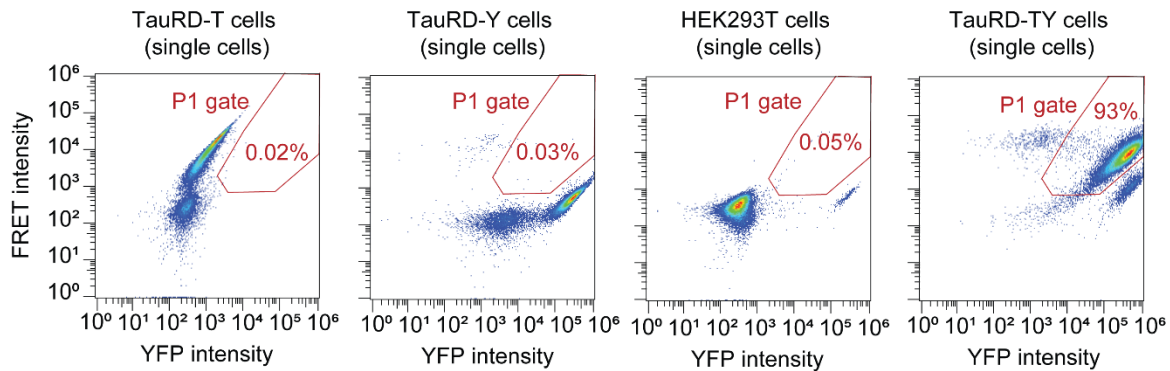
1. Selection of cells



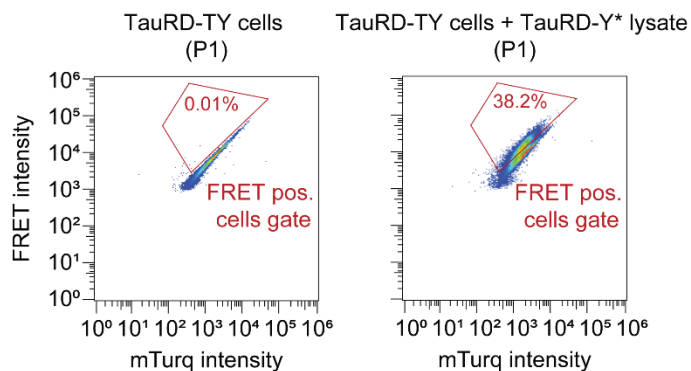
2. Selection of single cells



3. Exclusion of possible false positive FRET signal resulting from YFP excitation by the 405 nm laser (exclusion from P1 gate)¹



4. Selection of FRET positive cells from the P1 population using non-seeded cells as reference



241 **Supplementary Fig. 13: Flow cytometry strategy for quantification of FRET positive cells.**

242 To measure the mTurquoise2 and FRET fluorescence signals, cells were excited with 405 nm laser

243 light and fluorescence was determined using 440/50 and 530/30 filters, respectively. To measure

244 the YFP fluorescence signal, cells were excited at 488 nm and emission was recorded using a

245 530/30 filter. For each sample, 50,000 single cells were analyzed, using a gating strategy recently
246 described^{1,2}. First, cells were selected (1), followed by single cell selection (2). After gating single
247 cells, an additional gate (P1) was introduced to exclude YFP-only cells that show a false-positive
248 signal in the FRET channel due to excitation at 405 nm using TauRD-T cells, TauRD-Y cells and
249 HEK293T cells^{1,2} as reference (3). The FRET positive gate was set by plotting the FRET
250 fluorescence signal versus the mTurquoise2 fluorescence signal using non-seeded cells as
251 reference (4). Note that some panels in (1)-(3) were recently published describing the gating
252 strategy for a comparable experiment².

253

254 **Supplementary references**

- 255 1 Banning, C. *et al.* A flow cytometry-based FRET assay to identify and analyse protein-
256 protein interactions in living cells. *PLoS One* **5**, e9344 (2010).
- 257 2 Yuste-Checa, P. *et al.* The extracellular chaperone Clusterin enhances Tau aggregate
258 seeding in a cellular model. *Nature Communications* **12**, 4863 (2021).

259 **Supplementary Table 1. TauRD-Y interactome in TauRD-Y* cells**

260 List of proteins interacting with TauRD-Y in TauRD-Y* cells at steady state determined by stable isotope labelling by amino acids in cell
 261 culture (SILAC). TauRD-Y cells were used as control. Normalized SILAC ratios of TauRD-Y*/TauRD-Y [H/L] from 3 independent
 262 replicates are shown. Interactors were defined as proteins quantified in at least 2 out of 3 replicates with enrichment ≥ 2 fold. Proteins with
 263 known association to the ubiquitin-proteasome system are highlighted in green and VCP-cofactor complex in red. Intensity-based absolute
 264 quantification (iBAQ) values reflect measured molar protein amounts.

Protein ID	Protein name	Gene name	Fasta headers	Unique peptides	Mol. weight [kDa]	Norm. ratio [H/L] Rep.1	Norm. ratio [H/L] Rep.2	Norm. ratio [H/L] Rep.3	Median norm. ratio	iBAQ [H] Exp.1	iBAQ [H] Exp.2	iBAQ [H] Exp.3
Q9UNZ2;FZ	NSFL1 cofactor p47	NSFL1C	sp Q9UNZ2 NSF1C_HUMAN NSFL1 cofactor p47 OS=	14	40.572	42.702	80.022	11.719	42.702	59143000	112180000	13783000
Q9UQN3;AC	Charged multivesicular body protein 2b	CHMP2B	sp Q9UQN3 CHM2B_HUMAN Charged multivesicu	4	23.906	18.201	25.514	11.839	18.201	2093000	5417800	15472000
P55072;C9I2	Transitional endoplasmic reticulum ATPase	VCP	sp P55072 TERA_HUMAN Transitional endoplasmii	47	89.321	16.959	43.344	6.3181	16.959	29193000	94165000	26411000
Q9UNM6;J3	26S proteasome non-ATPase regulatory sub	PSMD13	sp Q9UNM6 PSD13_HUMAN 26S proteasome non-A	22	42.945	17.963	16.071	13.583	16.071	9313200	17290000	5085700
Q6PEV8	Protein FAM199X	FAM199X	sp Q6PEV8 F199X_HUMAN Protein FAM199X OS=H	5	42.801	41.449	15.154	15.115	15.154	9838300	30031000	10267000
F8VUA2;Q9	Charged multivesicular body protein 1a	CHMP1A	tr F8VUA2 F8VUA2_HUMAN Charged multivesicula	5	19.531	14.648	19.186	12.293	14.648	25912000	113020000	38592000
Q15773;F5H	Myeloid leukemia factor 2	MLF2	sp Q15773 MLF2_HUMAN Myeloid leukemia factor	6	28.147	16.867	13.819	6.564	13.819	74907000	153440000	42871000
O43242;H0Y	26S proteasome non-ATPase regulatory sub	PSMD3	sp O43242 PSMD3_HUMAN 26S proteasome non-A	34	60.977	13.413	15.879	6.9978	13.413	21734000	50167000	10257000
O00231;J3Q	26S proteasome non-ATPase regulatory sub	PSMD11	sp O00231 PSD11_HUMAN 26S proteasome non-A	26	47.463	13.086	22.385	7.5615	13.086	14133000	35102000	7362100
P62191;G3V	26S protease regulatory subunit 4	PSMC1	sp P62191 PRS4_HUMAN 26S proteasome regulat	20	49.184	12.739	13.685	6.7346	12.739	6082800	18968000	4723500
P17480	Nucleolar transcription factor 1	UBTF	sp P17480 UBF1_HUMAN Nucleolar transcription f	22	89.405	12.209	11.585	7.1602	11.585	94071000	144030000	43389000
O14545;F8V	TRAF-type zinc finger domain-containing pr	TRAFD1	sp O14545 TRAD1_HUMAN TRAF-type zinc finger c	12	64.84	7.2319	19.2	11.522	11.522	6914300	16022000	16301000
Q13501;E7E	Sequestosome-1	SQSTM1	sp Q13501 SQSTM1_HUMAN Sequestosome-1 OS=H	16	47.687	9.6152	22.927	11.41	11.41	27933000	113830000	115270000
Q13200;C9I	26S proteasome non-ATPase regulatory sub	PSMD2	sp Q13200 PSMD2_HUMAN 26S proteasome non-A	46	100.2	7.2067	11.267	11.267	11.267	4555900	9942100	6380700
H0Y6K2;A04	Bromodomain-containing protein 2	BRD2	tr H0Y6K2 H0Y6K2_HUMAN Bromodomain-contain	11	88.288	24.922	7.6855	10.958	10.958	6685300	16169000	6613700
H0YFD6;P4C	Trifunctional enzyme subunit alpha, mitoch	HADHA	tr H0YFD6 H0YFD6_HUMAN Trifunctional enzyme s	29	86.371	10.902	11.422	8.175	10.902	45516000	92103000	31426000
P55036;Q5V	26S proteasome non-ATPase regulatory sub	PSMD4	sp P55036 PSMD4_HUMAN 26S proteasome non-A	14	40.736	12.228	10.9	3.7986	10.9	19080000	82099000	8516700
Q6QNY1;J3K	Biogenesis of lysosome-related organelles	BLOC1S2	sp Q6QNY1 BL1S2_HUMAN Biogenesis of lysosom	3	15.961	10.78	15.848	2.0051	10.78	1892700	3652000	1718300
P55084;F5G	Trifunctional enzyme subunit beta, mitochc	HADHB	sp P55084 ECHB_HUMAN Trifunctional enzyme sul	25	51.294	9.9693	11.079	8.0079	9.9693	65103000	128900000	39724000
P25788;G3V	Proteasome subunit alpha type-3	PSMA3	sp P25788 PSA3_HUMAN Proteasome subunit alp	9	28.433	3.0605	14.754	9.9671	9.9671	2846500	1743900	2866700
A8MUA9;A6	Small ubiquitin-related modifier 4;Small ub	SUMO3;SUM	tr A8MUA9 A8MUA9_HUMAN SMT3 suppressor of	1	15.317	8.4377	11.126	9.78185	14432000	26087000	0	
Q8TAT6;J3L	Nuclear protein localization protein 4 homo	NPLOC4	sp Q8TAT6 NPL4_HUMAN Nuclear protein localiza	17	68.119	3.9291	15.451	9.69005	1208400	5604000	0	
P25789;H0Y	Proteasome subunit alpha type-4;Proteasor	PSMA4	sp P25789 PSA4_HUMAN Proteasome subunit alp	10	29.483	2.7706	16.307	9.5388	4339400	0	4387000	
Q9UHD9	Ubiquilin-2	UBQLN2	sp Q9UHD9 UBQL2_HUMAN Ubiquilin-2 OS=Homo	11	65.695	6.6843	11.794	9.23915	8201000	24600000	108990	
O14818;H0V	Proteasome subunit alpha type-7	PSMA7	sp O14818 PSA7_HUMAN Proteasome subunit alp	14	27.887	2.6045	9.1585	10.57	9.1585	3845500	10551000	10021000
Q9UID3;E9F	Vacuolar protein sorting-associated protein	VPS51	sp Q9UID3 VPS51_HUMAN Vacuolar protein sortin	11	86.041	12.8	5.2875	9.04375	603160	3513600	552200	
Q14596;B7Z	Next to BRCA1 gene 1 protein	NBR1	sp Q14596 NBR1_HUMAN Next to BRCA1 gene 1 pr	12	107.41	15.113	2.4528	8.7829	0	12693000	12934000	
Q92890;C9I	Ubiquitin fusion degradation protein 1 hom	UFD1L	sp Q92890 UFD1_HUMAN Ubiquitin recognition fa	9	34.5	11.411	6.134	8.7725	785590	5835400	721170	
Q15008;C9I	26S proteasome non-ATPase regulatory sub	PSMD6	sp Q15008 PSMD6_HUMAN 26S proteasome non-A	27	45.531	7.3639	9.6008	8.555	8.555	13494000	32338000	6986900

265
266

Continued on next page

Protein ID	Protein name	Gene name	Fasta headers	Unique peptides	Mol. weight [kDa]	Norm. ratio [H/L]	Rep.1	Norm. ratio [H/L]	Rep.2	Norm. ratio [H/L]	Rep.3	Median norm. ratio	iBAQ [H]	Exp.1	iBAQ [H]	Exp.2	iBAQ [H]	Exp.3
Q96DK7	Tripartite motif-containing protein 44	TRIM44	sp Q96DK7 TRIM44_HUMAN Tripartite motif-contain	5	38.472	10.369		6.5983				8.48365	708170	19187000	783500			
Q16643;D6f	Drebrin	DBN1	sp Q16643 DREB_HUMAN Drebrin OS=Homo sapie	16	71.428			13.93		2.7427		8.33635	123350	13631000	6342500			
A0A087X211	26S protease regulatory subunit 10B	PSMG6	tr A0A087X211 A0A087X211_HUMAN 26S proteaso	16	45.796	10.533		6.0398				8.2864	2266900	10434000	743130			
P51665;H3B	26S proteasome non-ATPase regulatory sub	PSMD7	sp P51665 PSMD7_HUMAN 26S proteasome non-A	14	37.025	8.2466		13.713		6.6956		8.2466	9133800	34517000	6064400			
P35998;A0A	26S protease regulatory subunit 7	PSMC2	sp P35998 PR57_HUMAN 26S proteasome regulat	24	48.633	7.5017		8.0742				8.5178	8531200	12549000	5021100			
B3KVL5;Q8I	Zinc finger CCHC domain-containing protein	ZCCHC10	tr B3KVL5 B3KVL5_HUMAN Zinc finger, CCHC domi	1	20.308			7.1775		8.4956		7.83655	18527000	60508000	11466000			
Q8IXW5	Putative RNA polymerase II subunit B1 CTD	RPAP2	sp Q8IXW5 RPAP2_HUMAN Putative RNA polymer	13	69.508	10.475		7.8181		3.3996		7.8181	1205400	8566200	4524400			
P62979;J3Q	Ubiquitin-40S ribosomal protein S27a;Ubiqu	RPS27A;UBB1	sp P62979 RS27A_HUMAN Ubiquitin-40S ribosoma	10	17.965	9.4683		7.6945		4.1911		7.6945	3164100000	7019100000	1951400000			
Q99460;A0A	26S proteasome non-ATPase regulatory sub	PSMD1	sp Q99460 PSMD1_HUMAN 26S proteasome non-A	42	105.84	6.684		7.415		7.8358		7.415	3058500	12531000	2851500			
P43686	26S protease regulatory subunit 6B	PSMC4	sp P43686 PR56B_HUMAN 26S proteasome regul	21	47.366	8.4576		2.5541		6.7907		6.7907	1137200	10458000	617140			
R4GMRS;K7	26S proteasome non-ATPase regulatory sub	PSMD8	tr R4GMRS R4GMRS_HUMAN 26S proteasome non	10	32.551	1.3779		6.6145		13.37		6.6145	491820	3751000	6211100			
POCAP2;H8	DNA-directed RNA polymerase II subunit Gf	POLR2M;GCC	sp POCAP2 GRL1A_HUMAN DNA-directed RNA pol	4	41.739	6.9552		6.1579				6.55655	2999600	6478700	0			
P49721;A0A	Proteasome subunit beta type-2	PSMB2	sp P49721 PSB2_HUMAN Proteasome subunit beta	10	22.836	2.6138		10.075				6.3444	526870	3115400	1949400			
Q9UQ35;J3L	Serine/arginine repetitive matrix protein 2	SRRM2	sp Q9UQ35 SRRM2_HUMAN Serine/arginine repet	44	299.61	8.8182		4.1061		6.3418		6.3418	40059000	69443000	34477000			
O75487	Glypican-4;Secreted glypican-4	GPC4	sp O75487 GPC4_HUMAN Glypican-4 OS=Homo sa	13	62.411	6.1176		9.697				6.1176	12306000	31449000	4359700			
Q9H307;G3P	Pinin	PNIN	sp Q9H307 PININ_HUMAN Pinin OS=Homo sapien	39	81.627	6.4613		5.9829				5.9829	180190000	359840000	205880000			
Q99615;K7E	DnaJ homolog subfamily C member 7	DNAJC7	sp Q99615 DNJC7_HUMAN DnaJ homolog subfami	35	56.44	32.017		5.9433				3.8506	58381000	56886000	13723000			
O95816	BAG family molecular chaperone regulator	BAG2	sp O95816 BAG2_HUMAN BAG family molecular ch	9	23.772	5.7371		8.5666				3.8905	5.7371	10758000	36658000	8833600		
Q9BYN8	28S ribosomal protein S26, mitochondrial	MRPS26	sp Q9BYN8 RT26_HUMAN 28S ribosomal protein S	7	24.211	5.6963		5.8954		3.1697		5.6963	51779000	55345000	11868000			
P10644;K7E	cAMP-dependent protein kinase type I- α	PRKAR1A	sp P10644 KAP0_HUMAN cAMP-dependent protei	12	42.981	5.6698		8.1797				5.6698	1804900	8873600	3456600			
A0A0C4DG6	ADP-ribosylation factor-like protein 6-inter	ARL6IP4	tr A0A0C4DG6 A0A0C4DG62_HUMAN ADP-ribosyl	5	24.591	6.5334		5.8168		2.4357		5.6534	11791000	37307000	7853000			
Q15545	Transcription initiation factor TFIID subunit	TAF7	sp Q15545 TAF7_HUMAN Transcription initiation f	5	40.259	6.7383		4.5475				5.6429	1917000	3824800	262590			
F5H442;Q9S	Tumor susceptibility gene 101 protein	TSG101	tr F5H442 F5H442_HUMAN Tumor susceptibility ge	8	40.917	6.9756		3.423				5.1993	1298100	2512100	0			
Q14677;H0N	Clathrin interactor 1	CUN11	sp Q14677 EPN4_HUMAN Clathrin interactor 1 OS=	17	68.259	4.5671		5.1051				4.8361	483270	1390800	0			
Q16531;F5C	DNA damage-binding protein 1	DDB1	sp Q16531 DDB1_HUMAN DNA damage-binding pr	51	126.97	5.1552		4.8124		4.7395		4.8124	2260500	20150000	818320			
Q14646;H0N	Chromodomain-helicase-DNA-binding protein	CHD1	sp Q14646 CHD1_HUMAN Chromodomain-helicasi	22	196.69	4.667		5.6909				4.667	1212300	6836700	855680			
G3V5Z7;P6G	Proteasome subunit alpha type;Proteasome	PSMA6	tr G3V5Z7 G3V5Z7_HUMAN Proteasome subunit a	12	28.147			5.4361		3.7845		4.6103	0	986560	3211200			
P17980;E9P	26S protease regulatory subunit 6A	PSMC3	sp P17980 PR56A_HUMAN 26S proteasome regula	21	49.203	5.2382		3.8803				4.55925	2297800	7983700	563940			
O00232;J3K	26S proteasome non-ATPase regulatory sub	PSMD12	sp O00232 PSD12_HUMAN 26S proteasome non-A	22	52.904	4.4642		2.2919		13.215		4.4642	5157500	5534500	3641700			
P61964;Y9C	WD repeat-containing protein 5	WDR5	sp P61964 WDR5_HUMAN WD repeat-containing p	5	36.588	2.7665		5.5202				4.14335	1116200	6218500	163100			
O00487;C9J	26S proteasome non-ATPase regulatory sub	PSMD14	sp O00487 PSDE_HUMAN 26S proteasome non-AT	10	34.577	4.4008		3.6454				4.0231	2763600	4175800	1273000			
P62195;J3Q	26S protease regulatory subunit 8	PSMC5	sp P62195 PR58_HUMAN 26S proteasome regulat	23	45.626	4.5333		4.0178		2.4837		4.0178	2401900	10162000	3258800			
P24928	DNA-directed RNA polymerase II subunit RF	POLR2A	sp P24928 RPB1_HUMAN DNA-directed RNA polyn	51	217.17	3.9675		4.1625		3.3865		3.9675	5036400	22719000	4400000			
O14974;F8V	Protein phosphatase 1 regulatory subunit 1	PPP1R12A	sp O14974 MYPT1_HUMAN Protein phosphatase 1	15	115.28	3.6323		4.1458				3.88905	135210	738040	0			
Q5VIR6;F6V	Vacuolar protein sorting-associated protein	VP53	sp Q5VIR6 VP53_HUMAN Vacuolar protein sortin	10	79.652			2.3872				5.2434	0	867750	158630			
Q8WV44;H	E3 ubiquitin-protein ligase TRIM41	TRIM41	sp Q8WV44 TRIM41_HUMAN E3 ubiquitin-protein li	5	71.669	4.3208		3.4885		3.7734		3.7734	613000	252640	1261800			
F8W118;F8V	59;B729C2;F8VRJ2	NAP1L1	tr F8W118 F8W118_HUMAN Nucleosome assembl	12	24.694	3.6447		4.8952		3.4073		3.6447	4807500	20158000	2227100			
E9PNW4;A	CD59 glycoprotein	CD59	tr E9PNW4 E9PNW4_HUMAN Uncharacterized pro	4	11.985			4.7462				2.1357	3.44095	5131200	54954000	35045000		
Q96BQ5	Coiled-coil domain-containing protein 127	CCDC127	sp Q96BQ5 CC127_HUMAN Coiled-coil domain-coi	4	30.834	4.0401						2.7807	3.4104	3768100	3178900	697410		
O43164	E3 ubiquitin-protein ligase Praja-2	PJA2	sp O43164 PJA2_HUMAN E3 ubiquitin-protein liga	15	78.213	3.3397		6.1296		2.2392		3.3397	4791500	29710000	8235700			
B8ZD4;Q8K	Tax1-binding protein 1	TAX1BP1	tr B8ZD4 B8ZD4_HUMAN Tax1-binding protein 1	14	93.609	9.5213		3.2831		3.1608		3.2831	409770	4896800	4112000			
P62857	40S ribosomal protein S28	RPS28	sp P62857 RS28_HUMAN 40S ribosomal protein S2	2	7.8409	3.7217		3.2677		1.1842		3.2677	18987000	32783000	6557100			
P62873;F6U	Guanine nucleotide-binding protein G(i)/G	(GNB1)	sp P62873 GBB1_HUMAN Guanine nucleotide-bind	13	37.377	3.2364		4.2746		1.6165		3.2364	2812200	17175000	35389000			
Q7L7X3;J3Q	Serine/threonine-protein kinase TAO1	TAOK1	sp Q7L7X3 TAOK1_HUMAN Serine/threonine-prot	15	116.07	1.3856		3.2072		3.0804		3.0804	2889600	6633200	6110200			
O75955;A0F	Flotillin-1	FLOT1	sp O75955 FLOT1_HUMAN Flotillin-1 OS=Homo sa	16	47.355	3.0802		3.6951		1.7534		3.0802	11366000	21730000	4780700			
Q12899;A2J	Tripartite motif-containing protein 26	TRIM26	sp Q12899 TRI26_HUMAN Tripartite motif-contain	7	62.165	4.126		2.001				3.0635	1519900	2525100	1427900			
O99986;H0N	Serine/threonine-protein kinase VRK1	VRK1	sp O99986 VRK1_HUMAN Serine/threonine-prot	14	45.476	3.4612		3.0568		1.1048		3.0568	2738700	26700000	18471000			
C9J2Y9;P30I	DNA-directed RNA polymerase;DNA-direct	POLR2B	tr C9J2Y9 C9J2Y9_HUMAN DNA-directed RNA poly	34	133.06	3.7497		3.0177		3.0513		3.0513	4282800	9848300	392790			
H3BV80;H3I	RNA-binding protein with serine-rich doma	RNPS1	tr H3BV80 H3BV80_HUMAN RNA-binding protein	6	24.561	3.0441		3.3076		2.5543		3.0441	139510000	204410000	94293000			
Q9UBI6	Guanine nucleotide-binding protein G(i)/G	(GNB12)	sp Q9UBI6 GBG12_HUMAN Guanine nucleotide-bi	3	8.0061	3.0438		4.9367		2.0117		3.0438	3890300	34430000	84342000			

267

268

Continued on next page

Protein ID	Protein name	Gene name	Fasta headers	Unique peptides	Mol. weight [kDa]	Norm. ratio [H/L]	Rep.1	Norm. ratio [H/L]	Rep.2	Norm. ratio [H/L]	Rep.3	Median norm. ratio	lBAQ [H] Exp.1	lBAQ [H] Exp.2	lBAQ [H] Exp.3	
I1E4Y6;QGY	PERQ amino acid-rich with GYF domain-cont	GIGYF2	tr I1E4Y6 I1E4Y6_HUMAN GRB10-interacting GYF pi	11	152.53	3.4506		2.6293				3.03995	571610	1017200	0	
P16403;P10	Histone H1.2;Histone H1.4	HIST1H1C;HIS	sp P16403 H12_HUMAN Histone H1.2 OS=Homo sa	12	21.364	3.0264		2.2983		3.593		3.0264	103310000	303900000	129810000	
P19387;H3B	DNA-directed RNA polymerase II subunit RF	POLR2C	sp P19387 RPB3_HUMAN DNA-directed RNA polyr	10	31.441	3.0233		3.8035		2.6379		3.0233	11207000	18173000	2879500	
Q5HYB6		DKFZp686J13	tr Q5HYB6 Q5HYB6_HUMAN Epididymis luminal pr	21	27.175	4.5555		2.9635		2.9779		2.9779	1471400	6297900	1443000	
P06748;E5R	Nucleophosmin	NPM1	sp P06748 NPM_HUMAN Nucleophosmin OS=Homo	17	32.575	3.5369		2.9192		1.7384		2.9192	45741000	124660000	102380000	
J3QLD9;E7E	Flotillin-2	FLOT2	tr J3QLD9 J3QLD9_HUMAN Flotillin-2 OS=Homo sa	15	47.142	2.9067		4.1686		1.6969		2.9067	8440000	26271000	11510000	
P62879;C9J	Guanine nucleotide-binding protein G(i)/G	GNB2	sp P62879 GBB2_HUMAN Guanine nucleotide-bin	12	37.331	2.9058		4.836		1.5201		2.9058	4881400	14551000	15388000	
Q53H12;E9F	Acylglycerol kinase, mitochondrial	AGK	sp Q53H12 AGK_HUMAN Acylglycerol kinase, mitc	18	47.137	1.1258		2.8627		4.0535		2.8627	4820100	15152000	13972000	
Q13112	Chromatin assembly factor 1 subunit B	CHAF1B	sp Q13112 CAF1B_HUMAN Chromatin assembly fa	4	61.492	2.844		2.8809				2.86245	512590	77757	0	
A0A087WV;DNA	directed RNA polymerases I, II, and III	POLR2E	tr A0A087WVZ9 A0A087WVZ9_HUMAN DNA-direc	7	21.459	3.1167		2.4935				2.8051	3322300	15849000	0	
Q92820	Gamma-glutamyl hydrolase	GGH	sp Q92820 GGH_HUMAN Gamma-glutamyl hydroly	8	35.964	2.8025		5.1253		2.0979		2.8025	2133200	7381800	1489700	
Q96GA3;A0	Protein LTV1 homolog	LTV1	sp Q96GA3 LTV1_HUMAN Protein LTV1 homolog C	15	54.854	1.3874		3.0356		2.7805		2.7805	11848000	15414000	11793000	
P60709;A0A	Actin, cytoplasmic 1;Actin, cytoplasmic 1, N-ACTB	ACTB	sp P60709 ACTB_HUMAN Actin, cytoplasmic 1 OS=	27	41.736	1.2178		3.5005		2.7751		2.7751	11323000	36019000	20782000	
Adde01;CON	_Q9U6Y5;I3L170		tr Adde01 TauYfp_HUMAN Tau Yfp	39	43.256	3.5063		2.7256				2.7256	4130100000	891400000	3833400000	
Q99613;B5A	Eukaryotic translation initiation factor 3 sub	EIF3C;EIF3CL	sp Q99613 EIF3C_HUMAN Eukaryotic translation ir	33	105.34	2.5577		2.8357				2.6967	855670	4670000	443520	
P28066	Proteasome subunit alpha type-5	PSMA5	sp P28066 PSA5_HUMAN Proteasome subunit alpi	13	26.411			3.108		2.254		2.681	713200	3627100	526020	
Q9HCM4	Band 4.1-like protein 5	EPB41L5	sp Q9HCM4 E41L5_HUMAN Band 4.1-like protein 5	9	81.855	2.1785		3.0182				2.59835	227100	3722200	0	
A0A087WVY	Slit homolog 2 protein;Slit homolog 2 prote	SLIT2	tr A0A087WVY5 A0A087WVY5_HUMAN Slit homol	9	159.98	2.0219		3.1071				2.5645	487410	1400300	599630	
A0A1W2PQ	DNA repair protein RAD50	RAD50	tr A0A1W2PQ90 A0A1W2PQ90_HUMAN Uncharact	25	142.94	2.5131		3.214		0.89296		2.5131	1024000	5250600	1514700	
Q9H0U4;E9I	Ras-related protein Rab-1B;Putative Ras-re	RAB1B;RAB1B	sp Q9H0U4 RAB1B_HUMAN Ras-related protein R	12	22.171			2.7446				2.1603	2.45245	682330	3902100	564680
Q13823;H0N	Nucleolar GTP-binding protein 2	GNL2	sp Q13823 NOG2_HUMAN Nucleolar GTP-binding	18	83.654	2.5228		2.3703				2.44655	504360	3938100	57885	
Q07021;I3L	Complement component 1 Q subcomponen	C1QBP	sp Q07021 C1QBP_HUMAN Complement compone	10	31.362	2.1285		5.1114		2.4395		2.4395	5133600	39902000	12700000	
Q72417	Nuclear fragile X mental retardation-interac	NUFIP2	sp Q72417 NUFP2_HUMAN Nuclear fragile X ment	15	76.12	2.9962		2.4364		2.0328		2.4364	5829600	7837800	5467700	
P08670;B0Y	Vimentin	VIM	sp P08670 VIME_HUMAN Vimentin OS=Homo sapi	45	55.651	2.4027		2.6728		1.6894		2.4027	59024000	131930000	146780000	
P19525;C9J	Interferon-induced, double-stranded RNA-;	EIF2AK2	sp P19525 E2AK2_HUMAN Interferon-induced, do	12	62.094	2.5648		2.384		2.0421		2.384	145870	749090	114650	
Q01082	Spectrin beta chain, non-erythrocytic 1	SPTBN1	sp Q01082 SPTB2_HUMAN Spectrin beta chain, no	120	274.61	2.354		5.0002		1.5658		2.354	14363000	46226000	27935000	
A0A0D95F54;A0A0D95F6;A0A0D95F6;A0A0D95F4;A0	SPTAN1		tr A0A0D95F54 A0A0D95F54_HUMAN Spectrin alpi	132	282.83	2.3502		5.0256		1.4746		2.3502	16833000	62862000	26440000	
P07948;E5R	Tyrosine-protein kinase Lyn	LYN	sp P07948 LYN_HUMAN Tyrosine-protein kinase L	12	58.573			2.3857		2.2951		2.3404	0	1032300	2217900	
Q9UN86;D6	Ras GTPase-activating protein-binding prote	G3BP2	sp Q9UN86 G3BP2_HUMAN Ras GTPase-activating	11	54.12	2.3338		1.3159		2.5495		2.3338	8272900	13070000	6033900	
P07900;G3V	Heat shock protein HSP 90-alpha	HSP90AA1	sp P07900 HS90A_HUMAN Heat shock protein HSP	63	84.659	2.277		4.0858		2.008		2.277	6729400	12647000	4596800	
P46013	Antigen Ki-67	MKI67	sp P46013 KI67_HUMAN Proliferation marker prot	17	358.69	2.3191		2.2468		2.2169		2.2468	524560	475360	44507	
P60228;E5R	Eukaryotic translation initiation factor 3 sub	EIF3E	sp P60228 EIF3E_HUMAN Eukaryotic translation in	25	52.22	2.3804		2.2127		1.9171		2.2127	1089300	1573400	1367200	
P49916;K7E	DNA ligase 3	LIG3	sp P49916 DNL3_HUMAN DNA ligase 3 OS=Homo	8	112.91	2.9178		2.203		2.1767		2.203	1532800	1039900	946440	
Q5RKV6	Exosome complex component MTR3	EXOSC6	sp Q5RKV6 EXOS6_HUMAN Exosome complex con	6	28.235	2.3573		2.1818		2.111		2.1818	11071000	15292000	4620400	
P12931	Proto-oncogene tyrosine-protein kinase Src	SRC	sp P12931 SRC_HUMAN Proto-oncogene tyrosine-	8	59.834	2.168		4.1415		1.8886		2.168	748320	2601200	1702500	
P63092;Q5J	Guanine nucleotide-binding protein G(s) su	GNA3	sp P63092 GNA32_HUMAN Guanine nucleotide-bi	13	45.664	2.1627		4.1417		1.5402		2.1627	1488700	9048500	3740200	
O75531;E9P	Barrier-to-autointegration factor;Barrier-to-	BANF1	sp O75531 BAF_HUMAN Barrier-to-autointegratio	6	10.058	2.1605		2.4895		1.4442		2.1605	167700000	464450000	175040000	
Q9Y265;E7E	RuvB-like 1	RUVBL1	sp Q9Y265 RUVB1_HUMAN RuvB-like 1 OS=Homo	24	50.227	1.8486		2.1597		2.5745		2.1597	2800700	6342500	382330	
O14578;H7E	Citron Rho-interacting kinase	CIT	sp O14578 CTRO_HUMAN Citron Rho-interacting k	11	231.43	3.1776		2.1397		0.96079		2.1397	57864	292140	49921	
P27986;H0Y	Phosphatidylinositol 3-kinase regulatory su	PIK3R1	sp P27986 P85A_HUMAN Phosphatidylinositol 3-k	6	83.597	1.5657		2.1169		2.5085		2.1169	745890	11166000	1210500	
Q6WCQ1;J3	Myosin phosphatase Rho-interacting protei	MPRIIP	sp Q6WCQ1 MPRIIP_HUMAN Myosin phosphatase	12	116.53	2.1049		2.173		0.79734		2.1049	588250	1624600	104110	
P08754	Guanine nucleotide-binding protein G(k) su	GNAI3	sp P08754 GNAI3_HUMAN Guanine nucleotide-bir	15	40.532	2.0157		4.9059		2.0813		2.0813	19273000	75469000	42160000	
O15234;J3K	Protein CASC3	CASC3	sp O15234 CASC3_HUMAN Protein CASC3 OS=Homo	8	76.277	2.067		2.0138		2.7423		2.067	698630	2073400	4126900	
P17987;E7E	T-complex protein 1 subunit alpha	TCP1	sp P17987 TCPA_HUMAN T-complex protein 1 sub	34	60.343	1.5294		2.2873		2.0582		2.0582	485300	1703400	621710	
Q5SRQ6;P6	Casein kinase II subunit beta	CSNK2B;CSN	tr Q5SRQ6 Q5SRQ6_HUMAN Casein kinase II subui	8	26.925	2.0436		2.4349		1.2233		2.0436	5899500	15187000	987590	
P08238;Q58	Heat shock protein HSP 90-beta	HSP90AB1	sp P08238 HS90B_HUMAN Heat shock protein HSP	64	83.263	1.9891		2.9912		2.02		2.02	7615400	29148000	15600000	
O95425;A04	Supervillin	SVIL	sp O95425 SVIL_HUMAN Supervillin OS=Homo sap	9	247.74	1.4281		3.0818		2.0134		2.0134	360680	1636100	213390	
Q14676;A2J	Mediator of DNA damage checkpoint protei	MDC1	sp Q14676 MDC1_HUMAN Mediator of DNA dama	20	226.66	2.1653		2.0075		1.5305		2.0075	303620	152960	60101	
Q14008;H0N	Cytoskeleton-associated protein 5	CKAP5	sp Q14008 CKAP5_HUMAN Cytoskeleton-associat	72	225.49	1.7242		2.0021		2.3599		2.0021	325010	2252600	1461800	

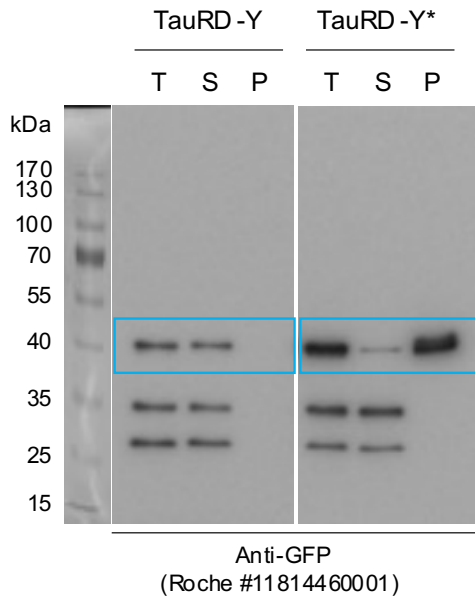
269

270

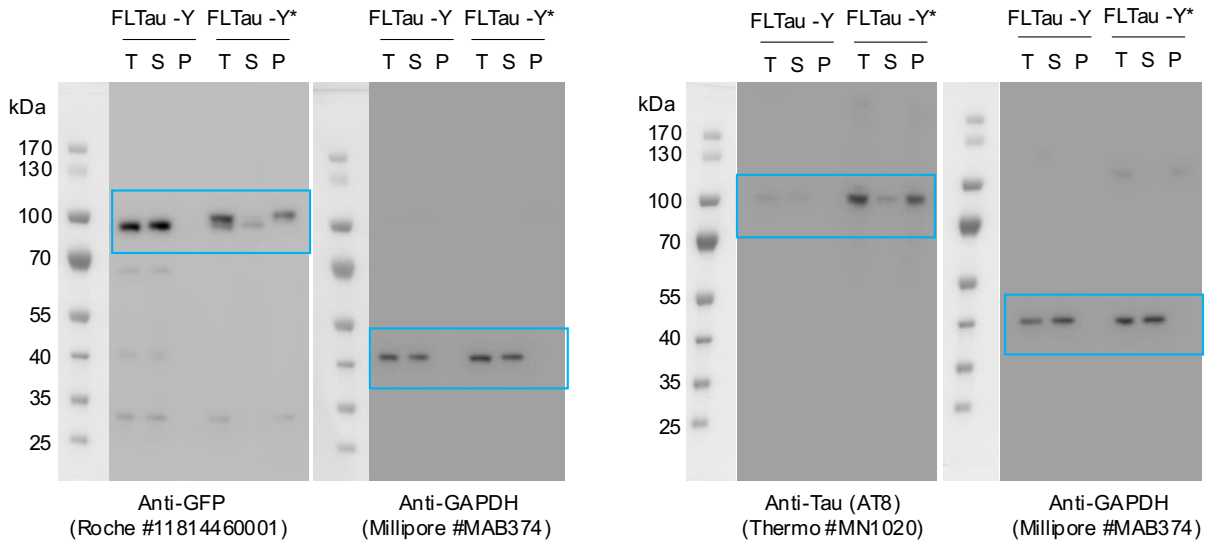
271 **Uncropped scans of blots**

272

Supplementary Fig. 1c

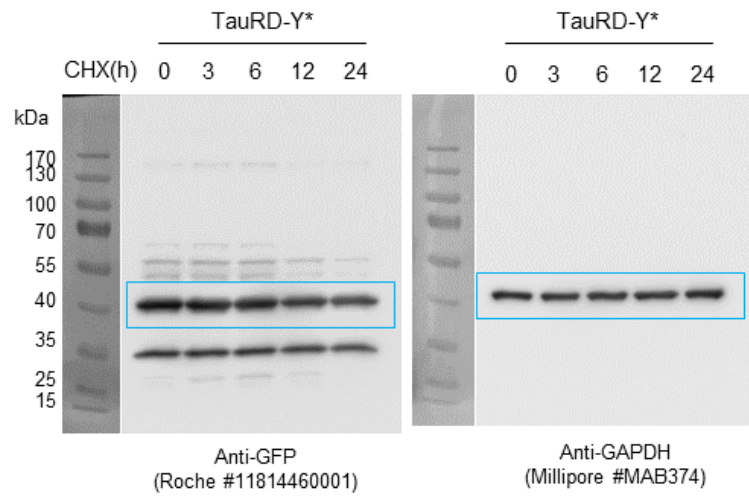
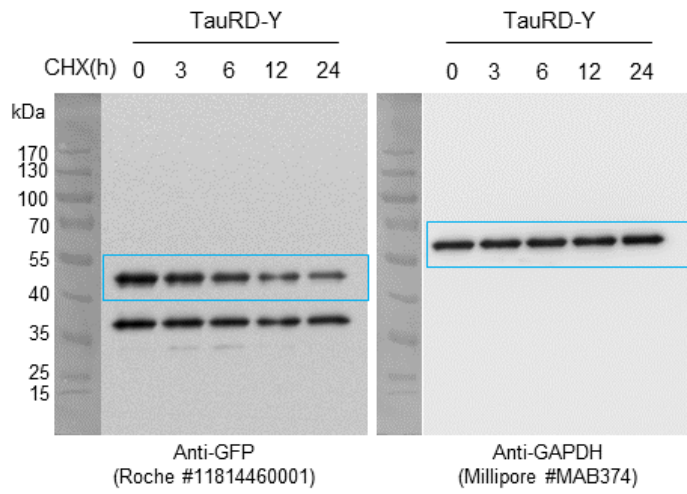


Supplementary Fig. 1e

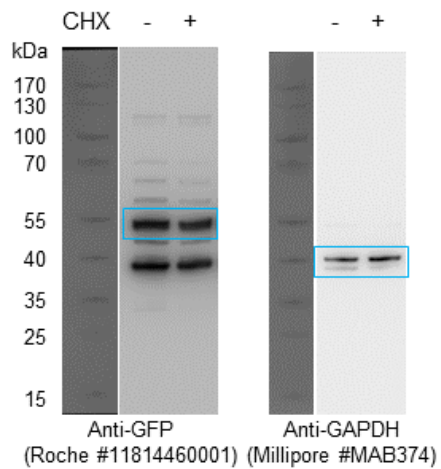


273

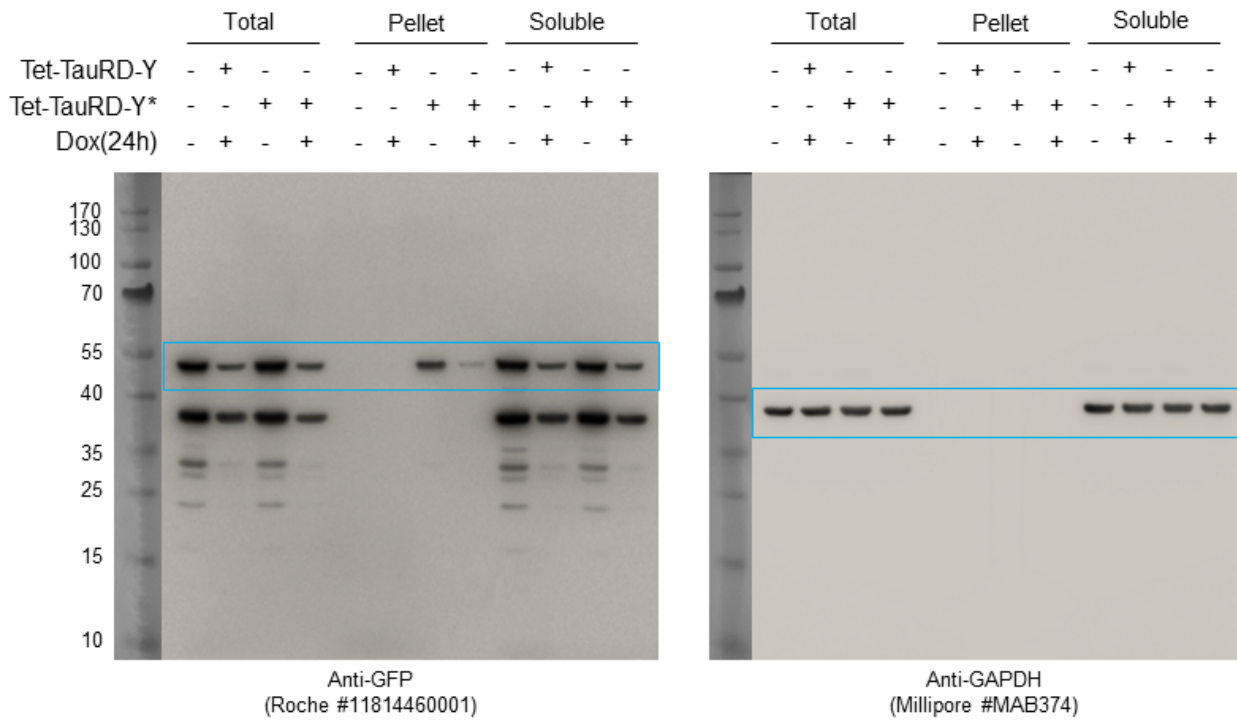
Supplementary Fig. 3a



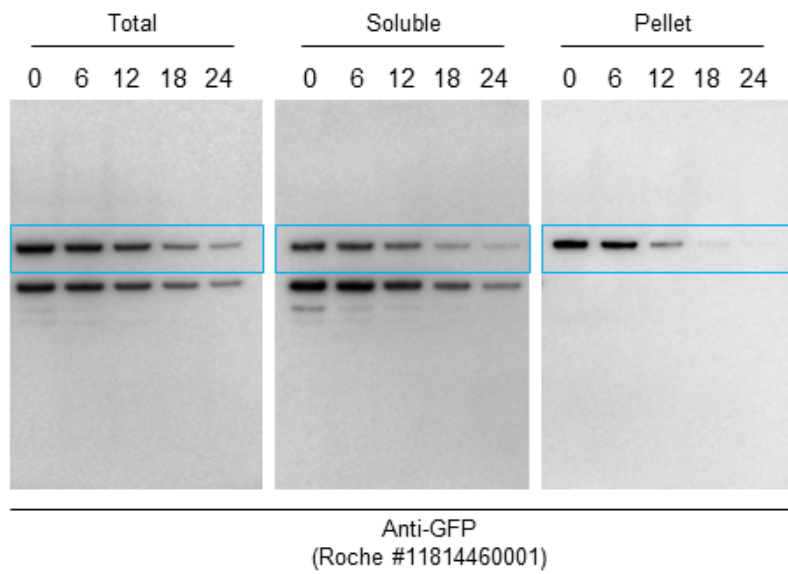
Supplementary Fig. 3b



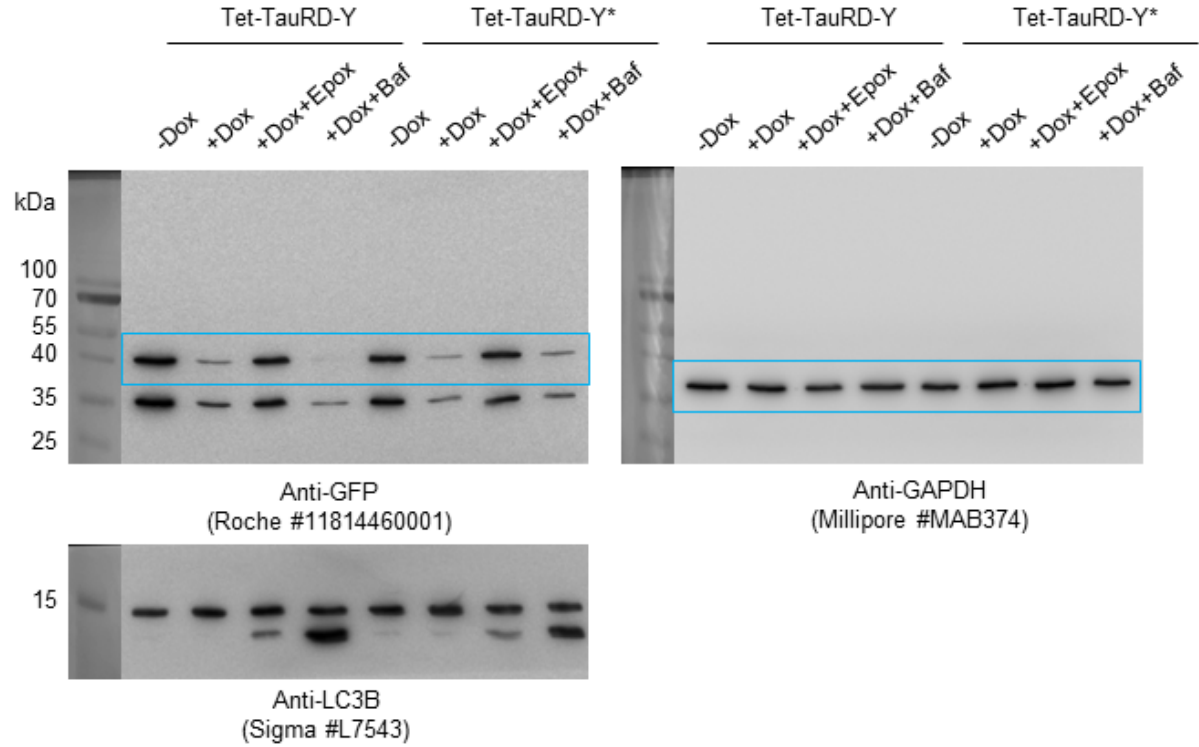
Supplementary Fig. 3c



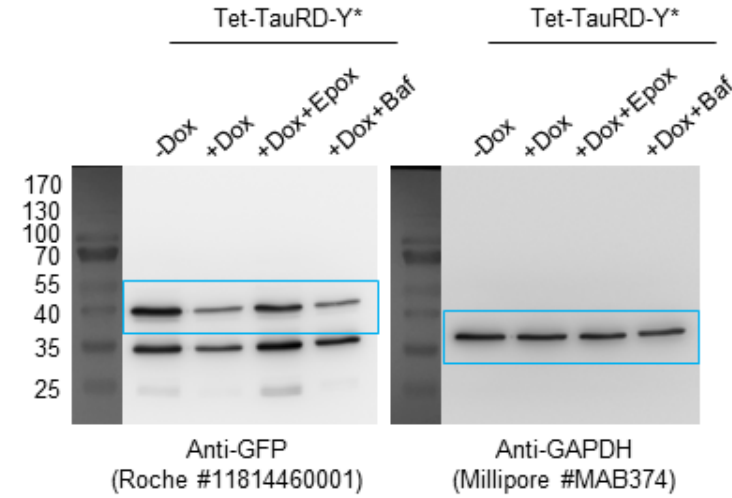
Supplementary Fig. 3c



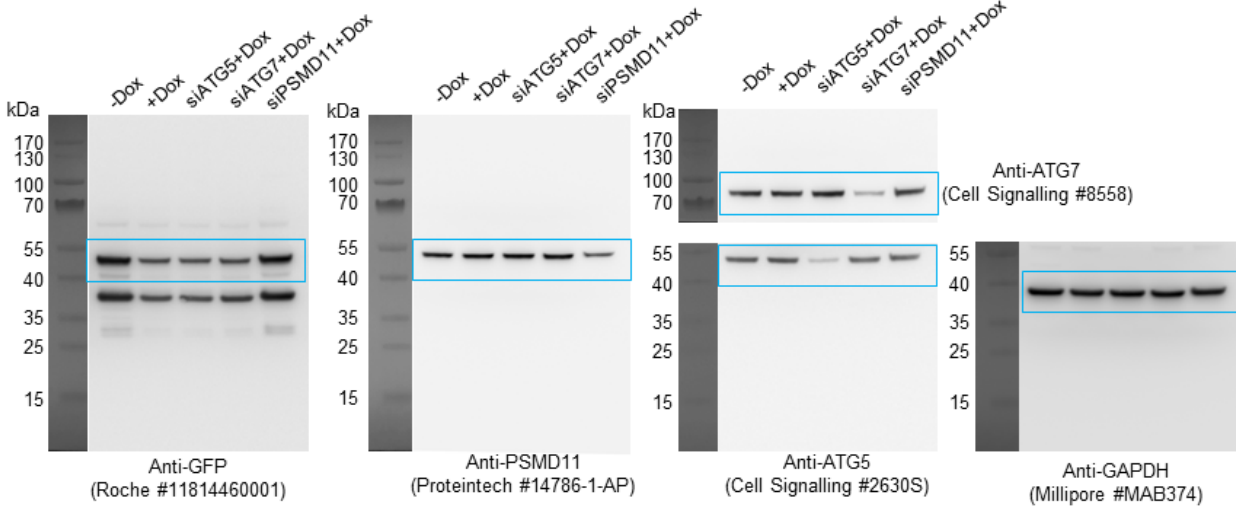
Supplementary Fig. 4a



Supplementary Fig. 4b

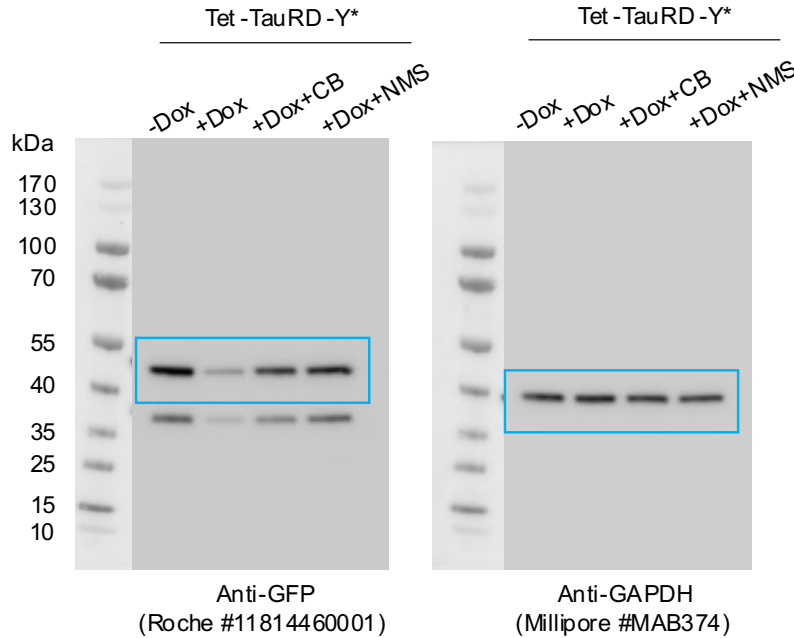


Supplementary Fig. 4e

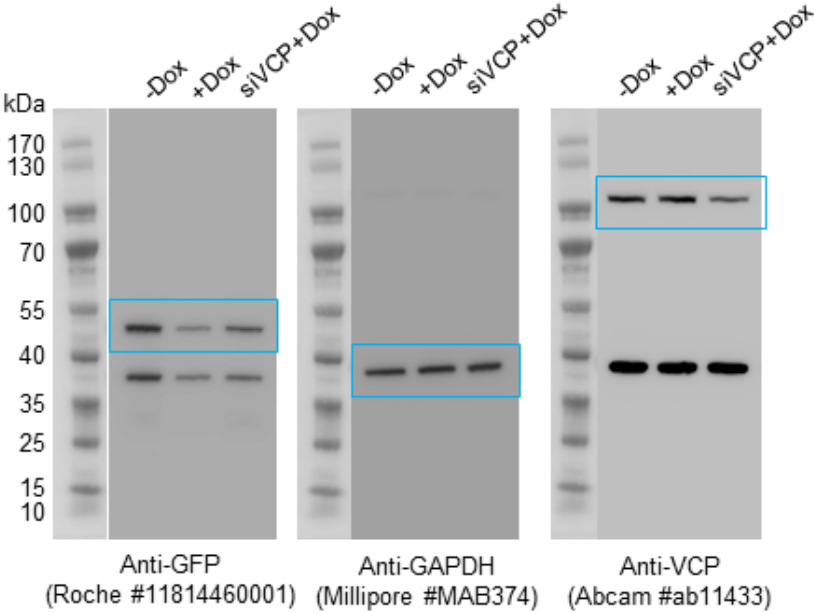


275
276

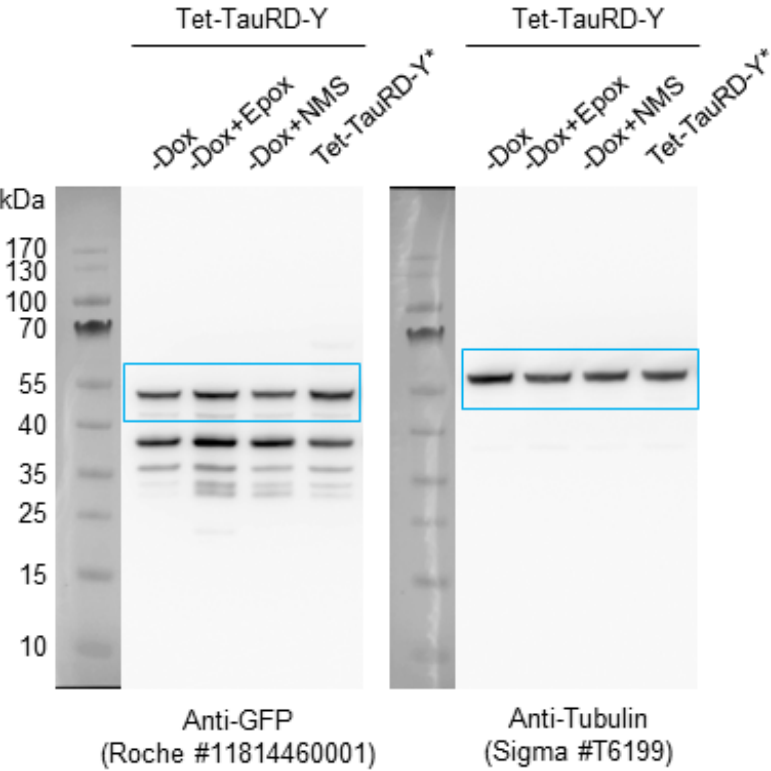
Supplementary Fig. 5e



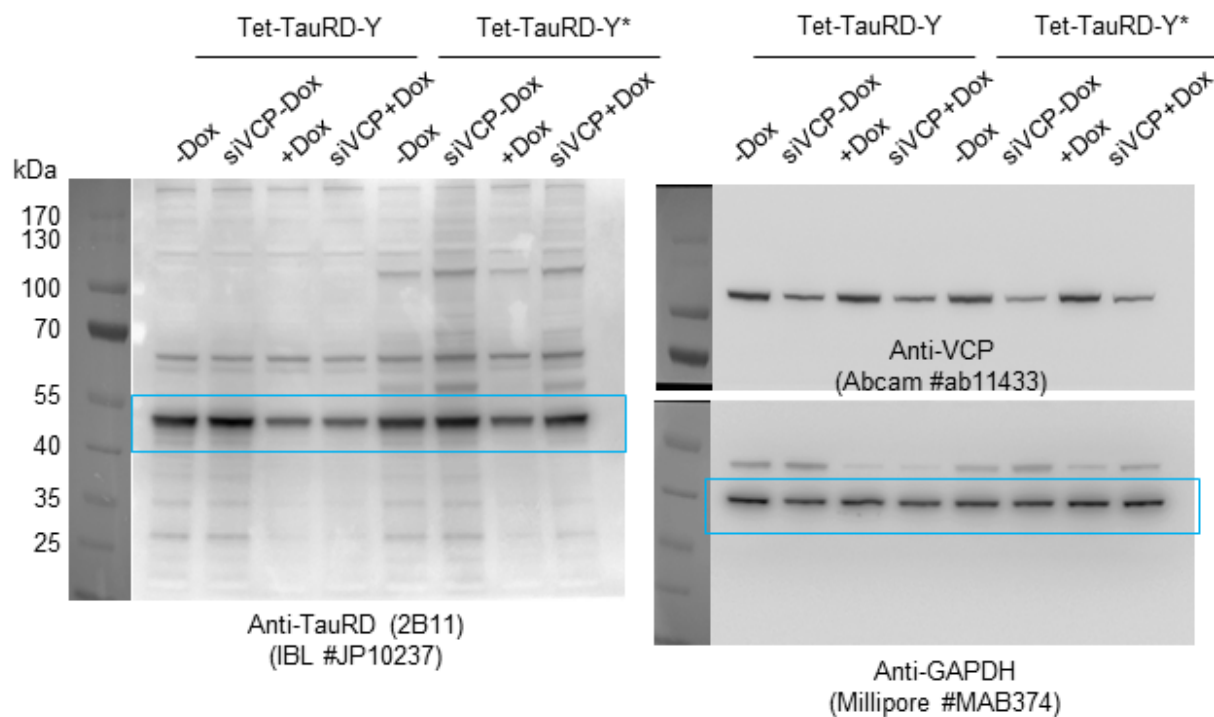
Supplementary Fig. 5g



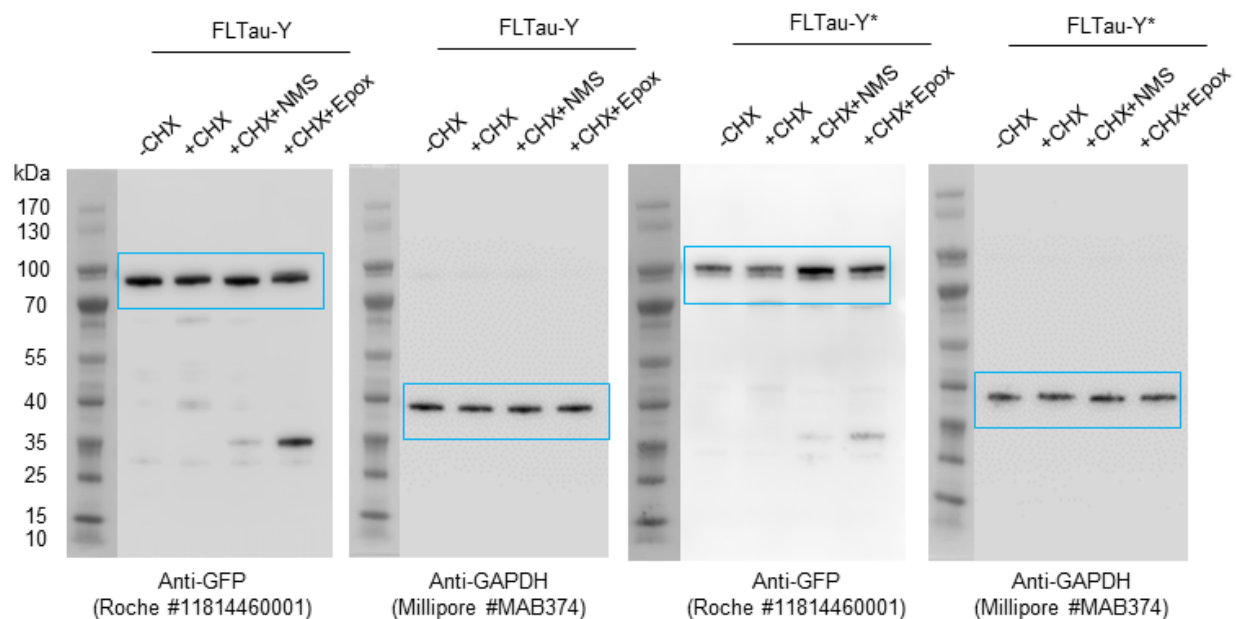
Supplementary Fig. 5i



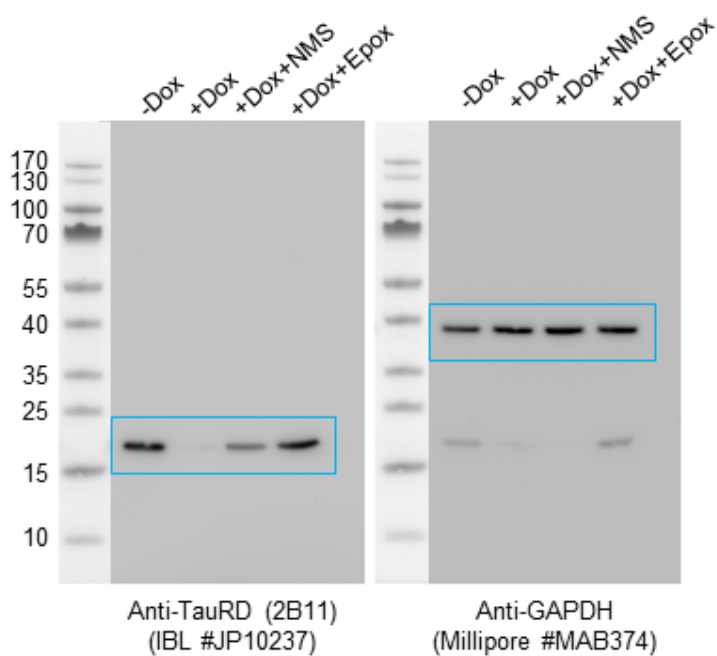
Supplementary Fig. 5k



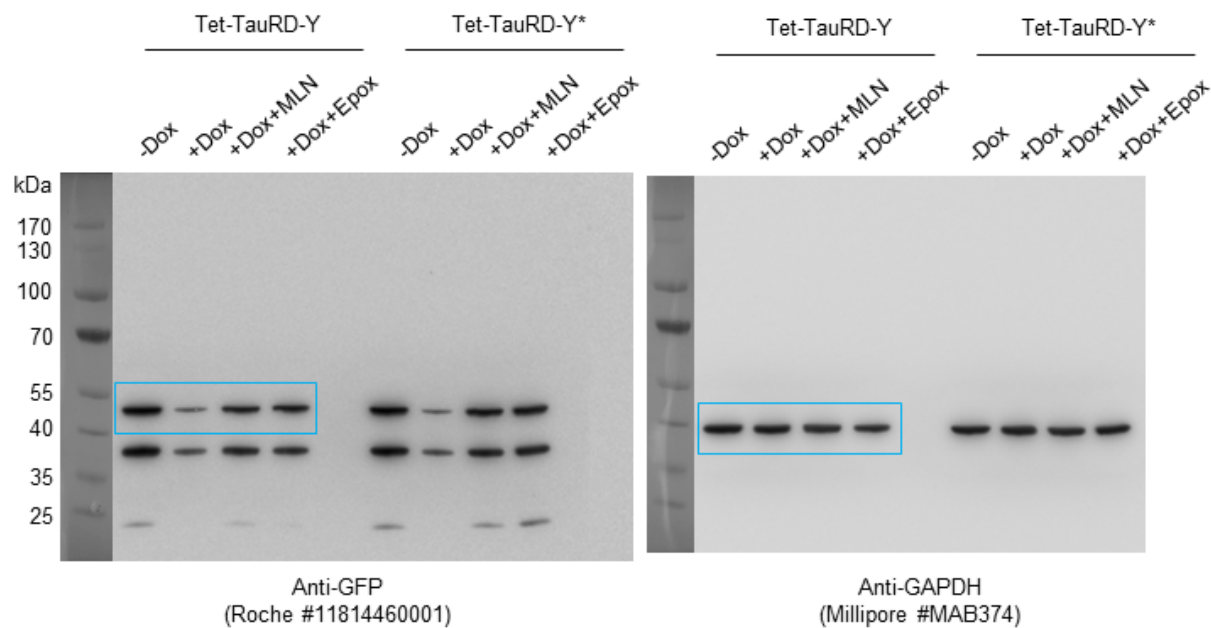
Supplementary Fig. 6c



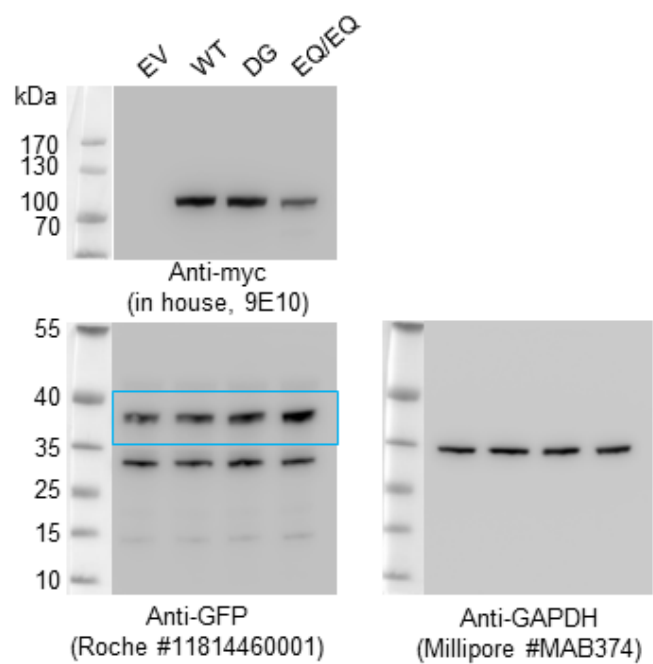
Supplementary Fig. 6e



Supplementary Fig. 8e



Supplementary Fig. 12c



277



Open Access This file is licensed under a Creative Commons Attribution 4.0 International License, which permits use, sharing, adaptation, distribution and reproduction in any medium or format, as long as you give appropriate credit to the original author(s) and the source, provide a link to the Creative Commons license, and indicate if changes were made. In the cases where the authors are anonymous, such as is the case for the reports of anonymous peer reviewers, author attribution should be to 'Anonymous Referee' followed by a clear attribution to the source work. The images or other third party material in this file are included in the article's Creative Commons license, unless indicated otherwise in a credit line to the material. If material is not included in the article's Creative Commons license and your intended use is not permitted by statutory regulation or exceeds the permitted use, you will need to obtain permission directly from the copyright holder. To view a copy of this license, visit <http://creativecommons.org/licenses/by/4.0/>.

REVIEWER COMMENTS

Reviewer #1 (Remarks to the Author):

In this manuscript, Saha et al. carry out experiments to demonstrate that the AAA+ chaperone VCP (p97) binds ubiquitylated Tau fibrils and disaggregates them. They demonstrate that inhibition of VCP activity stabilizes large Tau aggregates; however, this also results in the reduction in the amount of Tau species competent of prion like aggregate seeding in recipient cells. Therefore, the authors conclude that disaggregation by VCP generates seeding-active Tau as byproduct. Proper aggregate clearance requires the functions of Hsp70 and of the UPS system.

General impression

This is a very detailed study that presents a lot of data using multiple systems and multiple approaches to support the claims. However, it is mainly based on phenotypic observations. The authors have not done any of the needed in vitro experiments to show that isolated Tau fibrils can be disassembled by purified VCP. Furthermore, the role of Hsp70 is not well investigated and seems to be a side note in the manuscript.

Specific comments

1. The authors should quantify the inclusions/cell for Fig. 2d .
2. No filter-trap analysis done for CB-5083?
3. Filter-trap analysis of siVCP in Supplementary Fig. 4f are not very convincing, perhaps due to low efficiency of siRNA-mediated knockdown.
4. Line 171-172 vs line 203: Is the TauRD cell line tagged with myc or untagged? They are referred to differently in the two places indicated. If myc-tagged, naming conventions should be kept consistent, and should be renamed TauRD-M instead.
5. Claims of EQ/EQ mutants effects on TauRD-Y aggregates from lines 261-264 is not backed by actual data.
6. Is there a reason that the AE and RH mutants are not analyzed for whether they stabilize aggregates as the DG and EQ/EQ mutants in Fig. 5d? AE seems to colocalize nicely with aggregates in Fig. 5b.

Reviewer #2 (Remarks to the Author):

Thank you for writing a very comprehensive paper

A few general comments:
Lovely microscopy images!

Perhaps add into the title: "The AAA+ chaperone VCP disaggregates Tau fibrils and generates aggregate seeds " that this was a laboratory model

Please write out all abbreviations in the abstract for general readers who are not familiar with the

specific field: eg. valosin-containing protein (VCP)

In the abstract you state:

These findings identify VCP as a core component of the machinery for the removal of neurodegenerative disease aggregates and suggest that its activity can be associated with enhanced aggregate spreading in tauopathies.

Please add to your discussion how you relate your findings in the lab to what happens during neuro-inflammation in AD. Perhaps a figure could be added to the explanation.

VCP-mediated aggregate disassembly followed by proteasomal degradation provides an important alternative to autophagy as a mechanism for the elimination of terminally aggregated proteins.

Please add a diagram to explain autophagy and compare it to your VCP-mediated pathways and findings.

Please relate your findings directly to clinical application in AD. How do you foresee this research may impact clinical interventions?

Please elaborate or discuss in the conclusion if this work could be translated to other neuro-inflammatory diseases too? Parkinson's Disease?

Reviewer #3 (Remarks to the Author):

Saha et al. reported VCP disaggregates tau fibrils, however, it generates seeding-active tau as byproduct at the same time. These results suggest that VCP may have both neuroprotective and neurotoxic effects, although VCP mutations have been associated with aggregate deposition disorders such as vacuolar tauopathy and IBMPFD. Boosting cellular aggregate clearance, perhaps in combination with proteasome activation, may offer a potential therapeutic strategy as long as the production of seeding competent species can be controlled. This is an interesting study, which may raise the caution of targeting VCP alone for the therapeutics of tauopathies. I have a few comments on this manuscript.

1. The authors carried out excellent and detailed mechanistic studies mostly in cultured cell lines and a few in primary neurons, however, they did not show any evidence from animal models or human disease-related models. Thus, the reviewer is not sure how these findings in vitro can be applied in vivo and/or in humans.
2. The authors demonstrated the effect of the VCP disease mutations on disaggregation, if any, is only mild, suggesting that inhibition of aggregate clearance may not be the primary mechanism by which these mutations cause disease. This conclusion should be cautious since all the data are based on the studies using HEK293T cells. The authors may at least validate it using primary neurons. Also, the authors may discuss more about previous reports on VCP mutations and potential mechanisms.
3. Although the authors showed that the effects of VCP is macroautophagy independent, how about microautophagy or chaperone-mediated autophagy (CMA)? The authors did not show any data or discuss them. Also, previous studies have shown the macroautophagy could be one potential mechanism underlying the function of VCP. The authors should at least discuss this inconsistency between their data with others.

Reviewer #4 (Remarks to the Author):

Saha et al. describe an alternative mechanism of the tau fibril clearance by VCP chaperone which binds to ubiquitinated tau fibrils and recruits them for degradation by the proteasome. Using both the fluorescently labeled aggregation-prone region of tau and the full-length tau, the authors conducted experiments in HEK293T cells and in primary neurons which support their hypothesis and show that VCP is involved in tau fibril clearance. Overall, the manuscript is very well written and provides a large number of experiments to support the VCP role which lays a good ground for further work (by authors or others) to further confirm the VCP function using structural biology methods. This reviewer thinks that structural data describing the mechanism of VCP-Tau interaction at the molecular level would greatly improve the manuscript.

The methods section provides sufficient level of details.

This reviewer has the following recommendations to further improve the quality of the manuscript.

Major comments:

1. The authors discuss the role of VCP mutation in neurodegenerative diseases. In the light of the recent data from Shi et al. (Nature, 598), the tau fibril structure varies among different tauopathies. This may further confine VCP interaction and the mutation in VCP may not be the defining cause for the particular tauopathy. The discussion in this manuscript should reflect that.
2. The discussion about the potential role of VCP-Tau fragments forming the seeds for further fibrillization in other cells is not clear to this reviewer. Did the authors carry out experiments that such fragments can spread among the cells and seed further fibrillation?
3. The authors mention in the methods that they have carried out cryo-CLEM experiments. However, no cryo-CLEM data are shown in the manuscript. Actually, the correlation with fluorescence imaging would greatly improve the interpretation of Fig. 1d and 3c. In both cases, the authors denote the fibrillar objects in cryo-ET data as tau fibril. Although highly likely, this should be supported either by a control experiment or even better correlative imaging. In addition, Fig. 1d (right panel) gives a false notion that the filaments are restricted to a particular region of the depicted volume. There are obvious filaments of the same size in the top part of the image which are not shown in segmentation.

Minor comments:

1. "de novo", "in vitro" etc. shall be typeset in italic

Point-by-point response to reviewer comments

(all Page und line numbers in this response regard the document “Saha et al_Main-20220923_Plain Text_No edits.docx”)

Reviewer #1 (Remarks to the Author):

In this manuscript, Saha et al. carry out experiments to demonstrate that the AAA+ chaperone VCP (p97) binds ubiquitylated Tau fibrils and disaggregates them. They demonstrate that inhibition of VCP activity stabilizes large Tau aggregates; however, this also results in the reduction in the amount of Tau species competent of prion like aggregate seeding in recipient cells. Therefore, the authors conclude that disaggregation by VCP generates seeding-active Tau as byproduct. Proper aggregate clearance requires the functions of Hsp70 and of the UPS system.

General impression

This is a very detailed study that presents a lot of data using multiple systems and multiple approaches to support the claims. However, it is mainly based on phenotypic observations. The authors have not done any of the needed in vitro experiments to show that isolated Tau fibrils can be disassembled by purified VCP. Furthermore, the role of Hsp70 is no well investigated and seems to be a side note in the manuscript.

We thank the reviewer for these favorable comments.

This is the first study providing direct evidence that VCP in cooperation with the proteasome system mediates the disaggregation and disposal of Tau fibrils in cells. This activity has so far mostly been attributed to the Hsp70 chaperone system, although mainly on the basis of in vitro experiments.

In this manuscript we now show in cells that the system necessary for Tau disaggregation and degradation is very complex, and consists of at least three major machineries: VCP and its cofactors, the ubiquitin-proteasome system and the Hsp70 system. The Tau aggregates to be disaggregated must be modified by ubiquitylation by an E3 ligase(s) that remains to be

identified. Reconstitution of this process *in vitro* with purified components is highly challenging and is therefore outside the scope of this first study. One particular challenge, apart from having to express and purify VCP, cofactors and proteasome in functional form, is to produce the properly ubiquitylated Tau aggregates.

We agree with the reviewer that Hsp70 is mainly a side-note in this project, but we believe that the experiments presented are useful in providing a link to published literature. We have now included a sentence in the discussion (page 15, lines 332-334) to emphasize that due to the structural diversities of Tau fibrils, both the VCP pathway, described here, and a Hsp70 mediated reaction of disaggregation can exist in cells.

Specific comments

1. The authors should quantify the inclusions/cell for Fig. 2d.

The quantification of inclusions/cell is now shown in Fig. 2d. VCP and proteasome inhibition significantly stabilize aggregates in Tet-TauRD-Y* cells.

2. No filter-trap analysis done for CB-5083?

We added the filter-trap analysis for CB-5083 as Supplementary Fig. 5e. We observe similar effects of inhibiting VCP using CB-5083 as with NMS-873.

3. Filter-trap analysis of siVCP in Supplementary Fig. 4f are not very convincing, perhaps due to low efficiency of siRNA-mediated knockdown.

Yes, since VCP is essential for cell survival, it is indeed not trivial to deplete it completely from cells. To show the effect of VCP knockdown on the filter trap assay more clearly, we have added a quantification of the data in Supplementary Fig. 5g.

4. Line 171-172 vs line 203: Is the TauRD cell line tagged with myc or untagged? They are referred to differently in the two places indicated. If myc-tagged, naming conventions should be kept consistent, and should be renamed TauRD-M instead.

The TauRD cell line has a C-terminal myc tag as stated in line 173. This is now also indicated in line 213/214. We added new schematics to Fig.1a now including the non-fluorescent tagged FLTau and TauRD constructs.

5. Claims of EQ/EQ mutants effects on TauRD-Y aggregates from lines 261-264 is not backed by actual data.

We agree and have omitted this statement.

6. Is there a reason that the AE and RH mutants are not analyzed for whether they stabilize aggregates as the DG and EQ/EQ mutants in Fig. 5d? AE seems to colocalize nicely with aggregates in Fig. 5b.

We added the analysis of AE and RH mutants in Fig. 5d. We do not observe a significant stabilization of TauRD-Y aggregates upon expressing these mutants. This observation is consistent with the filter-trap analysis shown in Fig. 5c and current understanding that these mutations rather increase the ATPase activity and unfolding capacity of VCP.

Reviewer #2 (Remarks to the Author):

Thank you for writing a very comprehensive paper

A few general comments:
Lovely microscopy images!

We thank the reviewer for her/his positive comments.

Perhaps add into the title: "The AAA+ chaperone VCP disaggregates Tau fibrils and generates aggregate seeds " that this was a laboratory model

We have changed the title to "The AAA+ chaperone VCP disaggregates Tau fibrils and generates aggregate seeds in a cellular system" to emphasize that these experiments were done in a laboratory model.

Please write out all abbreviations in the abstract for general readers who are not familiar with the specific field: eg. valosin-containing protein (VCP)

We thank the reviewer for pointing this out. We have now written out VCP and Hsp70 in the abstract.

In the abstract you state:

These findings identify VCP as a core component of the machinery for the removal of neurodegenerative disease aggregates and suggest that its activity can be associated with enhanced aggregate spreading in tauopathies.

Please add to your discussion how you relate your findings in the lab to what happens during neuro-inflammation in AD. Perhaps a figure could be added to the explanation.

The reviewer has raised an interesting idea connecting our findings to neuroinflammation, which contributes critically to AD pathology. The general consensus about the contribution of protein aggregates to neuroinflammation in AD is that CNS-resident microglia recognize extracellular amyloid- β aggregates and Tau 'ghost tangles' via cell surface receptors and are activated by this process. Activated microglia secrete pro-inflammatory molecules and trigger reactions of the immune system leading to neuroinflammation. We surmise that disaggregated Tau seeds once released to the extracellular space, in addition to spreading aggregation to neighboring cells, may activate microglia and trigger an immune reaction,

thereby contributing to the characteristic neuroinflammation observed in AD. We have included this idea in the discussion (page 17, lines 365-368) of the revised manuscript.

VCP-mediated aggregate disassembly followed by proteasomal degradation provides an important alternative to autophagy as a mechanism for the elimination of terminally aggregated proteins.

Please add a diagram to explain autophagy and compare it to your VCP-mediated pathways and findings.

Autophagy is an important and complex cellular pathway that has been extensively studied and reviewed in the literature. Due to space limitations, we feel a review article would be the more appropriate format to elaborate on the interplay between VCP-mediated disaggregation, aggregate clearance by autophagy and other direct and indirect roles of VCP in the cell.

Please relate your findings directly to clinical application in AD. How do you foresee this research may impact clinical interventions?

We appreciate that the reviewer considers the possibility that our findings may impact clinical interventions in AD in the future. We currently state that (page 17, lines 371-376) 'Based on our results, both activation and inhibition of this pathway (i.e. disaggregation by VCP) may have beneficial effects dependent on the specific disease context. Non-human AAA+ ATPases with augmented disaggregase activity are currently being developed with the aim to reverse pathogenic protein aggregation. Boosting cellular aggregate clearance, perhaps in combination with proteasome activation, may offer a potential therapeutic strategy as long as the production of seeding competent species can be controlled.' Since VCP plays a role in different cellular pathways, we feel that larger claims may raise unfounded public expectations about the time necessary to transfer these results to a clinical setting.

Please elaborate or discuss in the conclusion if this work could be translated to other neuro-inflammatory diseases too? Parkinson's Disease?

Given that VCP colocalizes with Lewy bodies in patient brains from Parkinson's disease and dementia with Lewy bodies (Hirabayashi et al. Cell Death and Differentiation 2001, PMID: 11598795), it is possible that VCP is involved in modulating these aggregates as well. However, this activity has not yet been demonstrated. Also, it is unclear whether VCP would directly disaggregate Lewy body-resident α -synuclein aggregates or mediate its action via its role in autophagy. This is critical because the underlying molecular mechanism of VCP function would dictate whether or not seeding-competent species with possible downstream effects are generated. Future experiments with other disease-related aggregates and in relevant model systems will be necessary to test the generality of VCP-mediated disaggregation and the contribution to neuroinflammation. We believe that at this point it would be premature to speculate on the outcome of the interactions between alpha-synuclein aggregates and VCP.

Reviewer #3 (Remarks to the Author):

Saha et al. reported VCP disaggregates Tau fibrils, however, it generates seeding-active Tau as byproduct at the same time. These results suggest that VCP may have both neuroprotective and neurotoxic effects, although VCP mutations have been associated with aggregate deposition disorders such as vacuolar tauopathy and IBMPFD. Boosting cellular aggregate clearance, perhaps in combination with proteasome activation, may offer a potential therapeutic strategy as long as the production of seeding competent species can be controlled. This is an interesting study, which may raise the caution of targeting VCP alone for the therapeutics of tauopathies. I have a few comments on this manuscript.

1. The authors carried out excellent and detailed mechanistic studies mostly in cultured cell lines and a few in primary neurons, however, they did not show any evidence from animal models or human disease-related models. Thus, the reviewer is not sure how these findings *in vitro* can be applied *in vivo* and/or in humans.

We thank the reviewer for his/her positive comment. In this first study demonstrating VCP-mediated disaggregation of Tau fibrils, we have limited our experiments mainly to cultured mammalian cells and mouse primary neurons. In the revised draft, we have added new data from the tauopathy mouse model rTg4510 expressing human Tau with the P301L point mutation, where we tested whether VCP colocalizes with Tau aggregates in brain sections. Indeed, immunohistochemistry experiments show that VCP colocalizes with hyperphosphorylated Tau aggregates in the mouse brain. This result is now shown in Supplementary Fig. 6g. These observations further consolidate our findings in cultured cells. We have now emphasized the limitations of our model system in the discussion (page 16 line 340-341; page 17, line 353-354), and also altered the title of the manuscript to make this point clearer. Future studies will focus on a deeper investigation of VCP function in disaggregation in the *in vivo* model, but are outside the scope of the present manuscript.

The important role of VCP in modulating Tau aggregation in human brains is supported by a newly described neurodegenerative disease called vacuolar tauopathy, where patients carrying a hypomorphic VCP mutation, D395G, develop Tau aggregates in the brain (Darwich et al., Science 2020, PMID: 33004675). Furthermore, VCP colocalizes with Tau aggregates in Alzheimer's disease (Darwich et al., Science 2020, PMID: 33004675), inclusions of expanded polyglutamine protein huntingtin in Huntington's disease and Lewy bodies comprised of α -synuclein in Lewy Body Dementia (Hirabayashi et al. Cell Death and Differentiation 2001, PMID: 11598795). Therefore, it is plausible that VCP has a common function in protein disaggregation relevant to a wide range of human diseases - a topic for further investigation.

2. The authors demonstrated the effect of the VCP disease mutations on disaggregation, if any, is only mild, suggesting that inhibition of aggregate clearance may not be the primary mechanism by which these mutations cause disease. This conclusion should be cautious since all the data are based on the studies using HEK293T cells. The authors may at least validate it using primary neurons. Also, the authors may discuss more about previous reports on VCP mutations and potential mechanisms.

We agree with the reviewer that neurons may be more sensitive to VCP mutation than HEK293T cells. Accordingly, we have revised our conclusion (page 13, line 275-276) and extended the discussion on VCP mutations and potential mechanisms (page 16, lines 347-350). However, validating the mutants in neurons will require a substantial amount of testing and optimization. Such experiments, while not central to our main conclusions, would unduly delay publication.

3. Although the authors showed that the effects of VCP is macroautophagy independent, how about microautophagy or chaperone-mediated autophagy (CMA)? The authors did not show any data or discuss them. Also, previous studies have shown the macroautophagy could be one potential mechanism underlying the function of VCP. The authors should at least discuss this inconsistency between their data with others.

Emerging evidence indeed suggests that VCP also plays a role in autophagy. However, as shown in Supplementary Fig. 4a, we did not observe TauRD-Y stabilization upon inhibiting lysosomal degradation with BafilomycinA1, where all forms of autophagic degradation should be blocked, including microautophagy and CMA. We have clarified this in the text (page 7, lines 133-136). The independence of autophagy, whether or not a peculiarity of our model system, provides the advantage to unequivocally identify the function of VCP in disaggregation.

Reviewer #4 (Remarks to the Author):

Saha et al. describe an alternative mechanism of the tau fibril clearance by VCP chaperone which binds to ubiquitinated tau fibrils and recruits them for degradation by the proteasome. Using both the fluorescently labeled aggregation-prone region of tau and the full-length tau, the authors conducted experiments in HEK293T cells and in primary neurons which support their hypothesis and show that VCP is involved in tau fibril clearance. Overall, the manuscript is very well written and provides a large number of experiments to support the VCP role which lays a good ground for further work (by authors or others) to further confirm the VCP function using structural biology methods. This reviewer thinks that structural data describing the mechanism of VCP-Tau interaction at the molecular level would greatly improve the manuscript.

The methods section provides sufficient level of details.

We thank the reviewer for her/his positive comments, and agree with the assessment that understanding, in structural terms, how VCP interacts with Tau (and many of its other substrates) will be important. However, such experiments are clearly outside the scope of this first article on the mechanism of VCP-mediated fibril disaggregation and will require a separate study.

This reviewer has the following recommendations to further improve the quality of the manuscript.

Major comments:

1. The authors discuss the role of VCP mutation in neurodegenerative diseases. In the light of the recent data from Shi et al. (Nature, 598), the tau fibril structure varies among different tauopathies. This may further confine VCP interaction and the mutation in VCP may not be the defining cause for the particular tauopathy. The discussion in this manuscript should reflect that.

We agree and thank the reviewer for this comment. We have altered our discussion to better reflect this, and have added a statement that different forms of Tau aggregate may be more or less suitable for VCP-mediated disaggregation (page 15, line 332-334).

2. The discussion about the potential role of VCP-Tau fragments forming the seeds for further fibrillization in other cells is not clear to this reviewer. Did the authors carry out experiments that such fragments can spread among the cells and seed further fibrillation?

The experiments shown in Figures 6 and S12 have been mainly designed to detect oligomeric, seeding competent Tau species that when added to cells are imported and induce new Tau aggregates. However, the reviewer is correct in that we have not demonstrated that such oligomers or fragments can be exported from cells for uptake by neighboring cells. Further experiments will be required to investigate the mechanism of seed export and uptake. Such studies are ongoing in several laboratories. We discuss this now in more detail and point out the limitations of the present study (page 17, lines 361-365).

3. The authors mention in the methods that they have carried out cryo-CLEM experiments. However, no cryo-CLEM data are shown in the manuscript. Actually, the correlation with fluorescence imaging would greatly improve the interpretation of Fig. 1d and 3c. In both cases, the authors denote the fibrillar objects in cryo-ET data as tau fibril. Although highly likely, this should be supported either by a control experiment or even better correlative imaging. In addition, Fig. 1d (right panel) gives a false notion that the filaments are restricted to a particular region of the depicted volume. There are obvious filaments of the same size in the top part of the image which are not shown in segmentation.

We thank the reviewer for pointing this out. To address this comment, we introduced a new Supplementary Fig. 2 showing a schematic of the different steps of the cryo-ET procedure that was carried out for imaging the

inclusions in HEK293 cells and neurons (Supplementary Fig. 2a), and specific images from the cryo-CLEM workflow of the inclusions in neurons (Supplementary Fig. 2b-g). Additionally, we are providing a similar figure of the cryo-CLEM workflow in HEK293 cells here for the reviewer's assessment (Fig. I). Correlative imaging, in addition to the presence of YFP densities on the fibrils as shown in Supplementary Fig. S6f (as shown in Bäuerlein et al., Cell 2017, PMID: 28890085; Guo et al. Cell 2018, PMID: 29398115; Trinkaus et al. Nat Comm 2021, PMID: 33854052), confirms that the fibrils are indeed formed of TauRD-Y protein.

Regarding the additional fibrils in Fig. 1d, we think that the structures that the reviewer is referring to might be membranes, as shown here in the overlay of the tomogram with the segmentation (Fig. If). Moreover, the fibrils traced in the segmentation are representative and meant only for visualization. We have not used this data for any quantitative analysis of fibril abundance or specific localization, and cannot exclude the possibility that there may be some fibrils in other areas of the cell. The raw tomograms corresponding to Fig. 1d and 3c are available at EMDB (EMD-13739 and EMD-13740, respectively) for the reference of the readers and reviewers.

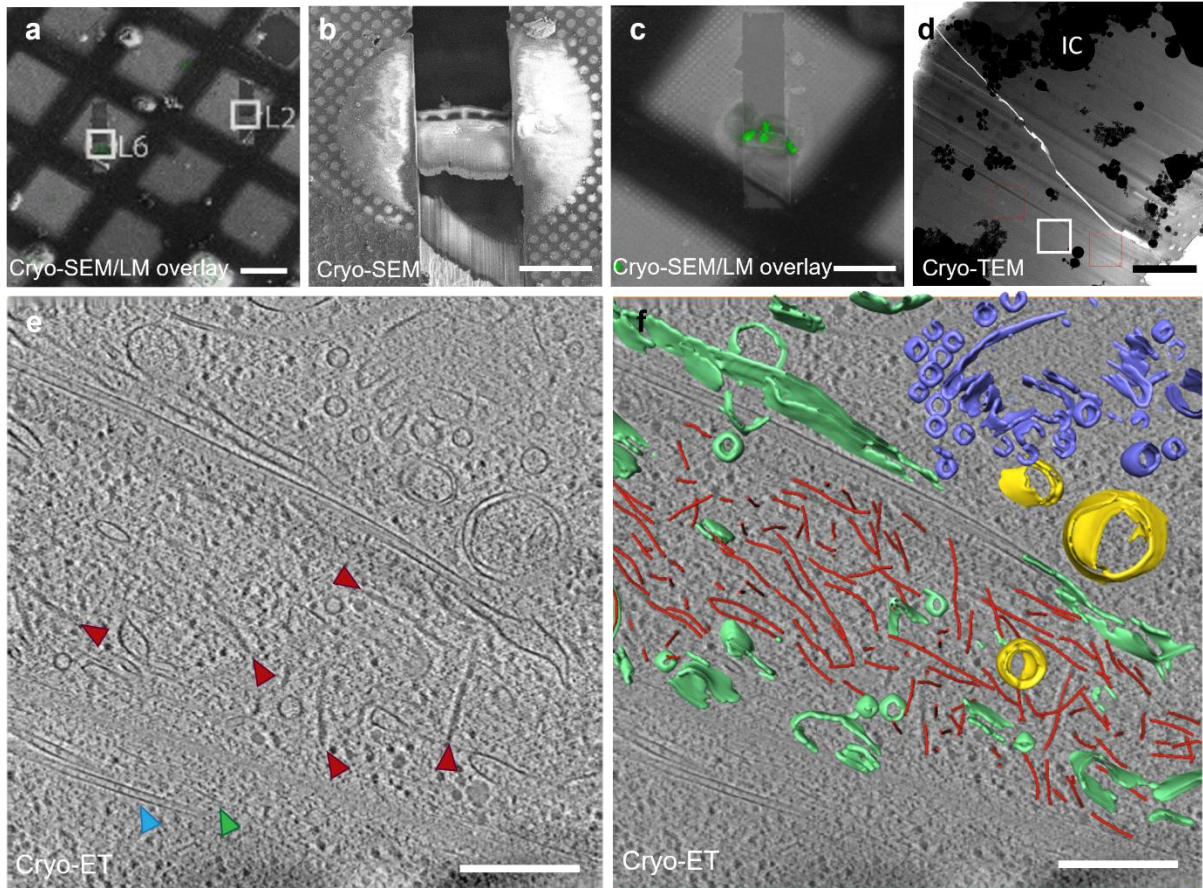


Fig 1: Cryo-correlative-light-electron microscopy (cryo-CLEM) workflow of HEK293 cells.

a TauRD-Y* cells containing TauRD inclusions were cultured on EM grids for 24 h and vitrified by plunge freezing. Thereafter, grids were imaged by cryo-LM (cryo-light microscopy) and cryo-SEM (cryo-scanning electron microscopy), and lamellae were generated by cryo-focused ion beam milling. An overlay of cryo-SEM and cryo-LM images is shown. A cell of interest is marked by box L6. L2 shows an additional lamella. Scale bar, 30 μm . **b** Magnified cryo-SEM image of the ~ 200 nm thick L6 lamella from (a). Scale bar, 15 μm . **c** Cryo-SEM and cryo-LM overlay at the location of the L6 lamella. Scale bar, 30 μm . **d** Cryo-TEM (cryo-transmission electron microscopy) overview of the lamella shown in (b, c). Tomograms were acquired in regions indicated by boxes. The tomogram shown in (e) was acquired in the area represented by the white box. IC: Ice crystal. Scale bar, 3 μm . **e** 1.7 nm thick tomographic slice of a TauRD inclusion from TauRD-Y* cells (shown in Fig. 1d). Red, blue and green arrowheads indicate representative TauRD-Y fibrils, microtubule and actin, respectively. Scale bar, 300 nm. **f** An overlay of the 3D rendering with the tomogram in (e) showing TauRD-Y fibrils (red), Golgi (purple), mitochondria (yellow) and ER (green). Scale bar, 300 nm.

Minor comments:

1. "de novo", "in vitro" etc. shall be typeset in italic

We agree this is normally the case, however, we followed the non-italicized style of Nature Communications to write 'de novo', 'in vitro', etc.

REVIEWER COMMENTS

Reviewer #1 (Remarks to the Author):

The authors have addressed my comments. I have no further comments.

Reviewer #3 (Remarks to the Author):

The authors provided new data and more discussions in their revision. The current version of the manuscript has been improved compared to the original submission. But I have a question about their new data in Supplementary Fig. 6g: Immunohistochemical staining of brain section of a 4-month-old Tau transgenic rTg4510 mouse with AT8 (green) and VCP (red) antibodies, and Nissl substance (cyan).

First, the staining of VCP in AT8-positive neuron shows the pattern very similar to AT8, i.e. mainly puncta staining in the cytosol. However, the staining of VCP in AT8-negative neuron shows the diffused staining like the background staining. The authors need to show the VCP staining of non-transgenic control mice, which will let us know the normal staining pattern of VCP, and how it changes in rTg4510 mice. Also, did the authors validate the specificity of this VCP antibody?

Second, if VCP is essential for pTau disaggregation, shouldn't the authors see reduced VCP expression or activity in AT8-positive neurons? However, the authors' data seems to be opposite. Maybe the puncta of VCP does not indicate the higher level of VCP, but actually suggesting the dysfunction of VCP or reduced activity of VCP?

Reviewer #4 (Remarks to the Author):

The authors have satisfactorily addressed my original comments. I fully support the acceptance of the manuscript for publication.

REVIEWER COMMENTS

Reviewer #3 (Remarks to the Author):

The authors provided new data and more discussions in their revision. The current version of the manuscript has been improved compared to the original submission. But I have a question about their new data in Supplementary Fig. 6g: Immunohistochemical staining of brain section of a 4-month-old Tau transgenic rTg4510 mouse with AT8 (green) and VCP (red) antibodies, and Nissl substance (cyan).

First, the staining of VCP in AT8-positive neuron shows the pattern very similar to AT8, i.e. mainly puncta staining in the cytosol. However, the staining of VCP in AT8-negative neuron shows the diffused staining like the background staining. The authors need to show the VCP staining of non-transgenic control mice, which will let us know the normal staining pattern of VCP, and how it changes in rTg4510 mice. Also, did the authors validate the specificity of this VCP antibody?

Second, if VCP is essential for pTau disaggregation, shouldn't the authors see reduced VCP expression or activity in AT8-positive neurons? However, the authors' data seems to be opposite. Maybe the puncta of VCP does not indicate the higher level of VCP, but actually suggesting the dysfunction of VCP or reduced activity of VCP?

To address the reviewer's first comment, we have added panels showing VCP immunostaining in the brain section of littermate control mice (Supplementary Fig. 6g). Both in control and transgenic mice, diffuse VCP signal is observed in neurons not containing pTau aggregates. Therefore, the punctate appearance of VCP in pTau positive neurons of rTg4510 mice is due to interaction with Tau aggregates.

The antibody that we used for these stainings NB100-1558 (Novus Biologicals) has previously been used for mouse brain immunofluorescence (Clemen et al. *Brain*, 2010; PMID: 20833645). We further validated the specificity of this antibody by immunoblotting (IB) and immunofluorescence (IF) analysis in VCP knockdown samples from mouse and human cell lines. Specifically, we used immortalized mouse neuronal Neuro2a cells, mouse embryonic fibroblast (MEF) and human HEK293T cells where VCP was down-regulated using siRNA. IB analysis showed that the intensity of the recognized band decreased when cells were treated with the VCP siRNA (Fig. 1a), confirming that the antibody recognized VCP in all three cell lines. The knockdown is relatively weak in mouse cell lines due to the inherently low transfection efficiency of these cell lines. Furthermore, IF analysis of VCP showed cells with reduced fluorescence intensity only under VCP knockdown condition (Fig. 1b). Additionally, immunoblot analysis of mouse brain lysates using this antibody showed a single band consistent with the molecular weight of VCP (Fig. 11b). These experiments validate the specificity of this antibody in recognizing mouse and human VCP for IB and IF applications.

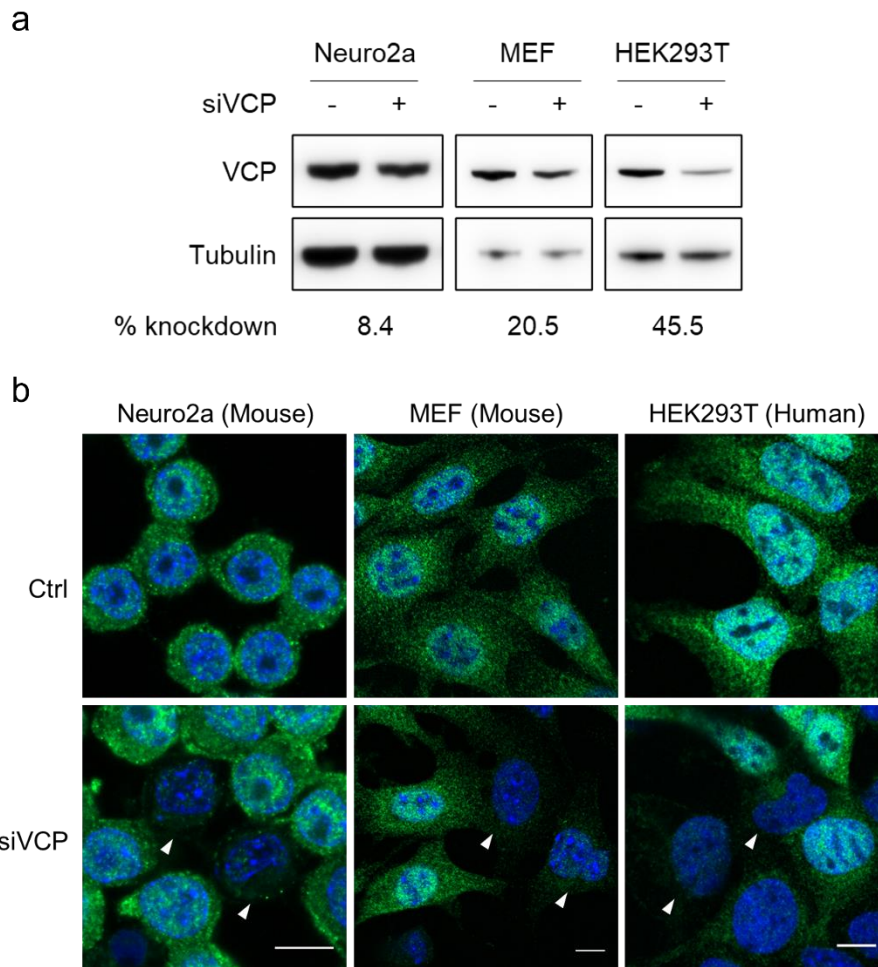


Figure I: Validation of VCP antibody NB100-1558 (Novus Biologicals).

a Analysis of VCP levels in Neuro2a, Mouse Embryonic Fibroblast (MEF) and HEK293T cells treated with control or VCP siRNA for 96 h. VCP was blotted using the antibody NB100-1558 (Novus Biologicals). Tubulin served as loading control. Percentage knockdown relative to control is indicated. **b** Immunofluorescence staining of VCP (green) in cells treated as in (a). White arrowheads indicate cells with reduced VCP levels. Scale bars, 10 μ m.

In the second point, the reviewer speculates that aggregate-containing neurons should have reduced VCP expression and that our data seems to be the opposite. While a (e.g. age related) reduction of VCP activity might contribute to a reduced Tau aggregate clearance in a disease context, we do not provide (and are not aware of) any evidence that Tau aggregation correlates with decreased VCP activity in tauopathy patients without VCP mutations. Indeed, VCP levels are not reduced in the human brain in AD (Bai et al. *Mol. Neurodegeneration*, 2021, PMID: 34384464), a fact that we now also mention in the manuscript. Note that in the tauopathy mouse model used the mutation is in Tau and there is no reason to assume that VCP levels are altered compared to control animals. In order to address the reviewer's question, we now quantified VCP fluorescence intensity in pTau+ and pTau- neurons in rTg4510 mouse brain. A mild but non-significant reduction

of VCP levels was observed in pTau+ neurons (Fig. IIa). We further compared VCP levels in lysates from the cortex of 4 - 4.5 months old control and rTg4510 mice. In line with the IF result, IB analysis showed no significant difference in the VCP levels between control and rTg4510 mice (Fig. IIb). Notably, a knock-in mouse model expressing hypomorphic VCP mutant D395G shows no Tau pathology (Darwich et al., Science, 2020, PMID: 33004675), indicating that reduced VCP activity is not sufficient to trigger Tau aggregation. Our results with NMS-873 treated cells are consistent with this idea (Supplementary Fig. 5i and 6c). Aggregates accumulate presumably due to overwhelmed disaggregation capacity of the cell. Additionally, a fully functional aggregate-clearance pathway requires the downstream Hsp70 chaperone system, the proteasome and under some conditions, autophagy. Perturbation of these pathways is often observed neurodegeneration models and likely to contribute to cellular aggregate load.

Assessing whether the aggregate-localized VCP is dysfunctional or actively disaggregates Tau in neurons *in vivo* is highly challenging and outside the scope of this manuscript. Notwithstanding, it is an exciting question and we are actively investigating this in living cells in an independent project using advanced microscopy techniques and cell culture models. In the present manuscript, we showed that disaggregation is blocked when VCP is not localized to the inclusions (Fig.4c,d), therefore we think that the presence of VCP on aggregates is meaningful.

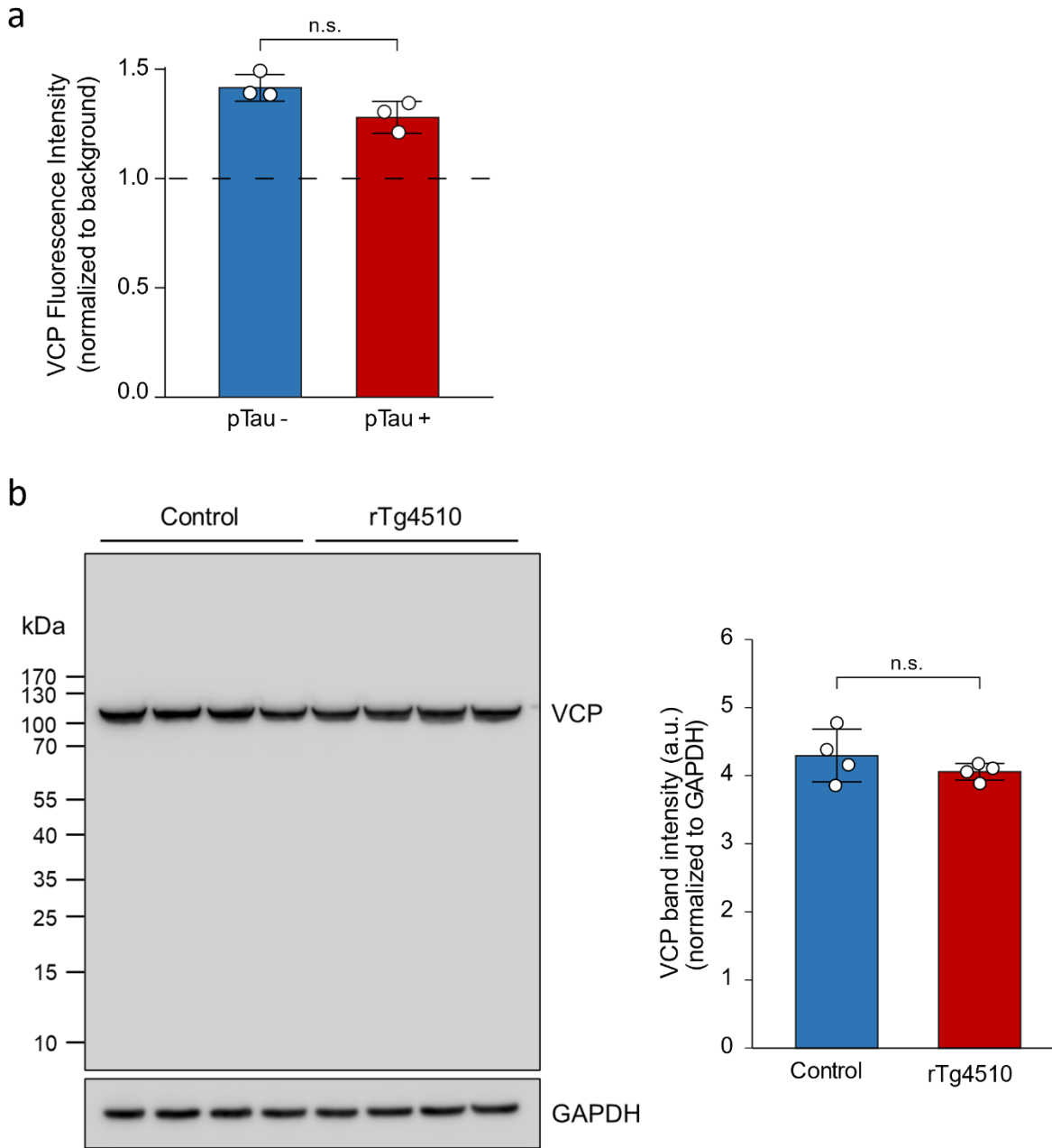


Figure II: Analysis of VCP levels in rTg4510 mice.

a Quantification of VCP fluorescence intensity in AT-8 negative (pTau-) and AT-8 positive (pTau+) neurons in rTg4510 brain sections (related to Supplementary Fig. 6g) co-stained with a validated VCP antibody NB100-1558 (Novus Biologicals). Mean \pm s.d.; $n=3$ mice, 50 neurons/mouse; n.s. non-significant ($p= 0.0616$) from unpaired t-test. **b** Left, immunoblot analysis of lysates from the cortex of control and rTg4510 mice. VCP was blotted using the antibody NB100-1558 (Novus Biologicals). GAPDH served as loading control. Right, quantification of VCP band intensity. Mean \pm s.d.; $n=4$ mice. n.s. non-significant ($p= 0.2920$) from unpaired t-test.

REVIEWERS' COMMENTS

Reviewer #3 (Remarks to the Author):

The authors have provided new data and discussions to address the reviewer's comments. I would like to recommend the acceptance of the manuscript for publication in Nature Communications.

Reporting Summary

Nature Portfolio wishes to improve the reproducibility of the work that we publish. This form provides structure for consistency and transparency in reporting. For further information on Nature Portfolio policies, see our [Editorial Policies](#) and the [Editorial Policy Checklist](#).

Statistics

For all statistical analyses, confirm that the following items are present in the figure legend, table legend, main text, or Methods section.

n/a Confirmed

- The exact sample size (n) for each experimental group/condition, given as a discrete number and unit of measurement
- A statement on whether measurements were taken from distinct samples or whether the same sample was measured repeatedly
- The statistical test(s) used AND whether they are one- or two-sided
Only common tests should be described solely by name; describe more complex techniques in the Methods section.
- A description of all covariates tested
- A description of any assumptions or corrections, such as tests of normality and adjustment for multiple comparisons
- A full description of the statistical parameters including central tendency (e.g. means) or other basic estimates (e.g. regression coefficient) AND variation (e.g. standard deviation) or associated estimates of uncertainty (e.g. confidence intervals)
- For null hypothesis testing, the test statistic (e.g. F , t , r) with confidence intervals, effect sizes, degrees of freedom and P value noted
Give P values as exact values whenever suitable.
- For Bayesian analysis, information on the choice of priors and Markov chain Monte Carlo settings
- For hierarchical and complex designs, identification of the appropriate level for tests and full reporting of outcomes
- Estimates of effect sizes (e.g. Cohen's d , Pearson's r), indicating how they were calculated

Our web collection on [statistics for biologists](#) contains articles on many of the points above.

Software and code

Policy information about [availability of computer code](#)

Data collection

ZEN 2011 SP7 (black) v14.0.2.201 (Zeiss LSM 780) - Confocal image acquisition
 LAS X v3.5.7.23225 (Leica SP8 FALCON) - Confocal image acquisition
 LAS X v3.5.7.23225 (Leica TCS SP8) - Confocal image acquisition
 LAS-4000 image analyzer (FujiFilm)- Immunoblot acquisition
 ImageQuant 800 control Software v1.2.0 (Amersham)- Immunoblot acquisition
 Attune NxT Software v2.4-3.1- Fluorescence-activated cell sorting
 FACSDiva v6.1.3 - FRET measurement
 MAPS v2.1 (FEI), K2align, IMOD package v4.9.0, TomoSegMemTV v1.0- Cryo-electron tomography workflow softwares

Data analysis

ImageJ v1.49s - Confocal image analysis and processing
 Adobe Photoshop CC 2018- Image processing
 AIDA Image Analyzer v4.27.039- Immunoblot quantification
 MS Excel 2019- Display of quantitative data and statistics
 GraphPad Prism 7- Statistics
 Origin 2019b- Exponential fitting, one-way ANOVA and Tukey post hoc test
 MaxQuant v1.5.4.1 - Protein identification and SILAC based quantification
 UNIPROT v2019-03-12- Database for protein identification
 Perseus v1.2.6.3 - Volcano plot for interactome analysis
 FlowJo v10.7.1 and V9 - Flow cytometry
 Amira v6.2 - Cryo-ET
 SerialEM v3.7.0 - Cryo-ET
 Motioncor2 v1.2.1 - Cryo-ET

For manuscripts utilizing custom algorithms or software that are central to the research but not yet described in published literature, software must be made available to editors and reviewers. We strongly encourage code deposition in a community repository (e.g. GitHub). See the Nature Portfolio [guidelines for submitting code & software](#) for further information.

Data

Policy information about [availability of data](#)

All manuscripts must include a [data availability statement](#). This statement should provide the following information, where applicable:

- Accession codes, unique identifiers, or web links for publicly available datasets
- A description of any restrictions on data availability
- For clinical datasets or third party data, please ensure that the statement adheres to our [policy](#)

All data supporting the findings of this study are included in the manuscript and the Supplemental Information. Source data are provided with this paper. Additional data is available from the corresponding authors upon reasonable request. The mass spectrometry proteomics data associated to Fig. 2a have been deposited to the ProteomeXchange Consortium via the PRIDE93 partner repository (<https://www.ebi.ac.uk/pride/archive/>) with the dataset identifier PXD023400. This PRIDE entry additionally contains analyses that are not a part of this study. The tomograms shown in Fig. 1d and Fig. 3c are available in the EMDB (<https://www.ebi.ac.uk/emdb/>) through the following information: EMD ID: EMD-13739 (Fig. 1d) and EMD-13740 (Fig. 3c).

Field-specific reporting

Please select the one below that is the best fit for your research. If you are not sure, read the appropriate sections before making your selection.

- Life sciences Behavioural & social sciences Ecological, evolutionary & environmental sciences

For a reference copy of the document with all sections, see nature.com/documents/nr-reporting-summary-flat.pdf

Life sciences study design

All studies must disclose on these points even when the disclosure is negative.

Sample size	No statistical methods were used to predetermine sample size. Based upon accepted standards in the field, quantitative experiments were performed in at least three independent replicates and statistical significance was evaluated. Animal experiment data is only qualitative and obtained from three animals per group.
Data exclusions	The original proteomics experiment shown in Fig. 2a was performed with three SILAC labels- Light (TauRD-Y), Heavy (TauRD-Y*), and Medium (a third cell line that is not a part of this study). The proteomics raw data in the PRIDE entry PXD023400 contains analyses of all the labels. Since the Medium labeled cell line is not a part of this study, the Medium label data was excluded from analysis shown in this study. No data other data were excluded from the rest of the experiments presented in this manuscript.
Replication	Experiments were carried out at least twice or in several independent replicates using protocols outlined in the Methods section. Similar results were observed.
Randomization	Mouse embryos of both sexes were chosen randomly for neuronal cell cultures. Animals of either sex were used in all experimental groups.
Blinding	Investigators were not blinded during the experiments. Blinding was not relevant for this study as no allocation of human/animal subjects was involved.

Reporting for specific materials, systems and methods

We require information from authors about some types of materials, experimental systems and methods used in many studies. Here, indicate whether each material, system or method listed is relevant to your study. If you are not sure if a list item applies to your research, read the appropriate section before selecting a response.

Materials & experimental systems

- | | |
|-------------------------------------|---|
| n/a | Involved in the study |
| <input type="checkbox"/> | <input checked="" type="checkbox"/> Antibodies |
| <input type="checkbox"/> | <input checked="" type="checkbox"/> Eukaryotic cell lines |
| <input checked="" type="checkbox"/> | <input type="checkbox"/> Palaeontology and archaeology |
| <input type="checkbox"/> | <input checked="" type="checkbox"/> Animals and other organisms |
| <input checked="" type="checkbox"/> | <input type="checkbox"/> Human research participants |
| <input checked="" type="checkbox"/> | <input type="checkbox"/> Clinical data |
| <input checked="" type="checkbox"/> | <input type="checkbox"/> Dual use research of concern |

Methods

- | | |
|-------------------------------------|--|
| n/a | Involved in the study |
| <input checked="" type="checkbox"/> | <input type="checkbox"/> ChIP-seq |
| <input type="checkbox"/> | <input checked="" type="checkbox"/> Flow cytometry |
| <input checked="" type="checkbox"/> | <input type="checkbox"/> MRI-based neuroimaging |

Antibodies

Antibodies used	VCP (AbCam #ab11433), anti-VCP (Novus Biologicals #NB100-1558), anti-GFP (Roche #11814460001), anti-Ubiquitin Lys48-specific (Millipore #05-1307), anti-ubiquitin Lys63-specific (AbCam #ab179434), anti-Ubiquitin (P4D1) (SantaCruz #sc-8017), anti-Tau (pS356) (GeneTex #GTX50165), anti-Phospho-Tau (S202, T205) (Thermo Fisher Scientific # MN1020), anti-NPLOC4 (Sigma #HPA021560), anti-UFD1L (AbCam #ab96648), anti-Ubiquitin FK2 (Millipore #04-263), anti-Tau (Tau-5) (Thermo #MA5-12808), anti-Human Tau/Repeat Domain (2B11) (IBL #JP10237), anti-LC3B (Sigma #L7543), anti-Atg5 (Cell Signalling #2630S), anti-Atg7 (Cell Signalling #8558), anti-PSMD11 (Proteintech #14786-1-AP), anti-GAPDH (Millipore #MAB374), anti-Tubulin (Sigma #T6199). Cy5-conjugated anti-mouse (Thermo #A10524), Cy-5 conjugated anti-rabbit (Thermo # A10523), Alexa Fluor 647 AffiniPure anti-mouse (Jackson ImmunoResearch #715-605-151), anti-mouse IgG peroxidase conjugate (Sigma #A4416), anti-rabbit peroxidase conjugate (Sigma #A9169), IRDye 680RD anti-mouse (LI-COR #926-68070), IRDye 800CW anti-rabbit (LI-COR #926-32211).
Validation	Most validations were performed by manufacturers: VCP (AbCam #ab11433) Abpromise guaranteed Immunocytochemistry (ICC) and western blotting (WB), anti-VCP (Novus Biologicals #NB100-1558) knockdown validated in-house for ICC/WB, anti-GFP (Roche #11814460001) validated for WB, anti-Ubiquitin Lys48-specific (Millipore #05-1307) validated for ICC, anti-ubiquitin Lys63-specific (AbCam #ab179434) validated for immunohistochemistry, anti-Ubiquitin (P4D1) (SantaCruz #sc-8017) validated for WB, anti-Tau (pS356) (GeneTex #GTX50165) validated for ICC, anti-Phospho-Tau (S202, T205) (Thermo Fisher Scientific # MN1020) validated for ICC and WB, anti-NPLOC4 (Sigma #HPA021560) validated for ICC, anti-UFD1L (AbCam #ab96648) validated for ICC, anti-Ubiquitin FK2 (Millipore #04-263) validated for ICC and WB, anti-Tau (Tau-5) (Thermo #MA5-12808) validated for ICC, anti-Human Tau/Repeat Domain (2B11) (IBL #JP10237) validation performed in Yuste-Checa et al., Nat Comm, 2021, anti-LC3B (Sigma #L7543) validated for WB, anti-Atg5 (Cell Signalling #2630S) validated for WB, anti-Atg7 (Cell Signalling #8558) validated for WB, anti-PSMD11 (Proteintech #14786-1-AP) validated for WB, anti-GAPDH (Millipore #MAB374) validated for WB, anti-Tubulin (Sigma #T6199) validated for WB.

Eukaryotic cell lines

Policy information about [cell lines](#)

Cell line source(s)	HEK293T cells were purchased from ATCC. Tet-FLTau and Tet-TauRD cell lines were generated in HEK293T background. Stable propagation of TauRD-Y aggregates was verified by YFP fluorescence microscopy.
Authentication	No authentication was performed.
Mycoplasma contamination	Cell lines were not PCR tested for mycoplasma contamination. No unusual DAPI staining was observed by microscopy.
Commonly misidentified lines (See ICLAC register)	None

Animals and other organisms

Policy information about [studies involving animals](#); [ARRIVE guidelines](#) recommended for reporting animal research

Laboratory animals	E15.5 CD-1 wild-type mouse embryos of both sexes were used for cortical neuronal cultures (breeding line MpiCrlcr:CD-1). rTg4510 mice were obtained by crossing tetO-tauP301L mice (JaxLabs, Stock number 015815) to the CamKII α -tTA line79 (JaxLabs, Stock number 003010) and maintained on a C57BL/6 genetic background. 4-month-old and 16-month-old animals of either sex were used for the experiments. Littermates were used as controls. Mice were housed in a specific pathogen free facility at 22 \pm 1.5 $^{\circ}$ C, 55 \pm 5% humidity, 14-hour light / 10-hour dark cycle.
Wild animals	The study did not involve wild animals.
Field-collected samples	The study did not involve animals collected from the field.
Ethics oversight	All experiments involving mice were performed in accordance with the relevant guidelines and regulations of the Government of Upper Bavaria (Germany).

Note that full information on the approval of the study protocol must also be provided in the manuscript.

Flow Cytometry

Plots

Confirm that:

- The axis labels state the marker and fluorochrome used (e.g. CD4-FITC).
- The axis scales are clearly visible. Include numbers along axes only for bottom left plot of group (a 'group' is an analysis of identical markers).
- All plots are contour plots with outliers or pseudocolor plots.
- A numerical value for number of cells or percentage (with statistics) is provided.

Methodology

Sample preparation	Creation of stable cell lines expressing the Tau repeat domain constructs fused to fluorescence proteins: HEK293T cells were
--------------------	--

transfected using Lipofectamine (Thermo). Cells were cultured in in Dulbecco's modified Eagle's medium (DMEM, Biochrom) supplemented with 10 % fetal bovine serum (FBS, GIBCO), 2 mM L-glutamine (GIBCO) and 1,000 µg/ml geneticin for selection. Polyclonal and monoclonal cell lines were generated by fluorescence-activated cell sorting. Upon selection, cells were cultured in medium supplemented with 200 µg/ml geneticin (Thermo) and penicillin/streptomycin (Thermo).

Quantification of FRET positive cells: Cells were harvested with TrypL Express Enzyme (Gibco), washed with PBS once and resuspended in PBS for analysis.

Instrument

Creation of stable cell lines: BD FACS Aria III (BD Biosciences) for cell sorting. FITC-A, DAPI-A lasers for YFP/GFP and mTurquoise2 detection, respectively.

Quantification of FRET positive cells: Attune NxT flow cytometer (Thermo Fisher Scientific) for FRET positive cells quantification. To measure mTurquoise2 and FRET fluorescence signals, cells were excited with 405 nm laser light and fluorescence was determined using 440/50 and 530/30 filters, respectively. To measure the YFP fluorescence signal, cells were excited at 488 nm and emission was recorded using a 530/30 filter.

Software

Creation of stable cell lines: FACSDiva Version 6.1.3.

Quantification of FRET positive cells: Analysis were performed with FlowJo V9.

Cell population abundance

Creation of stable cell lines: All sorted cells showed the corresponding fluorescence protein expression.

Quantification of FRET positive cells: For each sample, 50,000 single cells were collected and analyzed.

Gating strategy

Quantification of FRET positive cells: After gating single cells, an additional gate was introduced to exclude YFP-only cells that show a false-positive signal in the FRET channel due to excitation at 405 nm. The FRET positive gate was set by plotting the FRET fluorescence signal versus the mTurquoise2 fluorescence signal using non-seeded cells as reference.

Tick this box to confirm that a figure exemplifying the gating strategy is provided in the Supplementary Information.



SEP 06, 2022

Biochemical detection of aggregated Tau

Itika Saha¹, F. Ulrich Hartl¹, Mark S. Hipp^{2,3}

¹Department of Cellular Biochemistry, Max Planck Institute of Biochemistry, Am Klopferspitz 18, 82152 Martinsried, Germany;

²Department of Biomedical Sciences of Cells and Systems, University Medical Center Groningen, University of Groningen, Antonius Deusinglaan, 1, 9713 AV Groningen, The Netherlands;

³School of Medicine and Health Sciences, Carl von Ossietzky University Oldenburg, 26129 Oldenburg, Germany

OPEN  ACCESS**DOI:**

dx.doi.org/10.17504/protocols.io.n92ldpbx8l5b/v1

External link:

<https://www.biorxiv.org/content/10.1101/2022.02.18.481043v1.full>

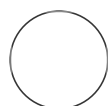
Protocol Citation: Itika Saha, F. Ulrich Hartl, Mark S. Hipp 2022. Biochemical detection of aggregated Tau.

protocols.io

<https://dx.doi.org/10.17504/protocols.io.n92ldpbx8l5b/v1>

MANUSCRIPT CITATION:

The AAA+ chaperone VCP disaggregates Tau fibrils and generates aggregate seeds
Itika Saha, Patricia Yuste-Checa, Miguel Da Silva Padilha, Qiang Guo, Roman Körner, Hauke Holthusen, Victoria A. Trinkaus, Irina Dudanova, Rubén Fernández-Busnadiego, Wolfgang Baumeister, David W. Sanders, Saurabh Gautam, Marc I. Diamond, F. Ulrich Hartl, Mark S. Hipp
bioRxiv 2022.02.18.481043;
doi:
<https://doi.org/10.1101/2022.02.18.481043>



Felix Kraus

ABSTRACT

This protocol describes the detection of aggregated Tau from HEK293 cells stably expressing and propagating aggregates of Tau repeat domain fused to YFP (Sanders et al. Neuron, 2014; Saha et al, BioRxiv, 2022). The filter trap assay is a modification of the membrane filter assay described previously (Wanker et al., Methods in Enzymology, 1999).

License: This is an open access protocol distributed under the terms of the [Creative Commons Attribution License](#), which permits unrestricted use, distribution, and reproduction in any medium, provided the original author and source are credited

Protocol status: Working
We use this protocol and it's working

Created: Sep 05, 2022

Last Modified: Dec 26, 2022

PROTOCOL integer ID:
69583

Keywords: ASAPCRN

Preparation of cell lysates

- 1 The protocol can be performed with freshly harvested cells or with frozen cell pellets. In either case, harvest cells by trypsinization and wash 1x with PBS before pelleting in 1.5 mL Eppendorf tubes.
- 2 Thaw frozen cell pellets on ice for at least 10 min. 10m
- 3 For cell pellets harvested from 1 well of a 12-well plate, add 75 μ L RIPA lysis buffer (Thermo) or 1% Triton X-100/PBS supplemented with protease inhibitor cocktail (Roche) and DNase, and resuspend pellets by pipetting.
- 4 When using 1% Triton X-100/PBS, briefly sonicate samples to lyse nuclei and achieve a homogenous lysate.
- 5 Incubate on ice for 30 min to 1 h. 1h

- 6 Centrifuge lysates at 1,000 x g for 5 min at 4 °C. Carefully remove supernatant without disturbing pelleted debris. 5m

Note

NOTE: Debris in the lysate can clog the filter in a filter trap assay.

- 7 Quantify protein concentration and normalize across all samples. The lysate can now be subjected to the centrifugation-based solubility assay or filter trap assay described below.

Solubility assay

- 8 Centrifuge lysate at 186,000 x g for 1 h at 4 °C. 1h
- 9 Remove supernatant and wash pellet with 200 µL PBS.
- 10 Centrifuge at 186,000 x g for 30 min at 4 °C. 30m
- 11 Remove PBS.
- 12 Add the same volume of PBS to the pellet as the lysis buffer initially used for the assay.

- 13 Disintegrate pellet by pipetting. Alternatively, sonication can be used.
- 14 Dilute total lysate, supernatant and pellet with SDS sample buffer and analyze by immunoblotting.

Filter trap assay

- 15 Equilibrate cellulose acetate membrane in 0.1% SDS/H₂O until completely wet.
- 16 Dilute up to 200 µg (Triton) or 100 µg (RIPA) total lysate in a total volume of 200 µL pre-cooled lysis buffer.
- 17 Mix samples by gentle vortexing and spin down in a mini centrifuge.
- 18 Affix equilibrated membrane to a filter trap apparatus (e.g. (PR648 Slot Blot Blotting Manifold, Hoefer). Ensure that there are no bubbles trapped over the membrane.
- 19 Load 200 µL 0.1% SDS/H₂O to the wells and apply vacuum. Observe whether the liquid is completely drawn through.
- 20 Load lysates and wait until they completely pass through the filter.

Note

NOTE: Filter clogging produces faulty results.

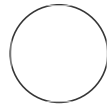
- 21 Wash wells 3 times with 200 μ L 0.1% SDS/H₂O followed by standard immunoblotting of the membrane.



Cell-based Tau seeding assay

Patricia Yuste-Checa¹

¹Max Planck Institute



Felix Kraus

ABSTRACT

This protocol details the procedure of cell-based Tau seeding assay.

ATTACHMENTS

[d5m9biezx.pdf](#)

GUIDELINES

Banning, C. et al. A flow cytometry-based FRET assay to identify and analyse proteinprotein interactions in living cells. PLoS One 5, e9344, doi:10.1371/journal.pone.0009344 (2010).

MATERIALS

TauRD-YT cell line: HEK293T cell line stably co-expressing the repeat domain of Tau (TauRD; residues 244-372 with FTD mutations P301L/V337M) fused to YFP or mTurquoise2.

FLTau-YT cell line: HEK293T cell line stably co-expressing FLTau (0N4R with FTD mutations P301L/V337M) fused to YFP or mTurquoise2.

DOI:

dx.doi.org/10.17504/protocols.io.x54v9jnrzg3e/v1

Protocol Citation: Patricia Yuste-Checa . Cell-based Tau seeding assay. **protocols.io** <https://dx.doi.org/10.17504/protocols.io.x54v9jnrzg3e/v1>

License: This is an open access protocol distributed under the terms of the [Creative Commons Attribution License](#), which permits unrestricted use, distribution, and reproduction in any medium, provided the original author and source are credited

Created: Aug 23, 2021

Last Modified: Dec 26, 2022

PROTOCOL integer ID: 52622

Keywords: Cell-based Tau seeding assay, HEK293T cell line, ASAPCRN

- 1 Plate 100,000 cells per well of HEK293T FRET reporter cell line (TauRD-YT, FLTau-YT or commercial cell line Tau RD P301S FRET Biosensor (ATCC, CRL- 3275)) into a 12-well plate.

Note

NOTE:

TauRD-YT cell line: HEK293T cell line stably co-expressing the repeat domain of Tau (TauRD; residues 244-372 with FTD mutations P301L/V337M) fused to YFP or mTurquoise2.

FLTau-YT cell line: HEK293T cell line stably co-expressing FLTau (0N4R with FTD mutations P301L/V337M) fused to YFP or mTurquoise2.

2 On the next day, seed aggregation in cells with Tau aggregates.

Note

Aggregates can be added directly to the media or transfection reagent can be used to circumvent cellular uptake pathways.

2.1 Seeding with transfection reagent:



- Prepare lipofectamine mix for n+1 samples: 50 μL Opti-MEM (Gibco) + flask icon 1.6 μL lipofectamine 3000 reagent (Thermo Fisher Scientific) per sample.
- Distribute flask icon 51.6 μL of the lipofectamine mix to individual tubes.
- Add corresponding amount of Tau aggregates.

Note

NOTE: For Tau seeding-competence quantification, Tau aggregate concentration should be determined experimentally by aggregate titration. Increasing amounts of aggregates should be added to the cells. Choose a concentration within the linear range of seeding. Tentative concentrations are:

- When using TauRD-YT cells as reporter cell line and TauRD aggregates produced in vitro (Tau residues 244-371, C291A/P301L/C322A/V337M, see protocol Tau aggregation reaction and thioflavin-T (ThT) fluorescence measurements), seeding with 14 ng TauRD aggregates (10 μ L of a 1:100 dilution in PBS of the aggregation reaction at 10 μ M) results in around 10-20% FRET positive cells.
- When using TauRD-YT cells as reporter cell line and FLTau (aggregates produced in vitro (FLTau 0N4R, see protocol Tau aggregation reaction and thioflavin-T (ThT) fluorescence measurements), seeding with 183 ng FLTau aggregates (40 μ L of a 1:100 dilution in PBS of the aggregation reaction at 10 μ M) results in 10-20% FRET positive cells.

NOTE: When lysates from cells containing aggregates are used as seeding material, lyse cell pellets with 0.05% Triton X-100/PBS, Complete EDTA-free protease inhibitor cocktail (Merck) and benzonase for 20 min on ice. Quantify total protein by Bio-Rad Protein Assay (Bio-Rad) or Pierce BCA Protein Assay Kit (Thermo Fisher Scientific). The amount of Tau protein can be quantified by SDS-PAGE and immunoblotting using purified Tau as standard or by ELISA. Tentative concentrations are:

- When using TauRD-YT cells as reporter cell line and lysate from TauRD-YT cells containing aggregates, seeding with 1 μ g total protein (around 8 ng TauRD-YFP and TauRD-mTurquoise2) results in 2-5% FRET positive cells. The residual concentration of Triton-X-100 in the seeds added to the cells is around 0.01%.
- When using TauRD-YT cells as reporter cell line and lysate from FLTau-YT cells containing aggregates, seeding with 10 ng total protein (around 200 pg FLTau-YFP and FLTau-mTurquoise2) results in 7% FRET positive cells. The residual concentration of Triton-X-100 in the seeds added to the cells is around 0.0001%.

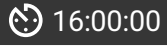
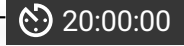
2.2 Seeding without transfection reagent:



- Mix Tau aggregates with  500 μ L fresh media.
- Replace cell media with this mix.

Note

NOTE: Tentative concentrations: When using TauRD-YT cells as reporter cell line and TauRD aggregates produced in vitro (Tau residues 244-371, C291A/P301L/C322A/V337M, see protocol Tau aggregation reaction and thioflavin-T (ThT) fluorescence measurements), seeding with 400 ng TauRD aggregates results in around 2-3% FRET positive cells after 48 h incubation.

3 Collect and quantify FRET positive cells after  16:00:00 |  20:00:00 (when using lipofectamine) or  48:00:00 (without lipofectamine or when using the FLTau-YT reporter cells): 3d 12h

3.1 Wash cells with PBS.



3.2 Add  100 μL TrypL Express Enzyme (Gibco).



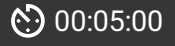
3.3 Collect the cells adding  400 μL of media and transfer them to an Eppendorf tube.

3.4 Centrifuge at  1000 x g for  00:05:00 . 5m



3.5 Discard the supernatant and wash the cell pellet with  200 μL PBS.



3.6 Centrifuge at  1000 x g for  00:05:00 . 5m



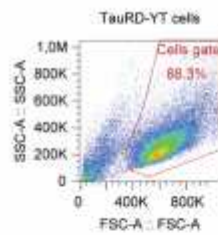
3.7 Discard supernatants and resuspend the cell pellet in  200 μL PBS.

Note

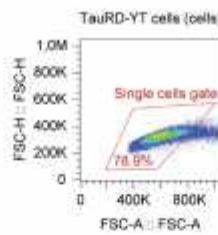
NOTE: Cells can be fixed after collection and stored at 4°C until quantification. After the PBS wash, resuspend the pellet with 400 μL 4% paraformaldehyde (PFA) and incubate at room temperature for 10 min. Centrifuge at 1000x g for 5 min, resuspend the pellet in PBS and store at 4°C.

3.8 Quantify FRET positive cells by flow cytometry. A minimum of 50,000 single cells should be analyzed. The FRET positive gate is set by plotting the FRET fluorescence signal versus the mTurquoise2 fluorescence signal using as reference nonseeded cells (See Figure below).

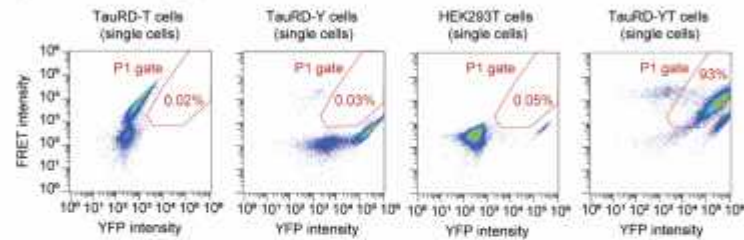
1. Selection of cells



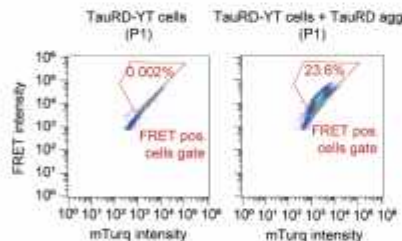
2. Selection of single cells



3. Exclusion of possible false positive FRET signal resulting from YFP excitation by the 405 nm laser (exclusion from P1 gate)



4. Selection of FRET positive cells from the P1 population using non-seeded cells as reference



Flow cytometry gating strategy for quantification of FRET positive cells. To measure the mTurquoise2 and FRET fluorescence signals, cells were excited with 405 nm laser light and fluorescence was determined using 440/50 and 530/30 filters, respectively. To measure the YFP fluorescence signal, cells were excited at 488 nm and emission was recorded using a 530/30 filter. For each sample, 50,000 single cells were analyzed. First, cells were selected (1), followed by single cell selection (2). After gating single cells, an additional gate (P1) was introduced to exclude YFP-only cells that show a false-positive signal in the FRET channel due to excitation at 405 nm using as reference TauRD-T cells, TauRD-Y cells and HEK293T cells¹ (3). The FRET positive gate was set by plotting the FRET fluorescence signal versus the mTurquoise2 fluorescence signal using as reference non-seeded cells (4). **Supplementary Fig. 10** from Yuste-Checa P., et al Nat commun xxx 2021).

Note

NOTE: When using TauRD-YT or FLTau-YT cells as reporter cell line, cells expressing just Tau-YFP and cells expressing just Tau-mTurquoise2 should also be analyzed as controls. After gating single cells, an additional gate is introduced to exclude YFP-only cells that show a false-positive signal in the FRET channel due to excitation at 405 nm¹. (See figure below for gating strategy).

NOTE: An Attune NxT flow cytometer (Thermo Fisher Scientific) can be used with the following settings:

mTurquoise2: Excitation 405 nm - Emission 440/50.

FRET: Excitation 405 nm - Emission 550/30.

YFP: Excitation 488 nm - Emission 550/30.



SEP 06, 2022

Detection of Tau ubiquitylation

Itika Saha¹, F. Ulrich Hartl^{2,3}, Mark S. Hipp^{2,3}

¹Department of Cellular Biochemistry, Max Planck Institute of Biochemistry, Am Klopferspitz 18, 82152 Martinsried, Germany;

²Department of Biomedical Sciences of Cells and Systems, University Medical Center Groningen, University of Groningen, Antonius Deusinglaan, 1, 9713 AV Groningen, The Netherlands;

³School of Medicine and Health Sciences, Carl von Ossietzky University Oldenburg, 26129 Oldenburg, Germany

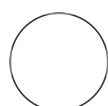
OPEN  ACCESS

DOI:
dx.doi.org/10.17504/protocols.io.3byl4je4rlo5/v1

External link:
<https://www.biorxiv.org/content/10.1101/2022.02.18.481043v1.full>

Protocol Citation: Itika Saha, F. Ulrich Hartl, Mark S. Hipp 2022. Detection of Tau ubiquitylation. **protocols.io** <https://dx.doi.org/10.17504/protocols.io.3byl4je4rlo5/v1>

MANUSCRIPT CITATION:
The AAA+ chaperone VCP disaggregates Tau fibrils and generates aggregate seeds
Itika Saha, Patricia Yuste-Checa, Miguel Da Silva Padilha, Qiang Guo, Roman Körner, Hauke Holthusen, Victoria A. Trinkaus, Irina Dudanova, Rubén Fernández-Busnadiego, Wolfgang Baumeister, David W. Sanders, Saurabh Gautam, Marc I. Diamond, F. Ulrich Hartl, Mark S. Hipp
bioRxiv 2022.02.18.481043;
doi:
<https://doi.org/10.1101/2022.02.18.481043>



Felix Kraus

ABSTRACT

This protocol describes the detection of ubiquitylated Tau from HEK293 cells stably expressing and propagating aggregates of Tau repeat domain fused to YFP (Sanders et al. Neuron, 2014; Saha et al, BioRxiv, 2022).

License: This is an open access protocol distributed under the terms of the [Creative Commons Attribution License](#), which permits unrestricted use, distribution, and reproduction in any medium, provided the original author and source are credited

Protocol status: Working
We use this protocol and it's working

Created: Sep 05, 2022

Last Modified: Dec 26, 2022

PROTOCOL integer ID:
69589

Keywords: ASAPCRN

- 1 Harvest cells from 2 confluent wells of a 6 well plate.
- 2 Lyse aggregate-containing cells by vortexing in cold RIPA buffer (Thermo) supplemented with protease inhibitor cocktail (Roche) and DNase. 20 mM N-ethylmaleimide should be included in the lysis buffer to inhibit the activity of deubiquitinating enzymes.
- 3 Briefly sonicate lysate and centrifuge at 2,000 x g for 5 min to remove cell debris. 5m
- 4 Collect supernatant, determine protein concentration and normalize across samples.
- 5 Dilute 1 mg protein in a total volume of 600 μ L RIPA buffer.

- 6 Add 50 μ L anti-GFP bead slurry (μ MACS GFP Isolation kit, Miltenyi Biotec) to diluted lysate.
- 7 Incubate for 1 h at 4 °C in a rotating wheel at 10 rpm. 1h
- 8 Before the end of 1 h, place μ -columns (Miltenyi Biotec) in the magnetic field of a μ MACS Separator (Miltenyi Biotec) and equilibrate columns by applying 250 μ L RIPA buffer. Allow complete flow-through.
- 9 Apply cell lysates and beads to μ -columns. Allow complete flow-through.
- 10 Wash columns 4 times with 1 mL 0.1% SDS/PBS.
- 11 Elute by applying 50 μ L pre-heated (95 °C) 1x SDS sample buffer.
- 12 Analyze eluates by immunoblotting with antibodies against GFP or ubiquitin.



SEP 06, 2022

Immunohistochemistry of rTg4510 mouse brain

Miguel Da Silva Padilha¹, Irina Dudanova¹, Itika Saha²,
F. Ulrich Hartl², Mark S. Hipp^{3,4}

¹Molecular Neurodegeneration Group, Max Planck Institute of Neurobiology, 82152 Martinsried, Germany;

²Department of Cellular Biochemistry, Max Planck Institute of Biochemistry, Am Klopferspitz 18, 82152 Martinsried, Germany;

³Department of Biomedical Sciences of Cells and Systems, University Medical Center Groningen, University of Groningen, Antonius Deusinglaan, 1, 9713 AV Groningen, The Netherlands;

⁴School of Medicine and Health Sciences, Carl von Ossietzky University Oldenburg, 26129 Oldenburg, Germany

OPEN  ACCESS

DOI:

dx.doi.org/10.17504/protocols.io.x54v9den4g3e/v1

External link:

<https://www.biorxiv.org/content/10.1101/2022.02.18.481043v1.full>

Protocol Citation: Miguel Da Silva Padilha, Irina Dudanova, Itika Saha, F. Ulrich Hartl, Mark S. Hipp 2022.

Immunohistochemistry of rTg4510 mouse brain.

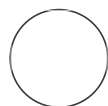
protocols.io

<https://dx.doi.org/10.17504/protocols.io.x54v9den4g3e/v1>

MANUSCRIPT CITATION:

Itika Saha, Patricia Yuste-Checa, Miguel Da Silva Padilha, Qiang Guo, Roman Körner, Hauke Holthusen, Victoria A. Trinkaus, Irina Dudanova, Rubén Fernández-Busnadiego, Wolfgang Baumeister, David W. Sanders, Saurabh Gautam, Marc I. Diamond, F. Ulrich Hartl, Mark S. Hipp
bioRxiv 2022.02.18.481043;
doi:

<https://doi.org/10.1101/2022.02.18.481043>



Felix Kraus

ABSTRACT

This protocol describes immunohistochemical staining of the Tau transgenic mice rTg4510 (Santacruz et al, 2005) brain section for Tau aggregates phosphorylated at Ser202/Thr205 and the AAA+ ATPase Valosin-containing protein (VCP). Experiments involving animal models must be performed in accordance with relevant institutional guidelines and regulations.

License: This is an open access protocol distributed under the terms of the [Creative Commons Attribution License](#), which permits unrestricted use, distribution, and reproduction in any medium, provided the original author and source are credited

Protocol status: Working
We use this protocol and it's working

Created: Sep 05, 2022

Last Modified: Dec 26, 2022

PROTOCOL integer ID:
69594

Keywords: ASAPCRN

1 Deeply anesthetize mice with 1.6% Ketamine/0.08% Xylazine and transcardially perfuse with PBS followed by 4% paraformaldehyde (PFA)(Santa Cruz) in PBS.

2 Dissect brains out of the skull and post-fix in 4% PFA in PBS overnight.

12h

3 Embed fixed tissue in agarose and section into 40 μm thick sections using a vibratome (VT1000S, Leica).

Note

NOTE: The sections can be stored in PBS 0.05% sodium azide at 4°C.

4 Permeabilize sections with 0.5% Triton X-100 and wash with PBS.

5 Incubate sections in blocking solution consisting of 0.2% BSA (w/v), 5% donkey serum (v/v)

30m

(abcam), 0.2% lysine (w/v) (Sigma-Aldrich), 0.2% glycine (w/v) (Sigma-Aldrich) in PBS for 30 min at room temperature (RT).

- 6** Incubate sections with primary antibodies (anti-phospho-Tau AT-8 (Thermo, Cat# MN1020, 1:300); anti-VCP (Novus Biologicals, Cat# NB 100-1558, 1:500) diluted in 0.3% Triton X-100 (v/v), 2% BSA (w/v) in PBS overnight at 4°C. 12h

- 7** Wash sections in PBS and incubate with secondary antibodies and Neurotrace 640/660 (ThermoFisher, Cat# N21483, 1:500) diluted in 0.3% Triton X-100, 3% donkey serum (v/v) for 2 h at RT. 2h

- 8** Stain nuclei with 0.5 µg/ml DAPI.

- 9** Mount sections on Menzer glass slides using Prolong Glass fluorescence (Invitrogen) mounting medium.

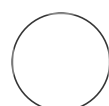


SEP 06, 2022

Lentivirus production

Itika Saha¹, F. Ulrich Hartl¹, Mark S. Hipp^{2,3}¹Department of Cellular Biochemistry, Max Planck Institute of Biochemistry, Am Klopferspitz 18, 82152 Martinsried, Germany;²Department of Biomedical Sciences of Cells and Systems, University Medical Center Groningen, University of Groningen, Antonius Deusinglaan, 1, 9713 AV Groningen, The Netherlands;³School of Medicine and Health Sciences, Carl von Ossietzky University Oldenburg, 26129 Oldenburg, GermanyOPEN  ACCESS**DOI:**dx.doi.org/10.17504/protocols.io.6qpvr4xn3gmk/v1**External link:**<https://www.biorxiv.org/content/10.1101/2022.02.18.481043v1.full>**Protocol Citation:** Itika Saha, F. Ulrich Hartl, Mark S. Hipp 2022. Lentivirus production.**protocols.io**<https://dx.doi.org/10.17504/protocols.io.6qpvr4xn3gmk/v1>**MANUSCRIPT CITATION:**

The AAA+ chaperone VCP disaggregates Tau fibrils and generates aggregate seeds
Itika Saha, Patricia Yuste-Checa, Miguel Da Silva Padilha, Qiang Guo, Roman Körner, Hauke Holthusen, Victoria A. Trinkaus, Irina Dudanova, Rubén Fernández-Busnadiego, Wolfgang Baumeister, David W. Sanders, Saurabh Gautam, Marc I. Diamond, F. Ulrich Hartl, Mark S. Hipp
bioRxiv 2022.02.18.481043;
doi:
<https://doi.org/10.1101/2022.02.18.481043>



Felix Kraus

ABSTRACT

This protocol describes the production of lentiviruses to transduce HEK293T cells and has to be performed in a biosafety level 2 laboratory

SAFETY WARNINGS

Has to be performed in a biosafety level 2 laboratory.

License: This is an open access protocol distributed under the terms of the [Creative Commons Attribution License](#), which permits unrestricted use, distribution, and reproduction in any medium, provided the original author and source are credited

Protocol status: Working
We use this protocol and it's working

Created: Sep 05, 2022

Last Modified: Dec 26, 2022

PROTOCOL integer ID:
69582

Keywords: ASAPCRN

Lentivirus production

1d 1h 10m

- 1 Plate $\sim 3.6 \times 10^6$ Lenti-X HEK293T cells (Takara) in 10 cm dish in 10 mL standard DMEM. Cells should be $\sim 80\%$ confluent at the time of transfection.

Note

NOTE: Only low passage cells should be used.

- 2 Next day, remove 5 mL medium and replenish with fresh medium.
- 3 Warm up reduced serum medium e.g. Opti-MEM (Gibco) and transfection reagent to room temperature (RT). This protocol was performed with Lipofectamine 3000 transfection reagent (Thermo).
- 4 Add 24 μL Lipofectamine 3000 to 600 μL Opti-MEM, mix by vortexing and incubate 5 min at RT.

5m

- 5 In another tube, mix 6 µg plasmid containing gene of interest, 5 µg packaging plasmid psPAX2 (RRID:Addgene_12260), 1 µg envelope plasmid pMD2.G (RRID:Addgene_12259) and 24 µL P3000 reagent (provided by manufacturer along with Lipofectamine 3000 reagent) in 600 µL Opti-MEM, mix by vortexing and incubate 5 min at RT.
- 6 Mix contents of both tubes and incubate for 15 min at RT. 15m
- 7 Add DNA-lipid complex to cells dropwise.
- 8 2 days later, collect virus-containing medium and centrifuge for 5 min at 1,000 x g. 2d
- 9 Collect supernatant in a fresh tube and proceed with concentration.

Concentration

1d 1h 10m

- 10 Add Lenti-X concentrator (Takara) to clarified virus-containing medium at 1:4 dilution and mix well by gently inverting tube.
- 11 Incubate overnight or 2 h at 4 °C. 1d
- 12 Next day, centrifuge for 45 min at 1,500 x g at 4 °C followed by gently aspirating supernatant. 45m



13 Resuspend viral pellet in 100 - 1000 μ L PBS, aliquot and store at -80 °C until use.



SEP 06, 2022

Lentivirus production for primary neuron transduction

Miguel Da Silva Padilha¹, Irina Dudanova¹, Itika Saha²,
F. Ulrich Hartl², Mark S. Hipp^{3,4}

¹Molecular Neurodegeneration Group, Max Planck Institute of Neurobiology, 82152 Martinsried, Germany;

²Department of Cellular Biochemistry, Max Planck Institute of Biochemistry, Am Klopferspitz 18, 82152 Martinsried, Germany;

³Department of Biomedical Sciences of Cells and Systems, University Medical Center Groningen, University of Groningen, Antonius Deusinglaan, 1, 9713 AV Groningen, The Netherlands;

⁴School of Medicine and Health Sciences, Carl von Ossietzky University Oldenburg, 26129 Oldenburg, Germany

OPEN ACCESS**DOI:**

dx.doi.org/10.17504/protocols.io.kqdg39eo1g25/v1

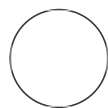
External link:

<https://www.biorxiv.org/content/10.1101/2022.02.18.481043v1.full>

Protocol Citation: Miguel Da Silva Padilha, Irina Dudanova, Itika Saha, F. Ulrich Hartl, Mark S. Hipp 2022. Lentivirus production for primary neuron transduction. **protocols.io** <https://dx.doi.org/10.17504/protocols.io.kqdg39eo1g25/v1>

MANUSCRIPT CITATION:

Itika Saha, Patricia Yuste-Checa, Miguel Da Silva Padilha, Qiang Guo, Roman Körner, Hauke Holthusen, Victoria A. Trinkaus, Irina Dudanova, Rubén Fernández-Busnadiego, Wolfgang Baumeister, David W. Sanders, Saurabh Gautam, Marc I. Diamond, F. Ulrich Hartl, Mark S. Hipp bioRxiv 2022.02.18.481043; doi: <https://doi.org/10.1101/2022.02.18.481043>



Felix Kraus

ABSTRACT

This protocol describes the production of lentiviruses to transduce mouse primary neurons and has to be performed in a biosafety level 2 laboratory

SAFETY WARNINGS



This protocol describes the production of lentiviruses to transduce mouse primary neurons and has to be performed in a biosafety level 2 laboratory

License: This is an open access protocol distributed under the terms of the [Creative Commons Attribution License](#), which permits unrestricted use, distribution, and reproduction in any medium, provided the original author and source are credited

Protocol status: Working
We use this protocol and it's working

Created: Sep 05, 2022

Last Modified: Dec 26, 2022

PROTOCOL integer ID:
69592

Keywords: ASAPCRN

- 1 Expand HEK293T cells (LentiX 293T cell line, Takara) for lentiviral packaging to 70-85% confluency in DMEM Glutamax (+4.5 g/L D-glucose, - pyruvate) supplemented with 10% Fetal Bovine Serum (FBS)(Sigma), 1% G418 (Gibco), 1% Non-Essential Amino Acids (Thermo Fisher) and 1% HEPES (Biomol).

Note

NOTE: Only low passage cells should be used.

- 2 For lentiviral production, plate cells ($\sim 4.8 \times 10^6$) in a three-layered 525 cm² flask (Falcon).
- 3 On the following day, transfect cells with 59.52 μ g expression plasmid, 35.2 μ g packaging plasmid psPAX2 (RRID:Addgene_12260) and 20.48 μ g envelope plasmid pVsVg (gift from Dieter Edbauer) using 345.6 μ l TransIT-Lenti transfection reagent (Mirus) in 9.6 mL DMEM without FBS. 1d
- 4 Incubate transfection mix for 20 min at room temperature and exchange the cell medium in the meantime. 20m

- 5 Add 10 mL of transfection mix to the flask, followed by incubation overnight.
- 6 Exchange the medium on the following day. 1d
- 7 After 48-52 h, collect culture medium containing the viral particles and centrifuge for 10 min at 1,200 x g. 2d
- 8 Filter the supernatant through 0.45 µm pore size filters using 50 mL syringes and add 20 mL Lenti-X concentrator (Takara) to filtered supernatant.
- 9 Incubate overnight at 4 °C and centrifuge samples at 1,500 x g for 45 min at 4 °C. 1d
- 10 Remove the supernatant and resuspend the lentivirus pellet in 150 µL TBS-5 buffer (50 mM Tris-HCl pH 7.8, 130 mM NaCl, 10 mM KCl, 5 mM MgCl₂).
- 11 After aliquoting, store lentivirus at -80 °C.
- 12 Thaw virus preparation immediately before adding to freshly prepared neuronal culture medium.
- 13 Remove a fifth of the medium from cultured neurons and add the equivalent volume of virus-

containing medium.

Note

NOTE: Volume of concentrated virus to be added to the neurons and the length of transduction should be determined empirically.



SEP 06, 2022

Native-PAGE analysis of VCP hexamer

Itika Saha¹, F. Ulrich Hartl¹, Mark S. Hipp^{2,3}

¹Department of Cellular Biochemistry, Max Planck Institute of Biochemistry, Am Klopferspitz 18, 82152 Martinsried, Germany;

²Department of Biomedical Sciences of Cells and Systems, University Medical Center Groningen, University of Groningen, Antonius Deusinglaan, 1, 9713 AV Groningen, The Netherlands;

³School of Medicine and Health Sciences, Carl von Ossietzky University Oldenburg, 26129 Oldenburg, Germany

OPEN  ACCESS**DOI:**

dx.doi.org/10.17504/protocols.io.36wgqjrzyvk5/v1

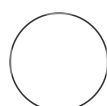
External link:

<https://www.biorxiv.org/content/10.1101/2022.02.18.481043v1.full>

Protocol Citation: Itika Saha, F. Ulrich Hartl, Mark S. Hipp 2022. Native-PAGE analysis of VCP hexamer. **protocols.io** <https://dx.doi.org/10.17504/protocols.io.36wgqjrzyvk5/v1>

MANUSCRIPT CITATION:

The AAA+ chaperone VCP disaggregates Tau fibrils and generates aggregate seeds
Itika Saha, Patricia Yuste-Checa, Miguel Da Silva Padilha, Qiang Guo, Roman Körner, Hauke Holthusen, Victoria A. Trinkaus, Irina Dudanova, Rubén Fernández-Busnadiego, Wolfgang Baumeister, David W. Sanders, Saurabh Gautam, Marc I. Diamond, F. Ulrich Hartl, Mark S. Hipp
bioRxiv 2022.02.18.481043;
doi:
<https://doi.org/10.1101/2022.02.18.481043>



Felix Kraus

ABSTRACT

Valosin-containing protein (VCP) is a homo-hexameric AAA+ ATPase in eukaryotic cells. This protocol describes the analysis of myc-tagged versions of VCP transiently transfected in HEK293 cells (stably expressing and propagating aggregates of Tau repeat domain fused to YFP) for hexamer formation.

License: This is an open access protocol distributed under the terms of the [Creative Commons Attribution License](#), which permits unrestricted use, distribution, and reproduction in any medium, provided the original author and source are credited

Protocol status: Working
We use this protocol and it's working

Created: Sep 05, 2022

Last Modified: Dec 26, 2022

PROTOCOL integer ID:
69590

Keywords: ASAPCRN

- 1** Plate 1.5×10^5 cells in 12-well plate.
- 2** Next day, transfect with plasmids expressing myc-tagged VCP variants (Saha et al. *BioRxiv*, 2022) using a standard transfection protocol.
- 3** Two days later, collect cells and lyse them in 50 μ L 0.5% Triton X-100/PBS supplemented with protease inhibitor cocktail (Roche) and DNase for 1 h on ice. 1h
- 4** Centrifuge lysates at 10,000 x g for 2 min and collect supernatant. 2m
- 5** Determine protein concentration in the supernatant and normalize across all samples.

6 Add 2x native sample buffer (40 % glycerol, 240 mM Tris pH 6.8, 0.04 % bromophenol blue) to 40 µg lysate.

7 Run samples on a Native PAGE gel (e.g. Novex Value 4 to 12% Tris-glycine gels (Thermo)) in 20 mM Tris 200 mM Glycine buffer at pH 8.4. 1h

8 Transfer proteins to nitrocellulose membrane in standard Tris-glycine buffer, block in 5% low-fat dry milk for 1 h at room temperature (RT). 2h

Note

NOTE: Nitrocellulose membranes produce less background than PVDF membranes with fluorescent secondary antibodies.

9 Dilute anti-myc (9E10) and anti-VCP (1:2000, Novus Biologicals) primary antibodies together in blocking solution and incubate membrane overnight.

10 Next day, wash membrane 3 times with TBST and incubate with anti-mouse (LI-COR Biosciences Cat# 926-68070, RRID:AB_10956588; 1:10,000) and anti-rabbit (LI-COR Biosciences Cat# 926-32211, RRID:AB_621843; 1:10,000) fluorescent secondary antibodies for 2 h at RT. 2h

11 Wash membrane 3 times with TBST.

12 Detect fluorescent myc and VCP signal on a fluorescent imager.



SEP 06, 2022

Primary neuronal cultures

Miguel Da Silva Padilha¹, Irina Dudanova¹, F. Ulrich Hartl¹,
Itika Saha², Mark S. Hipp^{3,4}

¹Molecular Neurodegeneration Group, Max Planck Institute of Neurobiology, 82152 Martinsried, Germany;

²Department of Cellular Biochemistry, Max Planck Institute of Biochemistry, Am Klopferspitz 18, 82152 Martinsried, Germany;

³Department of Biomedical Sciences of Cells and Systems, University Medical Center Groningen, University of Groningen, Antonius Deusinglaan, 1, 9713 AV Groningen, The Netherlands;

⁴School of Medicine and Health Sciences, Carl von Ossietzky University Oldenburg, 26129 Oldenburg, Germany

OPEN  ACCESS

DOI:

dx.doi.org/10.17504/protocols.io.ewov1ojwklr2/v1

External link:

<https://www.biorxiv.org/content/10.1101/2022.02.18.481043v1.full>

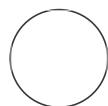
Protocol Citation: Miguel Da Silva Padilha, Irina Dudanova, F. Ulrich Hartl, Itika Saha, Mark S. Hipp 2022. Primary neuronal cultures.

protocols.io

<https://dx.doi.org/10.17504/protocols.io.ewov1ojwklr2/v1>

MANUSCRIPT CITATION:

Itika Saha, Patricia Yuste-Checa, Miguel Da Silva Padilha, Qiang Guo, Roman Körner, Hauke Holthusen, Victoria A. Trinkaus, Irina Dudanova, Rubén Fernández-Busnadiego, Wolfgang Baumeister, David W. Sanders, Saurabh Gautam, Marc I. Diamond, F. Ulrich Hartl, Mark S. Hipp
bioRxiv 2022.02.18.481043;
doi:
<https://doi.org/10.1101/2022.02.18.481043>



Felix Kraus

ABSTRACT

This protocol describes the preparation of primary neuronal cultures from E15.5 CD-1 wild type mouse embryos. Experiments involving animal models must be performed in accordance with relevant institutional guidelines and regulations.

License: This is an open access protocol distributed under the terms of the [Creative Commons Attribution License](#), which permits unrestricted use, distribution, and reproduction in any medium, provided the original author and source are credited

Protocol status: Working
We use this protocol and it's working

Created: Sep 05, 2022

Last Modified: Dec 26, 2022

PROTOCOL integer ID:
69593

Keywords: ASAPCRN

- 1 Sacrifice pregnant female mice by cervical dislocation.
- 2 Remove the uterus from the abdominal cavity and place into a 10 cm sterile Petri dish on ice containing dissection medium, consisting of Hanks' balanced salt solution (HBSS) supplemented with 0.01 M HEPES, 0.01 M MgSO₄ and 1% penicillin/streptomycin.
- 3 Isolate each embryo, decapitate the heads, remove the brains from the skull and immerse in ice-cold dissection medium.
- 4 Dissect cortical hemispheres, and remove meninges under a dissection microscope.
- 5 Collect the cortices in a 15 mL sterile tube and digest with 0.25% trypsin containing 1 mM ethylenediaminetetraacetic acid (EDTA) and 15 μ L 0.1% DNase I for 20 min at 37 °C.

- 6** Stop digestion by removing the supernatant and washing the tissue twice with Neurobasal medium (Invitrogen) containing 5% Fetal Bovine Serum.

- 7** Resuspend the tissue in 2 mL Neurobasal medium and triturate to achieve a single cell suspension.

- 8** Spin cells at 130 x g, remove the supernatant, and resuspend the cell pellet in Neurobasal medium with 2% B-27 supplement (Invitrogen), 1% L-glutamine (Invitrogen) and 1% penicillin/streptomycin (Invitrogen).

- 9** Plate cells at desired density in dishes or coverslips coated with 1 mg/mL poly-D-lysine (Sigma) and 1 µg/mL laminin (Thermo Fisher Scientific).



SEP 06, 2022

Size exclusion chromatography of cell lysates containing Tau aggregates

Patricia Yuste Checa¹, Itika Saha¹, F. Ulrich Hartl¹, Mark S. Hipp^{2,3}

¹Department of Cellular Biochemistry, Max Planck Institute of Biochemistry, Am Klopferspitz 18, 82152 Martinsried, Germany;

²Department of Biomedical Sciences of Cells and Systems, University Medical Center Groningen, University of Groningen, Antonius Deusinglaan, 1, 9713 AV Groningen, The Netherlands;

³School of Medicine and Health Sciences, Carl von Ossietzky University Oldenburg, 26129 Oldenburg, Germany

OPEN  ACCESS

DOI:

dx.doi.org/10.17504/protocols.io.4r3l27mjpg1y/v1

External link:

<https://www.biorxiv.org/content/10.1101/2022.02.18.481043v1.full>

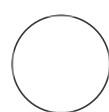
Protocol Citation: Patricia Yuste Checa, Itika Saha, F. Ulrich Hartl, Mark S. Hipp 2022. Size exclusion chromatography of cell lysates containing Tau aggregates.

protocols.io

<https://dx.doi.org/10.17504/protocols.io.4r3l27mjpg1y/v1>

MANUSCRIPT CITATION:

The AAA+ chaperone VCP disaggregates Tau fibrils and generates aggregate seeds
Itika Saha, Patricia Yuste-Checa, Miguel Da Silva Padilha, Qiang Guo, Roman Körner, Hauke Holthusen, Victoria A. Trinkaus, Irina Dudanova, Rubén Fernández-Busnadiego, Wolfgang Baumeister, David W. Sanders, Saurabh Gautam, Marc I. Diamond, F. Ulrich Hartl, Mark S. Hipp
bioRxiv 2022.02.18.481043;
doi:
<https://doi.org/10.1101/2022.02.18.481043>



Felix Kraus

ABSTRACT

This protocol can be used to fractionate Tau aggregates from cell lysates by size exclusion chromatography. The protocol was optimized using HEK293 cells stably expressing and propagating aggregates of Tau repeat domain, containing the disease-related mutations P301L and V337M, fused to YFP (Clone 10 from Sanders et al., Neuron, 2014). However, any cell line containing Tau aggregates can be used.

License: This is an open access protocol distributed under the terms of the [Creative Commons Attribution License](#), which permits unrestricted use, distribution, and reproduction in any medium, provided the original author and source are credited

Protocol status: Working
We use this protocol and it's working

Created: Sep 05, 2022

Last Modified: Dec 26, 2022

PROTOCOL integer ID:
69591

Keywords: ASAPCRN

- 1 Lyse cell pellets with Triton buffer, Complete EDTA-free protease inhibitor cocktail (Roche) and benzonase for 20 min on ice. NOTE: Triton buffer: 0.05% Triton X-100/PBS or 1% Triton X-100/PBS (more efficient lysis) can be used to lyse cell pellets. 30m

- 2 Clarify the lysates by centrifugation at 1,000 x g for 5 min at 4 °C and filter the supernatant with a PVDF 0.22 µm filter (Millex, #SLGVX13NL). 5m

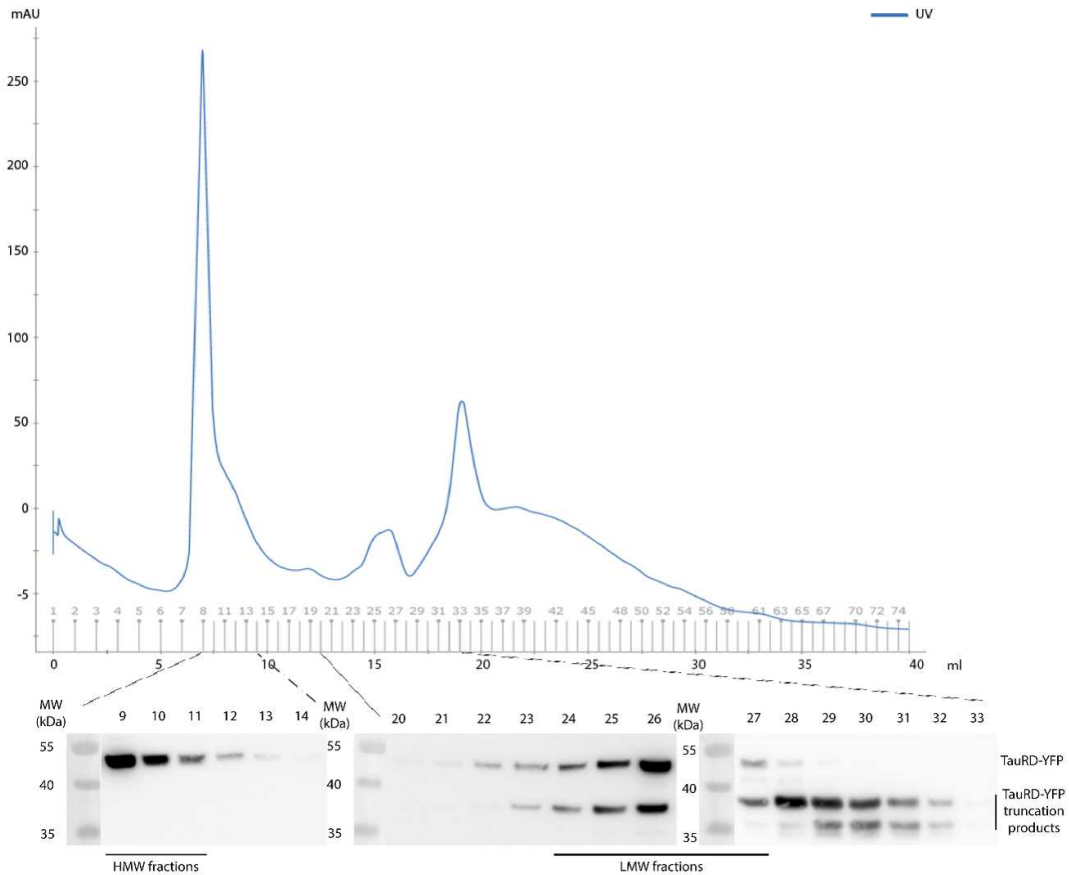
- 3 Quantify total protein by Bio-Rad Protein Assay (Bio-Rad) or Pierce BCA Protein Assay Kit (Thermo Fisher Scientific).

- 4 Load 3 mg total protein on a Superose 6 HR10/30 (GE 875 Healthcare) column previously equilibrated with PBS.

- 4.1 NOTES: Cells from a confluent T75 flask lysed with 800 µL lysis buffer results in ~ 8-10 mg/mL total protein. Superose 6 HR10/30 (GE Healthcare): Flow rate 0.5 mL/min; 1mL fractions up to void volume of the column and 0.5 mL fractions from void volume to the end.

- 5** Analyze and quantify individual fractions by Western blot. NOTES: Use 15 μ l of each fraction to detect TauRD-YFP by immunoblotting with anti-GFP antibody (Roche #11814460001).

5.1



High molecular weight (HMW) species are detected in the void volume of the column while low molecular weight (LMW) species are detected around 15 mL elution volume (fractions ~24-27). TauRD-YFP cleaved products are detected along with TauRD-YFP in the LMW fractions.

- 6** The corresponding fractions, HMW and LMW species, can be pooled and quantified (using purified TauRD-YFP as standard) by immunoblotting to perform other biochemical assays or cell-based Tau seeding assays.

Note

NOTE: Seeding with 0.5 ng HMW species from TauRD-YFP Clone 10 results in ~20% FRET positive cells while 0.5 ng LMW species results in ~1-2% FRET positive cells following the protocol "Cell-based Tau seeding assay" (Yuste-Checa et al., Nature Communication, 2021).